REPORT DOCUMENTATION PAGE

Form Approved
OMB No. 0704-0188

1. REPORT DATE (DD-MM-YYYY) 19-12-2011	2. REPORT TYPE Journal Article	3. DATES COVERED (From - To)

4. TITLE AND SUBTITLE

New Insights into Structure-Property Relationships in Thermosetting Polymers from Studies of Co-Cured Polycyanurate Networks (preprint)

5a. CONTRACT NUMBER

5b. GRANT NUMBER

5c. PROGRAM ELEMENT NUMBER

6. AUTHOR(S)

Andrew J. Guenthner, Kevin R. Lamison, Vandana Vij, Josiah T. Reams, Gregory R. Yandek and Joseph M. Mabry

5d. PROJECT NUMBER

5f. WORK UNIT NUMBER
23030521

7. PERFORMING ORGANIZATION NAME(S) AND ADDRESS(ES)

Air Force Research Laboratory (AFMC)
AFRL/RZSM
9 Antares Road
Edwards AFB CA 93524-7401

8. PERFORMING ORGANIZATION REPORT NUMBER

9. SPONSORING / MONITORING AGENCY NAME(S) AND ADDRESS(ES)

Air Force Research Laboratory (AFMC)
AFRL/RZS
5 Pollux Drive
Edwards AFB CA 93524-7048

10. SPONSOR/MONITOR'S ACRONYM(S)

11. SPONSOR/MONITOR'S NUMBER(S)
AFRL-RZ-ED-JA-2011-583

12. DISTRIBUTION / AVAILABILITY STATEMENT

Approved for public release; distribution unlimited (PA #12037).

13. SUPPLEMENTARY NOTES
For publication in Macromolecules.

14. ABSTRACT

Studies of the physical properties of the co-cured networks formed from three similar dicyanate ester monomers revealed a number of unexpected variations from simple linear mixing rules. These variations shed light on important synergistic effects in co-cured thermosetting networks and their possible causes. The monomers utilized were the dicyanate esters of Bisphenol A (BADCy), Bisphenol E (LECy), and the silicon-containing analog of Bisphenol A (SiMCy). The most important of the synergistic effects was a decrease of approx. 25% in moisture uptake seen only in co-networks of LECy and SiMCy. For all other systems, a clear relationship between moisture uptake and the number density of cyanurate rings was observed. This relationship generally applies to many types of cyanate esters and gives an indication of the importance of specific sites (as opposed to free volume alone) in moisture uptake. Numerous additional examples of non-linear mixing relations were observed in the glass transition temperature, density, and thermochemical stability of fully cured networks. Interestingly, the most widespread deviations from linear behavior were observed for co-networks of SiMCy and LECy, suggesting that factors such as the mismatch in network segment size may be more important than differences in flexibility or symmetry in driving significant physical interactions among co-network components.

15. SUBJECT TERMS

16. SECURITY CLASSIFICATION OF:			17. LIMITATION OF ABSTRACT	18. NUMBER OF PAGES	19a. NAME OF RESPONSIBLE PERSON Dr. Joseph M. Mabry
a. REPORT Unclassified	b. ABSTRACT Unclassified	c. THIS PAGE Unclassified	SAR	109	19b. TELEPHONE NUMBER (include area code) N/A

Standard Form 298 (Rev. 8-98)
Prescribed by ANSI Std. 239.18

New Insights into Structure-Property Relationships in Thermosetting Polymers from Studies of Co-Cured Polycyanurate Networks

Andrew J. Guenthner,[1*] Kevin R. Lamison,[2] Vandana Vij,[2] Josiah T. Reams,[3] Gregory R. Yandek,[1] and Joseph M. Mabry[1]

[1]Air Force Research Laboratory, Propulsion Directorate, Edwards AFB, CA 93524
[2]ERC Incorporated, Air Force Research Laboratory, Edwards AFB, CA 93524
[3]National Research Council, Air Force Research Laboratory, Edwards AFB, CA 93524

Author e-mail: andrew.guenthner@edwards.af.mil

Abstract

Studies of the physical properties of the co-cured networks formed from three similar dicyanate ester monomers revealed a number of unexpected variations from simple linear mixing rules. These variations shed light on important synergistic effects in co-cured thermosetting networks and their possible causes. The monomers utilized were the dicyanate esters of Bisphenol A (BADCy), Bisphenol E (LECy), and the silicon-containing analog of Bisphenol A (SiMCy). The most important of the synergistic effects was a decrease of approx. 25% in moisture uptake seen only in co-networks of LECy and SiMCy. For all other systems, a clear relationship between moisture uptake and the number density of cyanurate rings was observed. This relationship generally applies to many types of cyanate esters and gives an indication of the importance of specific sites (as opposed to free volume alone) in moisture uptake. Numerous additional examples of non-linear mixing relations were observed in the glass transition temperature, density, and thermochemical stability of fully cured networks. Interestingly, the most widespread deviations from linear behavior were observed for co-networks of SiMCy and

LECy, suggesting that factors such as the mismatch in network segment size may be more important than differences in flexibility or symmetry in driving significant physical interactions among co-network components.

Keywords: cyanate ester, silicon-containing polymers, moisture uptake, polymer blends, co-networks

Introduction

Cyanate ester resins[1-4] have gained increasing prominence as "next generation" thermosetting monomers used as adhesives and composite resins in a wide range of high-performance aerospace,[5] electronics,[6, 7] and alternative energy[8] applications. The low toxicity, low shrinkage, and low generation of volatiles during thermal cure of cyanate esters (primarily *via* cyclotrimerization) to form polycyanurates, along with the ability to be used in fabrication processes as varied as filament winding,[9] resin transfer molding,[10-12] and nanostructure casting,[13] make polycyanurates highly attractive for commercial product development. In addition, the highly selective nature of the cure reaction,[14, 15] along with the ease of detection of both the extent of cure and side reactions in the solid state,[1] make cyanate esters especially useful in fundamental studies of macromolecular network formation, structure, and properties. Thus, a well-developed understanding of the relationships among network physical and chemical characteristics, processing, and resultant solid-state properties for cyanate esters is not only highly feasible, it also has the potential to significantly improve the design and performance of thermosetting resins used in many technologically important products ranging from micro-capacitors[6] to interplanetary space probes.[16]

One of the major challenges associated with developing structure-property relationships for cyanate esters, or for any thermosetting polymer, involves the ability to examine the physical

structure of the cured macromolecular network at the molecular level. Though much useful information can be ascertained from examination of the soluble fraction in a partially polymerized system, as described by Kasehagen and Macosko[17] for the dicyanate ester of bisphenol A (hereafter "BADCy"), the structure arising from the later, post-vitrification stages of cure is much more difficult to examine. Georjon and Galy,[18] for instance, have shown through positron annihilation studies that a substantial amount of free volume develops during the final stages of cyanate ester cure, with significant impacts on properties such as moisture uptake. While infrared and solid-state NMR spectroscopy can provide useful data on the chemical structures present even after complete conversion, and X-ray data can provide valuable information on local ordering and orientation, much desirable information on physical aspects of the network structure is extremely difficult to obtain directly. As a result, indirect methods such as the study of volumetric changes or examination of primary and secondary thermomechanical transitions[19] must be used to gather evidence of these aspects. There exists, therefore, a critical need for innovative approaches to further expand the available repertoire of indirect experimental methods that can be used to probe the molecular level structures and interactions in thermosetting polymer networks. Such innovative techniques will reveal important clues to help understand the nature of the networks and facilitate considerable progress in developing structure/property relationships.

In this paper, we illustrate the use of three-component co-cured network studies to probe the molecular level interactions in well-defined thermosetting polymer networks. Most physical properties of interest in these co-cured networks are expected to follow simple linear rules of mixing because phase separation is absent and the components are highly similar. Using three-component systems, not only can the presence of nonlinear behavior be detected, but

nonlinearities that apply equally to all the components are easily distinguished from those that appear only for certain combinations of components. These component-specific nonlinearities serve as an indication of important interactions. Thus, by mapping the compositional patterns of property variations, and in particular patterns of systematic deviation from expected values, unexpected interactions among the components of co-cured networks can be discovered.

Furthermore, by utilizing the synthetic flexibility afforded by cyanate esters to formulate and compare co-networks with well-defined and systematic differences in segment structure, important information may be inferred on the roles played by various structural parameters (such as the rigidity of network segments or the distance between cross-links) in controlling physical properties of interest. Whereas previous two-component co-cured cyanate ester network studies[20-24] have provided some tantalizing hints that synergistic and/or unexpected interactions among components may frequently take place, the carefully crafted three-component studies presented herein reveal many synergistic interactions (such as unexpectedly low moisture uptake) offer significant opportunities for exploitation. Consequently, the techniques and results described herein provide a vivid illustration of how well-designed studies of molecular level interactions in co-cured networks enable substantial advances in the development of structure-property relationships and improved performance not only for cyanate esters but for thermosetting polymers in general.

Results and Discussion

Due to the large number of variables (thirty-one in all) and compositions studied, only the most significant highlights of the results are discussed in detail in this section. A comprehensive description of all of the variables examined, and all of the results for all of the properties of

interest, including those not discussed in detail herein such as "wet" T_g values and char yields, are provided in Supporting Information.

The three monomers utilized for the study of co-networks constituted a set of highly similar dicyanate monomers, two of which (Primaset® BADCy and its asymmetric and more flexible counterpart, Primaset® LECy, are commonly used commercial products). The third monomer, a silicon-containing analog of BADCy known as SiMCy, retains the symmetry of BADCy while affording more flexible network segments as in LECy but with a larger segmental volume. The set thus allows a systematic study of the interactions among rigid / flexible, symmetric / asymmetric, and larger / smaller network segments.

It should be noted that, due to the highly similar nature of the monomers, phase separation (at scales of 0.1 µm and above) was avoided both during the mixing of monomers (as evidenced by their transparent and homogeneous appearance when melted), as well as in the co-cured networks (which always showed single glass transitions over a range no broader or less well-defined for multiple component networks than for single component networks), and for which sample castings always appeared transparent and homogeneous. Moreover, examination of the cured networks by infrared spectroscopy showed no indications of the formation of significant amounts of side products or other unexpected chemical structures that might give rise to nonlinear rules of mixing in multi-component networks. The reliable formation of networks with well-defined chemical structures by curing in an inert atmosphere at relatively low temperatures is in accord with the expected chemical behavior of cyanate ester networks.

To study the interactions among components, robust regressions were performed on all sample data, with particular effort given to identifying meaningful deviations from linearity caused by compositional variations specific to two components, which is the signature

5

characteristic of significant molecular level interactions. In addition, the data were also examined for correlations among properties as well as the segment structure on the estimated physical property values for pure components. Table 1 summarizes the key results obtained from the robust regression analyses in terms of the predicted values of the properties for BADCy, LECy, and SiMCy, along with the effect of conversion. Note that the conversion for all samples was in the range 0.95 – 1.00, and, in cases where it was found to be a significant factor, variations due to differences in conversion among samples were specifically included in the regression models.

Moisture Uptake. Figure 1 shows both the individually measured moisture uptake values (not adjusted for degree of conversion, as dots) and a grid depicting the smoothed values of moisture uptake (at full conversion). As explained in the Experimental section, the smoothed values were utilized to identify any systematic deviations from linearity as a function of composition. Robust regression of the data showed that the moisture uptake was predicted with a standard error of just 0.12% (absolute) when the degree of conversion was taken into account. As reported previously,[25] SiMCy exhibits a significantly lower moisture uptake compared to BADCy and LECy. In addition, as first reported for BADCy by Georjon and Galy,[18] the degree of cure had a strong influence on moisture uptake (statistically significant at 94% confidence). Interestingly, Georjon and Galy showed that the free volume in BADCy increased with increasing conversion for the range of conversions investigated (85-100%). The report is consistent with earlier data[26-28] reporting an increase in molar volume at room temperature at conversions above the gel point for many cyanate esters, as well as with our own density measurements. The increase in free volume was naturally linked to the increased water uptake. Our results, however, show a clear decrease in water uptake with increasing SiMCy content, even though, as discussed in the section on density, the overall free volume in the system increased with increasing amounts of SiMCy.

Table 1. Key properties of single component cyanate ester networks obtained from robust regressions of data for co-networks

Parameter (data source)	Unit	Value (from robust regression, at full cure)			Effect of Cure[c]
		BADCy	LECy	SiMCy	
T_g (uncured, DSC)	°C	-38 ± 2	-47 ± 2	-46 ± 2	n/a
T_g (fully cured, TMA)[a]	°C	309 ± 7	294± 8	266 ± 7	n/a
T_g (fully cured, DSC)[b]	°C	300 ± 5	290 ± 5	267 ± 5	n/a
Density (as-cured)[a]	g/cc	1.195 ± 0.003	1.220 ± 0.003	1.175 ± 0.003	-0.14 ± 0.06
CTE (as-cured, TMA)[a]	ppm/°C	59 ± 2	64 ± 2	74 ± 2	-30 ± 14
CTE (fully cured, TMA)[b]	ppm/°C	56 ± 3	62 ± 3	69 ± 3	n/a
Water Uptake (as-cured)[a]	wt%	2.34 ± 0.12	2.36 ± 0.13	1.76 ± 0.11	+4.9 ± 2.3
T-5% Loss (TGA, N_2)	°C	418 ± 2	419 ± 2	418 ± 2	n/a
T-5% Loss (TGA, Air)	°C	417 ± 2	417 ± 2	415 ± 2	n/a
Char Yield (TGA, N_2)	wt%	49 ± 4	57 ± 3	48 ± 3	n/a
Char Yield (TGA, Air)	wt%	20 ± 6	41 ± 6	51 ± 6	n/a

[a] "As-cured" in the description of the data source means that the reported values were obtained from a regression of co-network data on samples cured at 210 °C for 24 hrs, which resulted in conversions of 95-100%, in which the extent of cure was included as a regression variable (the reported values thus represent an extrapolation to full cure)

[b] "Fully cured" in the description of the data source means the values were obtained from a regression of co-network data on samples that had been previously heated to 350 °C to ensure full cure

[c] "Effect of cure" denotes the expected change in value for a hypothetical 100% increase in conversion (note that the data is only valid for conversions of 95-100%, however)

The results of the co-network study, therefore, indicate that moisture uptake in cyanate esters is not simply a matter of free volume, but rather appears to depend on the availability of a specific type of free volume. The free volume that is presumably "frozen in" during the later stages of cure was noted by Georjon and Galy to possess a larger characteristic size, according to positron annihilation lifetime data, than the free volume initially present in the system. It is reasonable to expect that such free volume would form at characteristic locations near the triazine rings in the developing cyanate ester network, where, during vitreous cure (the glass transition temperature of the polycyanurate networks is significantly higher than the cure temperature during the late stages of cure), van der Waals volume is reduced by cross-linking, creating free volume that is unable to relax or diffuse away to any significant extent. On the other hand, it is reasonable to expect that the extra free volume in SiMCy as compared to
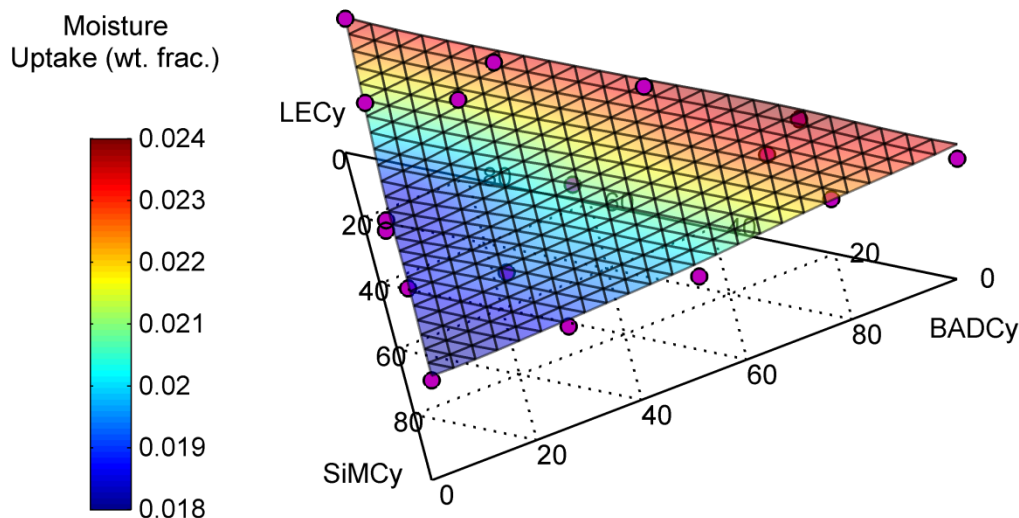
Figure 1. Moisture uptake as a function of composition. The dark circles indicate individual measurements (at varying conversions of 0.95 – 1, while the grid indicates the calculated values of the smoothed data (extrapolated to full conversion), thereby highlighting the effect of composition.

BADCy or LECy would be associated with the longer and more flexible Si-C bonds that discourage tight packing of chain segments, and hence, that such free volume is not likely to be concentrated near cyanurate rings. This concept is illustrated graphically in Figure 2, which depicts a model of a dicyanate ester network segment, with the likely locations of pockets of unoccupied volume pointed out.

Thus, it appears that a specific type of free volume, located near cyanurate rings and formed presumably because vitrification of the network prevents shrinkage, serves as a preferred site for moisture uptake in cyanate esters. If the aforementioned hypothesis is correct, then there
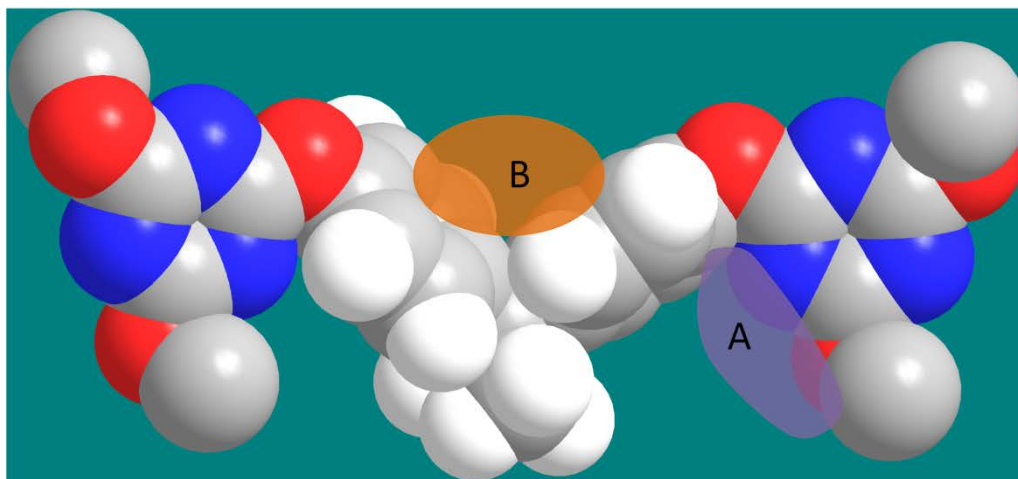
Figure 2. Space-filling model of a cured BADCy network segment, (electronic version colors: nitrogen = blue, oxygen = red) showing two full cyanurate rings. Regions where unoccupied volume might be expected to form are labeled "A" and "B". The affinity of water molecules for regions "A" and "B" is expected to be quite different.

should be a positive correlation between the number density of cyanurate rings and moisture uptake in cyanate esters. In Figure 3, the moisture uptake data (plotted as the number density of water molecules in the saturated system) is plotted as a function of the number density of cyanurate rings, based on the molar volume of the system and the extent of cure determined *via* the diBenedetto equation.[29] A strong positive correlation was indeed observed, as is evident by comparison with a similar plot (Figure 4) showing moisture uptake as a function of total molar free volume. There was, however, a notable outlier, a SiMCy / LECy co-network with anomalously low moisture uptake behavior that was reproduced in two subsequent, independent tests. As discussed later, such anomalous behavior was a characteristic of the SiMCy / LECy co-
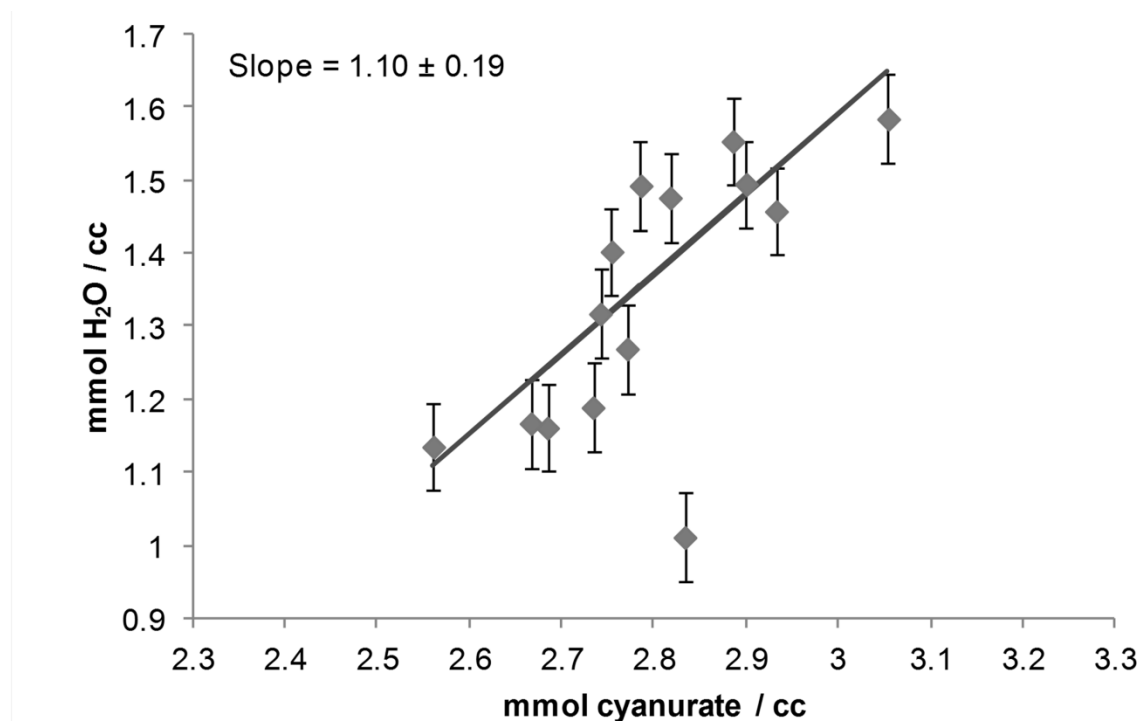
Figure 3. Water uptake as a function of cyanurate ring concentration in cyanate ester co-networks. Note that the ring density specifically takes into account the extent of cure, and the fitted regression line excludes the single outlying data point (50 wt% LECy, 50 wt% SiMCy, outlying value successfully replicated in two additional tests).

networks in particular, but this specific effect was perhaps the most technologically significant among all those that were discovered.

It should be noted that the hypothesis discussed above appears to be at least approximately true for a number of different cyanate esters. Such external validation is important because, considering only the co-cured network data, a number of properties may correlate with moisture uptake due to confounding with compositional variation. In systems with a modestly lower cyanurate ring density, such as the trifluoromethyl analog of BADCy and ortho-methylated BADCy, moderately lower moisture uptake (1.8 wt% and 1.4 wt%,
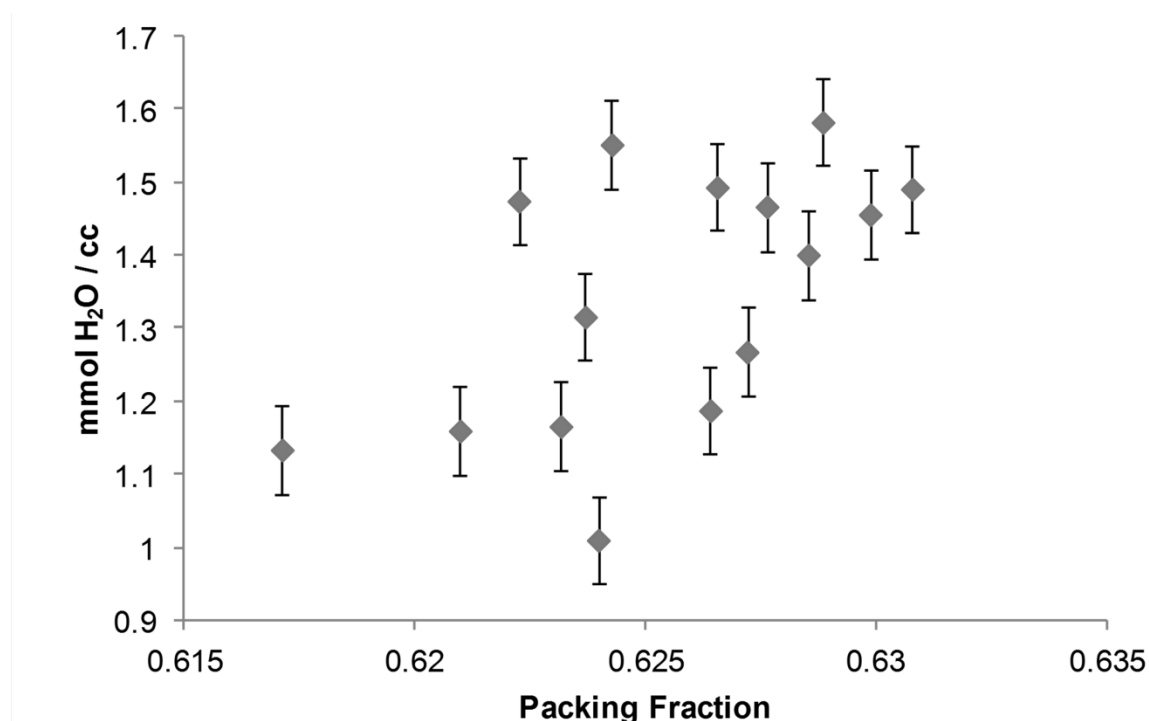
Figure 4. Water uptake as a function of packing fraction at 20 °C in cyanate ester co-networks.

respectively)[1, 24] has been observed, while systems with considerably lower cyanurate ring density, such as the dicyclopentadiene-containing dicyanates (1.2 wt%)[1] and the bisphenol M analog of BADCy (0.6 wt%)[1] have shown considerably lower water uptake. On the other hand, systems with a higher cyanurate ring density, such as the experimental monomers REX371 (3.8 wt%)[1] and ESR255 (2.8 wt%)[24] have exhibited higher water uptake values. (Quantitative comparisons are difficult due to a lack of data on the extent of cure and as-cured density of these previously reported systems.)

Both the three-component co-network data reported herein and the aforementioned data on similar compounds all indicate a higher sensitivity of moisture uptake to cyanurate ring density than would be expected based on a simple model wherein the density of favorable sites

11

for moisture uptake is simply proportional to the density of cyanurate rings. For instance, a 10% decrease in cyanurate ring density in SiMCy (compared to BADCy) leads to a 25% decrease in moisture uptake, while a 30% decrease in cyanurate ring density in the Bisphenol M analog leads to a 75% decrease in moisture uptake. The high sensitivity to cyanurate ring density may be due to the need for multiple cyanurate rings in close proximity to create favorable sites for moisture uptake, either because interacting or closely spaced cyanurate groups are needed to create a sufficiently hydrophilic environment, or perhaps because flexible linkages between cyanurate rings lessen the amount of free volume created during the post-gel stage of cure. Additional studies of free volume formation and moisture uptake as a function of conversion may provide clarification.

Finally, the idea that free volume formed during vitreous cure of thermosetting polymers may be an especially important determinant of moisture uptake has important implications for the design of thermosetting polymers with both a high glass transition temperature (which is generally aided by high densities of both hydrophilic groups that strongly interact with one another as well as high cross-link densities) and low moisture uptake. In particular, a thermosetting polymer designed to include hydrophilic groups that are shielded and/or located away from cross-linking sites (as in polybenzoxazines) may be well-suited to both high glass transition temperatures and low moisture uptake, as has been observed. [30, 31] On the other hand, hydrophobic groups, if placed in rigid groups in positions away from hydrophilic cross-linking sites, may decrease moisture uptake less than expected.

Density and packing. Figure 5 shows the individually measured density values as well as the smoothed density data at full conversion (grid) as a function of composition. From Table 1 and Figure 5 it can be seen that SiMCy forms the network with the lowest density of all three
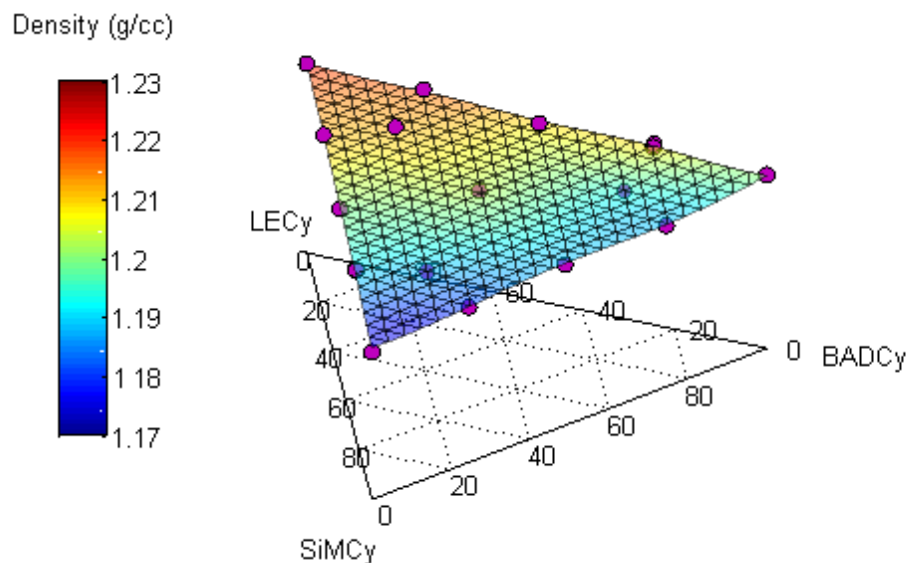
Figure 5. Density at 20 °C as a function of composition. The dark circles indicate individual measurements, while the grid indicates the calculated values of the smoothed data at full cure, thereby highlighting the effect of composition.

studied, with LECy exhibiting the highest density. The reported values for the pure components are similar to previously reported values[1, 25] when the effects of catalyst and the extent of cure are considered. Regression analysis indicated a statistically significant effect (p = 0.03) of the extent of cure on density, with a decrease in density of about 0.014 g/cm^3 for every 10% increase in the extent of cure, similar to the levels observed by Georjon and Galy for BADCy (at conversions of 0.85 to 1.00).[18] Thus, the data indicates that even for more flexible network segments, the formation of cyanurate rings at high conversions leads to the creation of additional free volume. The free volume associated with cyanurate ring formation was calculated on a molar basis for the different compositions studied, and found to be 34 – 40 cc/mol, with an uncertainty of approx. 15 cc/mol. Based on the slope of the line in Figure 3, roughly one additional mole of water uptake occurs for each additional mole of cyanurate rings formed at

high conversion in these systems. Thus, about half of the free volume created by cyanurate ring formation at late stages of cure appeared to be occupied by water under saturated conditions. These data clearly indicate that free volume associated with cyanurate ring formation is likely to be a far greater influence on system properties than the comparatively small differences (2-3 cc/mol) due to packing of the network segments.

The three monomers studied each exhibited subtle differences in packing fraction. Using the van der Waals volume calculated from the Bicerano correlation,[32] the packing fractions at 20 °C were determined for all blend compositions. Extrapolated values at 0 K and the cure temperature (210 °C) were also calculated, and the results are tabulated in Supporting Information. LECy exhibited the highest packing fraction in all cases, with the difference being largest (about 0.007) at 0 K. SiMCy, on the other hand, showed the lowest packing fraction at room temperature and above, but exhibited an almost identical packing fraction to BADCy when extrapolated to 0 K. Thus, intrinsically better packing was seen in LECy, while the looser packing seen in SiMCy was associated with a greater coefficient of thermal expansion, which is perhaps traceable to the generally lower dissociation energy of silicon-carbon bonds[33] (thereby rendering the bond length more sensitive to thermal fluctuations).

Additional physical properties. Figures 6 displays the individual and smoothed linear coefficient of thermal expansion data for the fully cured networks obtained by TMA after multiple heating cycles, while Figure 7 illustrates the deviation of the smoothed data from linearity. The coefficient of thermal expansion for SiMCy is quite a bit larger than that of LECy, which is slightly greater than that of BADCy. Measurements of the "as-cured" samples revealed
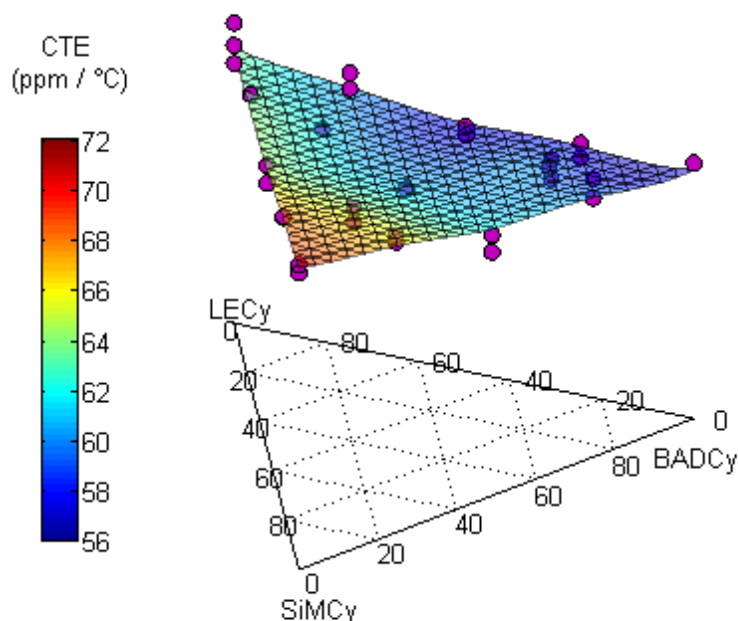
Figure 6. Linear coefficient of thermal expansion (measured on fully cured samples) as a function of composition (note there are two measurements per sample). The dark circles indicate individual measurements, while the grid indicates the calculated values of the smoothed data, thereby highlighting the effect of composition.

a statistically significant effect due to the extent of cure, with about a 3 ppm / °C decrease for every 10% increase in conversion. Although there did seem to be a reasonable negative correlation between the coefficients of thermal expansion and the glass transition temperatures of the fully cured networks (Figure 8), the differences in thermal expansion were much greater than expected from relationships (such as the one proposed by Seitz[34] for polymers) based on T_g values. The systematic deviations shown in Figure 7 clearly point to a lower than predicted (based on a linear rule of mixtures) coefficient of thermal expansion when network segments of
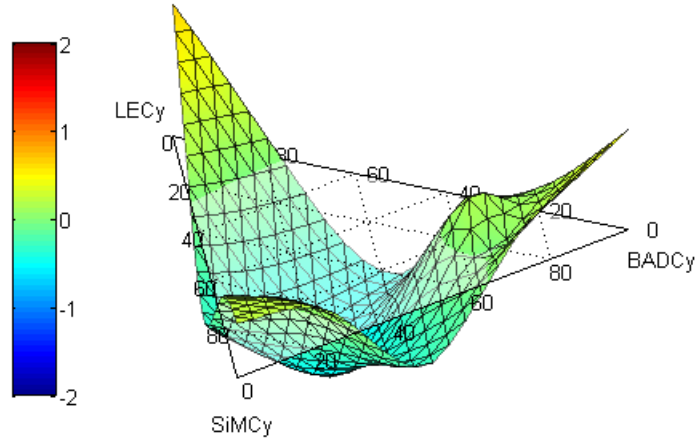
Figure 7. The smoothed deviation from predicted values based on a robust linear regression for the linear coefficient of thermal expansion (in units of Studentized residuals, measured on fully cured samples) as a function of composition. The data treatment is designed to reveal the nonlinear effects of composition, and shows systematically low values for all multi-component samples.

more than one type are co-cured. This result is a good example of a non-linearity that does not indicate component specific interactions, and is expected based on a very simple model for thermal expansion that assumes equal displacement of interpenetrating network segments (see Supporting Information), provided there is a difference in the bulk modulus of the component networks segments, and that increased bulk modulus correlates with decreased thermal expansion (as is typical). The formula for a ternary co-network is:

$$\alpha_{eff} = \frac{\alpha_1 \phi_1 K_1 + \alpha_2 \phi_2 K_2 + \alpha_3 \phi_3 K_3}{\phi_1 K_1 + \phi_2 K_2 + \phi_3 K_3} \tag{1}$$

in which α_{eff} is the effective linear coefficient of thermal expansion, and α_i, ϕ_i, and K_i refer to the linear coefficient of thermal expansion, volume fraction, and bulk elastic modulus of the ith
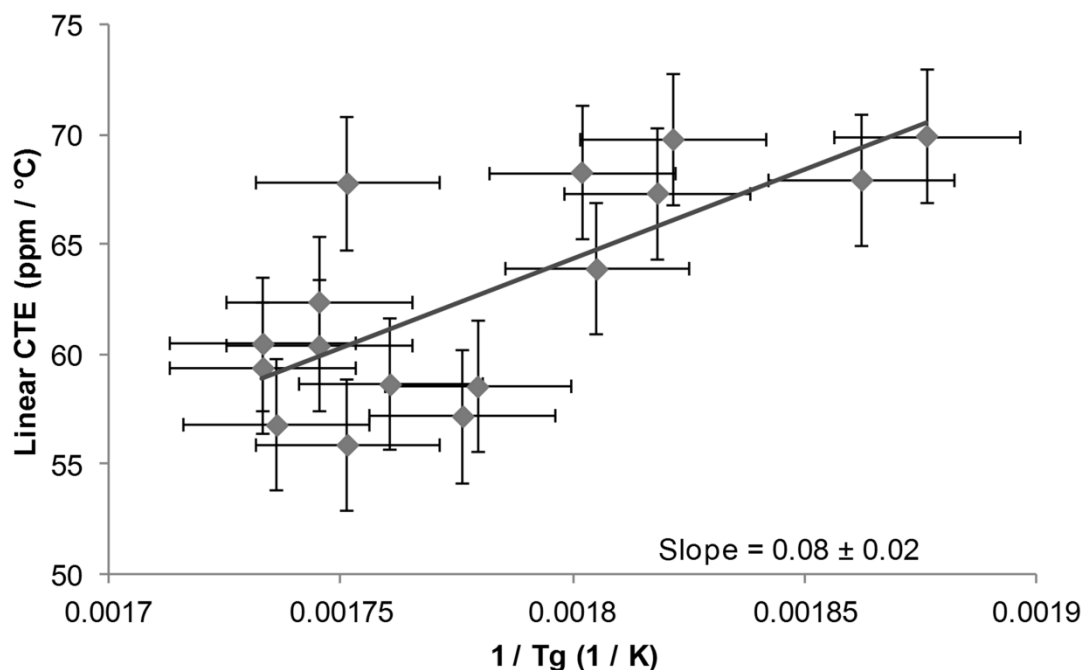
Figure 8. Linear coefficient of thermal expansion of fully cured co-networks as a function of the inverse of the fully cured glass transition temperature.

component, respectively. Using the data for fully cured samples, it was possible to extract a rough estimate of the bulk modulus ratios involved, with the result that the modulus of LECy segments was 10 - 40% that of BADCy segments and the modulus of SiMCy segments was 20-40% that of BADCy segments. These ratios, while qualitatively matching expectations based on the molecular structure of the segments, seem quantitatively too small. More sophisticated models that take into account both shear and bulk moduli, which have generated useful predictions for cyanate ester nanocomposites,[35] may thus be needed.

A similar non-specific interaction among components can be seen in thermochemical stability properties, as shown in Figures 9 and 10. In Figure 9, the maximum decomposition rate under nitrogen is plotted (rates under air were quite similar, see Supporting Information) as
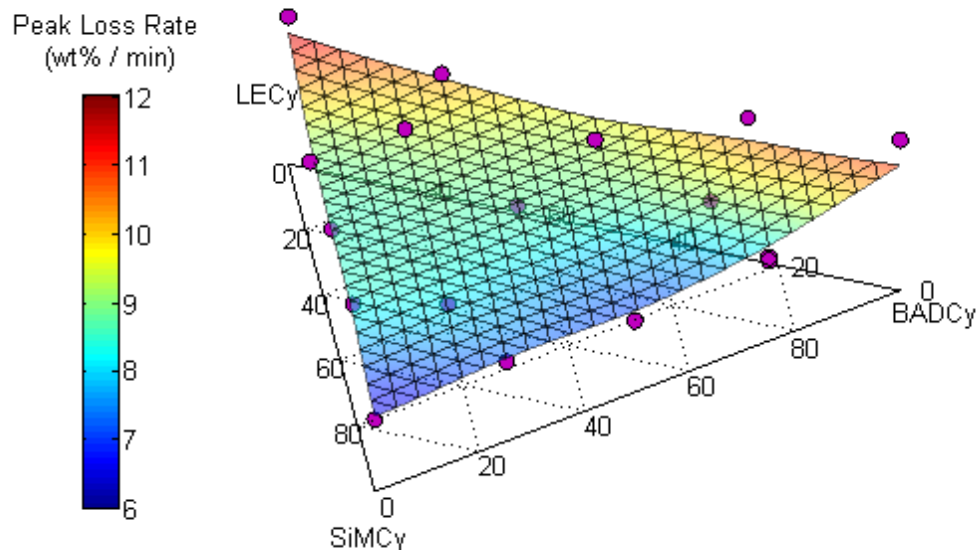
Figure 9. Maximum decomposition rate (under N_2) as a function of composition. The dark circles indicate individual measurements, while the grid indicates the calculated values of the smoothed data, thereby highlighting the effect of composition.

individual and smoothed data. Figure 10 illustrates the deviation from a weight fraction-based linear rule of mixtures. The multi-component networks all show a fairly marked negative deviation in maximum loss rate, presumably because the chemically more heterogeneous nature of the samples causes the thermal decomposition to unfold at slightly different times in different segments, leading to a broadening of the mass loss rate curve. (A similar effect is seen in the char yield data as well). This effect is in addition to the differences among the single-component networks, which can be seen in the individual TGA curves (Figure 11). It should be noted that, as previously observed,[25] SiMCy provided greater char yields than BADCy or LECy in air,

18
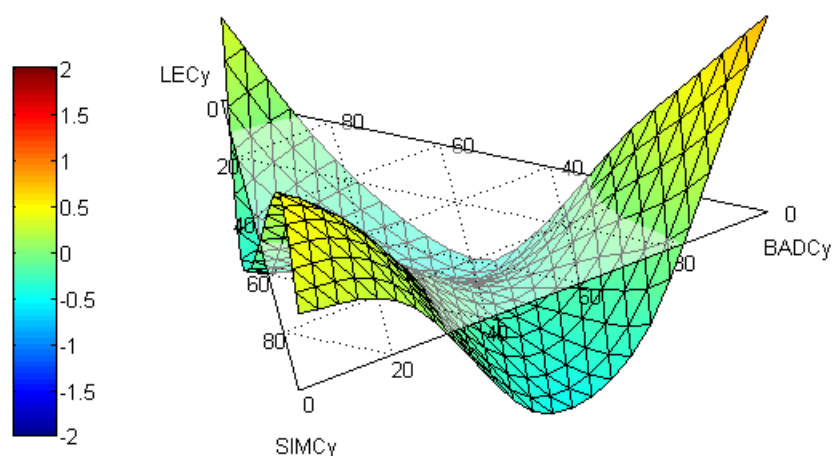
Figure 10. The smoothed deviation from predicted values based on a robust linear regression for the maximum decomposition rate under N_2 (in units of Studentized residuals) as a function of composition. The data treatment is designed to reveal the nonlinear effects of composition, and shows systematically low values for multi-component samples.

however it was also observed (see Supporting Information) that the char yield was greatest in co-networks containing around 25 wt% SiMCy segments and 75 wt% LECy segments.

In addition to analysis of individual variables, a *meta*-analysis of all of the variables and deviations from linearity was undertaken (see Supporting Information, Tables S2 and S3). The most important result was that in the majority of cases in which a significant deviation from linearity in the smoothed data was found based on the interaction of two components, the two components were SiMCy and LECy. Specific deviations for co-networks containing significant amounts of SiMCy and LECy included unusually low moisture uptake, high char yields in nitrogen and air, high decomposition onset temperature in air, low glass transition temperature at full cure, and increased packing fraction at O K. An example of data indicating such a component-specific interaction is shown in Figure 12, in which the deviation from the Gordon-
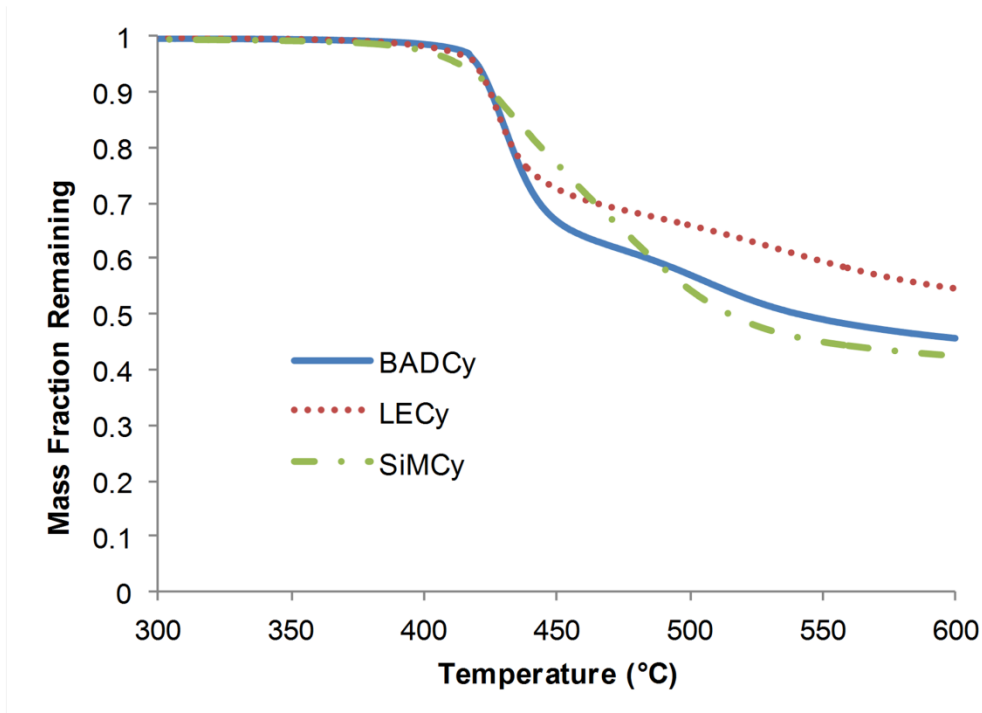
Figure 11. TGA curves of BADCy, LECy, and SiMCy single-component networks under nitrogen.

Taylor equation for the fully cured glass transition temperature of the network, found by DSC, is plotted. The same DSC scan detected no anomalies in the cure kinetics, and a separate TMA scan exhibited a similar negative deviation (though less clearly distinguished from random error) in the value of the fully cured T_g.

Thus, the interactions between SiMCy and LECy segments appear to be significantly greater than those between BADCy and LECy segments, or BADCy and SiMCy segments. Among the three components, segments made from LECy and SiMCy differed the most in terms of their molar volume, or, alternatively, their average distance between network junctions. The fact that SiMCy / LECy networks were more prone to deviations from simple rules of mixtures
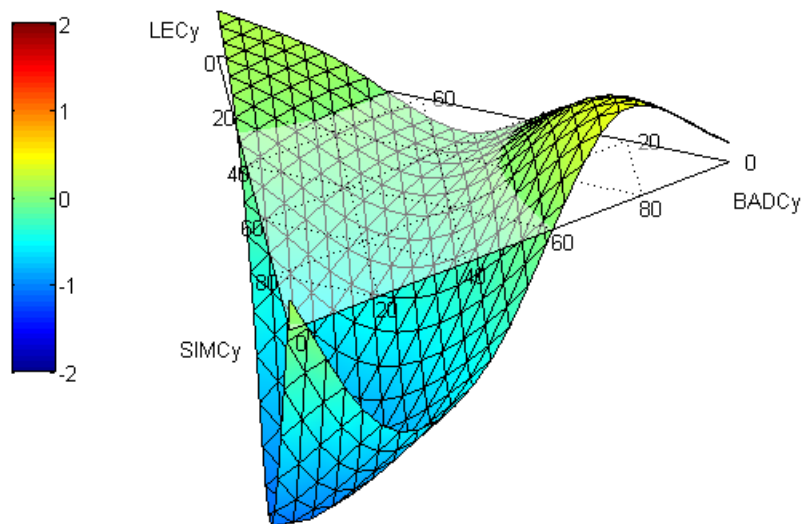
Figure 12. The smoothed deviation from the prediction of the Gordon-Taylor equation for the fully cured DSC glass transition temperature (in units of Studentized residuals) as a function of composition. The data treatment is designed to reveal the effects of interaction among components, and shows systematically low values for SiMCy / LECy co-networks.

in their physical properties therefore suggests that differences in segment size may be more readily exploited for the purpose of creating useful synergistic interactions in thermosetting polymer networks than, for instance, differences in symmetry (most prominent in BADCy / LECy and SiMCy / LECy networks), or in flexibility (most prominent in BADCy / SiMCy networks). Though such a hypothesis is speculative, it represents a good starting point for future investigations of synergistic interactions in highly cross-linked polymer networks. Skillful prediction of such synergism may enable significant technological advances in fields such as aerospace and microelectronics, for which the physical properties of such networks are of great importance.

Conclusions

Studies of three-component co-cured networks formed from similar dicyanate ester monomers have revealed a number of interesting and unexpected deviations from linear rules of mixtures for physical properties, thus confirming the importance of molecular level interactions among network segments. Among the most interesting results was an unexpected 25% reduction in moisture uptake for co-networks of equal amounts of LECy and SiMCy segments. For all other co-networks, a clear relationship between moisture uptake and the number density of cyanurate rings was observed. This relationship appears to hold generally for many types of cyanate esters. When combined with previously reported studies of density changes during cure, it is apparent that the net increase in free volume at room temperature associated with the final stages of cure provides favorable sites for moisture uptake, whereas increased free volume due to less efficient packing of network segments has, comparatively, very little influence on moisture uptake. In addition, a *meta*-analysis of all of the reproducible deviations from linear rules of mixtures for the physical properties of the co-cured networks was performed. The analysis showed that the majority of the deviations from linearity that appeared to be driven by interactions among components occurred in samples containing mixtures of SiMCy and LECy segments, suggesting that interactions between segments that differ substantially in molar volume may be useful for generating synergies in the physical properties of highly cross-linked polymer networks.

Experimental

Materials.

2,2'-Bis(4-cyanatophenyl)propane (the dicyanate ester of Bisphenol A, or BADCy), and 1,1'-bis(4-cyanatophenyl)ethane (the dicyanate ester of Bisphenol E, or LECy) were purchased from Lonza and used as received. Nonylphenol (technical grade) was purchased from Aldrich, and Copper (II) acetylacetonate was purchased from ROC/RIC; both were used as received. Bis(4-cyanatophenyl)dimethylsilane (SiMCy) was synthesized based on the procedure first reported by Wright[36] and later elaborated by Guenthner et al.[25] A typical synthesis was as follows.

General Synthetic Methods. All manipulations of compounds and solvents were carried out using standard Schlenk line techniques. Tetrahydrofuran (THF), ether, hexane and toluene were dried by passage through columns of activated alumina under a nitrogen atmosphere and then degassed prior to use. Dichlorodimethylsilane and triethylamine were purchased from Aldrich Chemical Co. and were distilled before use. 4-(Benzyloxy)bromobenzene was obtained from Aldrich and recrystallized from acetone before use. Cyanogen bromide, n-butyllithium, and 10% palladium on carbon (wet, Degussa type) were obtained from Aldrich Chemical Co. and used as received. ^{1}H, ^{13}C and ^{29}Si NMR measurements were performed using a Bruker AC 300 or Bruker 400 MHz instrument. ^{1}H and ^{13}C NMR chemical shifts are reported relative to the deuterated solvent peak (^{1}H, ^{13}C: acetone-d6, δ 2.05 ppm, δ 29.9 ppm). ^{29}Si NMR chemical shifts are reported relative to external tetramethylsilane at 0 ppm. Hydrogenation was done using a Parr Hydrogenator equipped with pressure safe vessels and viton seals. Samples were run on a TA Instruments Q2000 Differential Scanning Calorimeter (DSC) under nitrogen flowing at 50 mL/ min, with 5 minutes for equilibration at the maximum and minimum temperatures, to establish the melting point from a consistent thermal condition. Elemental

analyses were performed on Perkin Elmer EA2400 Series II combustion analyzer. Syntheses are modified from the reported literature.

Preparation of bis(4-benzyloxyphenyl)dimethylsilane (1). A chilled (-78 °C) THF (400 mL) solution of 4-(benzyloxy)bromobenzene (20.00 g, 76.0 mmol was treated with 2.2M n-BuLi (34.6 mL, 76 mmol) and allowed to react with stirring for 1 h at -78 °C. This mixture, now heterogeneous, was treated with slow addition of dichlorodimethylsilane (4.90 mL, 40 mmol, diluted with THF) and the cooling bath removed. The mixture was allowed to react with stirring for an additional 2 hr and then diluted with ether (600 mL) and stirred for 10-15 min. The organic layer was washed with water (2 X 200 mL) and brine (200 mL) and then dried over MgSO$_4$, stirring for ½ hr. The mixture was filtered, and the solvents were removed under reduced pressure on a rotary evaporator. The crude product was re-dissolved in a minimum amount of chloroform and precipitated into methanol (400 mL). This was stirred overnight, filtered and dried under nitrogen to afford **1** as a white solid (14.1 g, 87% yield). ^{1}H NMR (acetone-d6) δ: 7.48 -7.01 (m, 18), 5.12 (s, 4 H), 0.49 (s, 6 H). ^{13}C NMR (acetone-d6) δ: 160.75 (C1), 138.39 (C6), 136.43 (C3), 130.40 (C4), 129.34 (C7), 128.67 (C9), 128.67 (C8), 115.36 (C2), 70.21 (C5), -1.88 (SiCH$_3$). ^{29}Si NMR (acetone-d6) δ: -9.26. Anal. Calcd for C$_{28}$H$_{28}$O$_2$Si: C, 79.20; H, 6.65; N, 0.00. Found: C, 78.77; H, 6.75; N, 0.01
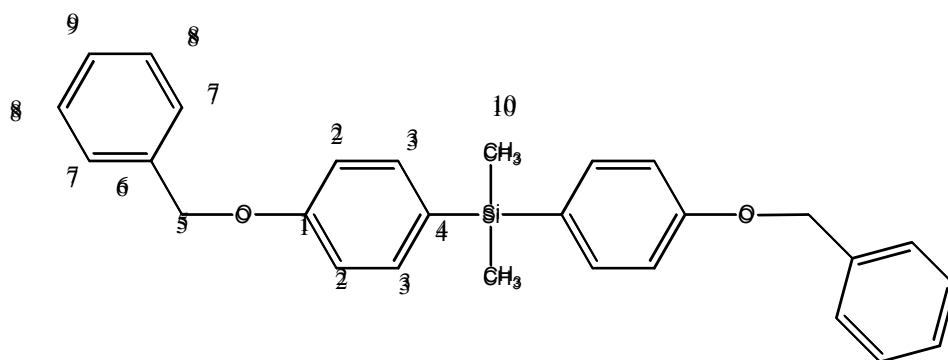

Preparation of bis(4-hydroxyphenyl)dimethylsilane (2). A THF (200 mL) solution containing 1 (10.00 g, 23.55 mmol) and 10 wt % palladium on carbon (600 mg), was placed in a 1000 mL

pressure safe vessel equipped with viton seals and connected to a hydrogenator. This was placed under an atmosphere of hydrogen (35 psi) and allowed to react with stirring for 24 hr. The catalyst was removed by filtration through celite, and the solvent was removed under reduced pressure to afford 4.80 g (83 % yield) of **2** as an off-white solid. For purification, compound **2** was washed twice with dry hexane, dried and then stirred overnight in dry toluene, and filtered. The white product was then dried under dynamic vacuum. ^{1}H NMR (acetone-d6) δ: 8.40 (s, 2H), 7.38-6.84 (dd, 8 H), 0.46 (s, 6 H). ^{13}C NMR (acetone-d6) δ: 159.70 (C1), 136.49 (C3), 128.89 (C4), 115.92 (C2), -1.65 (SiCH$_3$). ^{29}Si NMR (acetone-d6) δ: -9.59. Anal. Calcd. for C$_{14}$H$_{16}$O$_2$Si: C, 68.81; H, 6.60; N, 0.00. Found: C, 67.67;H, 6.75; N, 0.01.
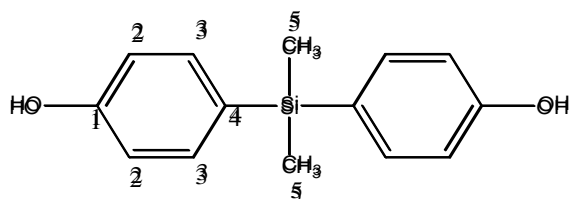
Preparation of bis(4-cyanatophenyl)dimethylsilane (3). A chilled (-20 °C) ether (50 mL) solution containing bis(4-hydroxyphenyl)dimethylsilane, **2**, (3.75 g, 15.4 mmol) and cyanogen bromide (4.05 g, 38.2 mmol) was treated with triethylamine (3.90 g, 38.5 mmol) in a dropwise manner. This mixture was allowed to react for 2 hr with stirring at -20 °C. The mixture was filtered to remove the hydrobromide salt, and the organic layer was washed with (2 X 100 mL) DI water, followed by a brine wash and then dried over MgSO$_4$. The solvents were removed under reduced pressure, and crude product (3.79 g, 84 % yield) was recrystallized from ether to afford 2.7 g (60 % yield) of 3 as white crystalline solid (mp 60.17 °C). ^{1}H NMR (acetone-d6) δ: 7.76- 7.40 (dd, 8H), 0.6 (s, 6H). ^{13}C NMR (acetone-d6) δ: 158.02(C1), 137.87 (C4), 137.59 (C3), 115.73 (C2), 109.52(OCN), -2.47 (SiCH$_3$).). ^{29}Si NMR (acetone-d6) δ: -7.08. Anal. Calcd for C$_{16}$H$_{14}$N$_2$O$_2$Si: C, 65.28; H, 4.79; N, 9.52. Found: C, 65.17; H, 4.83; N, 9.45.
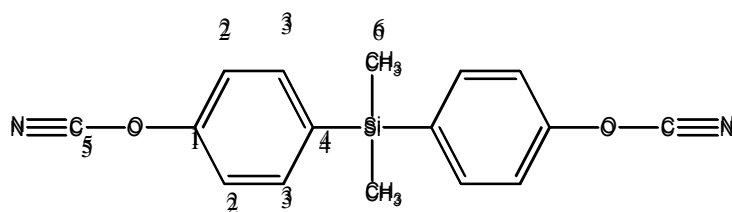
Design of Experiments

Compositions for analysis were chosen based on an experimental design that roughly followed a Simplex lattice for 16 samples with 3 components. The design featured equally spaced binary co-networks with a mass fraction difference of 0.25 (accounting for 12 points), along with four ternary co-networks, three in which each of the three components comprised a substantial majority and one at the compositional centroid (equal mass of all components). This design afforded slightly more data for the ternary co-networks than an equally spaced design would have provided, allowing for distinctions to be drawn between systems for which one component dominates versus the case where no component dominates. The difference of 0.25 in mass fraction for binary co-networks was taken as sufficiently small to reliably capture any systematic trends, while minimizing the number of data points required. At least one additional composition was chosen as a replicate for each type of experiment conducted. In addition, all significant outliers were subjected to replication in order to better understand their anomalous nature.

Sample Fabrication

Batches of catalyst comprised of 30 parts by weight nonylphenol to one part by weight copper (II) acetylacetonate were prepared by mixing the ingredients in a vial and heating to 60 °C, while stirring vigorously until complete dissolution took place (typically one to two hours). These batches were retained for up to 30 days. Due to the low humidity ambient environment, the only precautions taken when storing the Primaset® BADCy and LECy resins were the use of tightly sealed containers and avoidance of exposure to high humidity environments. However,

for the novel material SiMCy, for which the stability data are unknown, the sample was stored at or below 4 °C as an added precaution.

Uncured samples for Differential Scanning Calorimetry (DSC) analysis were prepared by mixing prescribed ratios of the three monomers with 2.0 parts per hundred by weight of catalyst at 95 °C. The mixture was then partially de-gassed at 95 °C for 30 minutes under reduced pressure (300 mm Hg), and approx. 5 mg was transferred to a DSC pan. To prepare cured samples, silicone molds made from R2364A silicone from Silpak Inc. (mixed at 10:1 by weight with R2364B platinum-based curing agent and cured overnight at room temperature, followed by post-cure at 150 °C for 1 hour) were prepared by de-gassing for 60 minutes at 95 °C and 300 mm Hg. The uncured cyanate ester mixture was mixed and de-gassed using the method for preparing DSC samples described above, and then poured into the prepared mold (no release agent was used). The open mold and sample were then placed under flowing nitrogen at 95 °C, ramped 5 °C/min to 150 °C and held for 1 hour , then ramped 5 °C/min to 210 °C and held for 24 hours to produce void-free discs measuring approximately 11.5-13.5 mm in diameter by 1-3 mm thick and weighing 200-400 mg. Multiple discs were used for oscillatory thermomechanical analysis (TMA), density measurements, and hot water exposure tests. In addition, small chips weighing approx. 5 mg were removed from the discs, crushed, and utilized for thermogravimetric analysis (TGA).

Characterization

DSC was performed on a TA Instruments Q2000 calorimeter under 50 mL/min. of flowing nitrogen. Uncured samples for heat of cyclotrimerization and cured glass transition temperature analysis were heated to 350 °C, then cooled to 100 °C, and re-heated to 350 °C, all at 10 °C/min. Uncured samples used for melting point determination were subjected to a program consisting of alternate heating and cooling steps at 5 °C/min. between 0 °C and 100 °C. For uncured samples used to determine the glass transition temperature prior to onset of cure, alternate heating and cooling ramps at 5 °C/min. between -70 °C and 0 °C were used. Finally,

when used to determine extent of cure for partly cured samples (for diBenedetto equation validity checks), uncured samples were heated to 200 °C at 5 °C/min, then cooled to 0 °C and re-heated to 350 °C, at 10 °C/min.

TGA was conducted on a TA Instruments Q5000 thermogravimetric analyzer under both nitrogen and air at a flow rate of 25 mL / min. by heating samples at 10 °C / min. to 600 °C. Oscillatory TMA was conducted with a TA Instruments Q400 series analyzer under 50 mL/min of nitrogen flow. The discs were held in place via a 0.2 N initial compressive force with the standard 5 mm diameter flat cylindrical probe while the probe force was modulated at 0.05 Hz over an amplitude of 0.1 N (with a mean compressive force of 0.1 N) and the temperature was ramped twice (heating and cooling) between 100 °C and 200 °C (to determine thermal lag) followed by heating to 350 °C, cooling to 100 °C, and re-heating to 350 °C , all at 10 °C/min. For samples previously exposed to hot water, the heating rate was increased to 20 °C/min and the thermal lag determination was performed after, rather than before, the first heating to 350 °C, in order to minimize drying before determination of the glass transition temperature. Details of the oscillatory TMA technique and the determination of thermal lag have been published elsewhere.[37] The oscillatory TMA experiments provided both coefficient of thermal expansion data as well as glass transition temperatures based on changes in the oscillatory response of the sample.

Densities were determined by placing sample discs in solutions of $CaCl_2$ (as the dihydrate) and deionized water and varying the $CaCl_2$ concentration until neutral buoyancy was observed on bubble-free samples over a period of several minutes at 20 °C. The density of the neutrally buoyant solution was determined by placing 10.00 mL in a volumetric flask (calibrated with deionized water at 20 °C) and weighing, and checked against the predicted density of the solution at ambient temperature based on the known concentration of $CaCl_2$. For hot water exposure testing, sample discs were placed in approximately 300 mL of deionized water at 85 °C for 96 hours, with sample weight measured before and after exposure. The exposed samples were then analyzed *via* oscillatory TMA to provide "wet" glass transition temperature data.

Analysis of Co-Network Data

From the numerous tests conducted, key response variables were analyzed as a function of several different compositional variables, with mass fraction being the default choice. Density and coefficient of thermal expansion data were analyzed as a function of volume fraction using the measured density values for single components to convert from mass fraction. Although slightly different estimates for the pure component densities were subsequently determined using the analysis methods described below, the effect on the previously calculated volume fractions was well within their experimental uncertainties, thus an iterative process of correction was judged unnecessary. Moisture uptake and heat of reaction data were analyzed on a mole fraction basis, while glass transition temperature values were analyzed on the adjusted weight fraction basis provided by the Gordon-Taylor equation, with the measured glass transition temperatures (*via* DSC) of the pure components at full cure used as the basis for conversion. As with the volume fraction, these values differ slightly from subsequent estimates, but the effect was sufficiently small that iteration was judged unnecessary.

For samples heated to 210 °C for 24 hours, the degree of conversion was determined using the diBenedetto equation, as follows. First, as part of the normal procedure for oscillatory TMA measurements, two measurements of the glass transition temperature were performed on the first and second heating to 350 °C. Trials of different heating rates (reported in detail elsewhere)[38] confirmed that the heating rates used were sufficiently rapid to avoid significant in-situ cure and to capture the "as-cured" glass transition temperature on the first heating. The glass transition temperature measured on the second heating (after exposure to 350 °C) was then taken as the "fully cured" glass transition temperature. The fully cured glass transition temperature obtained *via* oscillatory TMA was then compared to the fully cured glass transition temperature obtained *via* DSC after heating to 350 °C. The oscillatory TMA values were found to be 4 ± 9 °C higher than the DSC values on average.

Since the difference was not statistically significant (it was similar to the value of the random error in the TMA glass transition temperature measurements), the two measurements were considered similar enough that the glass transition temperatures of the uncured resin (obtainable only by DSC) were used without modification in the diBenedetto equation, along with the as-cured and fully cured glass transition temperature values obtained by TMA. Based on measurements of partly cured samples, a value of 0.37 was estimated and subsequently used for the parameter λ in the diBenedetto equation. The uncertainty in λ was relatively large, at about 0.1, however, changes in the value of λ did not affect the significance of conversion as a regression variable, only the value of the regression coefficient. Moreover, the standard errors of these regression coefficients were 25-50% of their respective values, hence a relative error of 25% in λ produced only a marginal increase in the uncertainty associated with the regression coefficient.

Using the appropriate measure of composition and, where appropriate, the degree of conversion, as independent variables, the key experimental parameters (31 in total) were analyzed *via* robust regression, using a bisquare weighting function and an iterative weighting algorithm available in MATLAB and described in detail in the references listed in the program.[39-42] For iteration, the default weighting parameter of 4.655 was utilized. Given the large numbers of data points analyzed, the likelihood of encountering apparent outliers due to random variation was quite high. The use of the robust regression, which assigned lower weight to the outliers, but did not ignore them, was considered the most appropriate method for dealing with these outliers. In cases where the degree of cure was not significant at the 90% confidence level, it was excluded as an independent variable for further analysis.

For each regression, the (external) Studentized residuals were analyzed in multiple ways. In addition to visual examination of the normal distribution plot and a plot of residuals versus predicted value, the residuals were analyzed for any systematic deviations as a function of composition. Systematic deviations were identified by smoothing the Studentized residuals using a Gaussian blur (treating the two independent compositional variables as plotted on a

triangular ternary diagram) with a characteristic radius of 0.25. The smoothed data was then plotted on a ternary diagram and inspected for discernible patterns. (All plots are provided in Supporting Information, and were generated using the MATLAB routine "ternplot.m" written by Carl Sandrock.) Utilizing a few sets of pseudo-random numbers generated by Microsoft Excel in place of the dependent variable, it was observed that the smoothing procedure resulted in smoothed Studentized residuals with a standard deviation of around 0.3, with absolute values exceeding 0.5 in only about 10% of cases. We thus used an absolute value of 0.5 as a rough cut-off value for assessing the significance of the smoothed residuals. In particular, when such a residual was encountered, the values of neighboring residuals were examined. Since very large single outliers can substantially influence their neighbors in the smoothed data, we also examined the unsmoothed Studentized residuals of neighboring points. These cases, along with a diagram identifying all "neighboring" compositional points, are discussed in detail in the Supporting Information.

The final result of these procedures was a set of identified deviations from linearity, for which a *meta*-analysis was undertaken. The deviations were classified according to three types: deviations in unsmoothed data (absolute value of t > 2), isolated deviations in smoothed data (absolute value of t > 0.5), and deviations in smooth data comprising a cluster of neighboring points. The deviations were then tabulated based on their numbers, and sub-totaled based on the corresponding network compositions (with tables provided in Supporting Information). It was found that all of the clusters of significant deviation in the smoothed data contained at least 50% of the components SiMCy or LECy, with the majority of these clusters containing co-networks composed primarily of SiMCy and LECy. Similar, but less dramatic, trends were seen for the other categories of deviations, with deviations being most common in SiMCy-rich co-networks, and in co-networks with at least 50% SiMCy or LECy.

Supporting Information Available

Sections S1.1 – S1.31 (results and discussion on a variable-by-variable basis), Tables S1-S3, Figures S1.1-S1.31, S2.1-S2.31, and S3.1-S3.31 (normal probability, residual, and smoothed residual plots for all variables, respectively), and Section S2 (derivation of CTE model) are available as Supporting Information. This content is available free of charge on the Internet at http://pubs.acs.org.

References

1. Hamerton, I., Ed., *Chemistry and Technology of Cyanate Ester Resins*. Chapman & Hall: London, 1994.

2. Nair, C. P. R.; Mathew, D.; Ninan, K. N. "Cyanate ester resins, recent developments" in *New Polymerization Techniques and Synthetic Methodologies*, 2001; Vol. 155, pp 1-99.

3. Fang, T.; Shimp, D. A., Polycyanate Esters -- Science and Applications. *Prog. Polym. Sci.* **1995,** *20*, 61-118.

4. Hamerton, I.; Hay, J. N.. *High Performance Polymers* **1998,** *10*, 163-174.

5. McConnell, V. P., Resins for the Hot Zone Part II: BMIs, CEs, Benzoxazines & Phthalonitriles. *High Performance Composites* September 2009, pp 43-49.

6. Chao, F.; Bowler, N.; Tan, X. L.; Liang, G. Z.; Kessler, M. R. *Composites Part A* **2009,** *40*, 1266-1271.

7.   Buckley, L. J.; Snow, A. W.,. *Abstr. Pap. Am. Chem. Soc.* **1996,** *211*, 37-POLY.

8.   Savary, F.; Bonito-Oliva, A.; Gallix, R.; Knaster, J.; Koizumi, N.; Mitchell, N.; Nakajima, H.; Okuno, K.; Sborchia, C., *IEEE Trans. Appl. Supercond.* **2010,** *20* (3), 381-384.

9.   Esslinger, J. R., Jr.; Fruchtnicht, O. C. *SAMPE J.* **2004,** *40*, 9-15.

10.   Das, S.; Castelli, L. M.; Falchetto, A. In "Novel use of cyanate esters: VARTM, filament winding and pultrusion", SAMPE Conf. Proc., Society for the Advancement of Material and Process Engineering: 2004; pp 1895-1904.

11.   He, S. B.; Liang, G. Z.; Yan, H. X.; Wang, J. H.; Yang, L. L.,. *Polymers for Advanced Technologies* **2009,** *20*, 143-146.

12.   Abali, F.; Shivakumar, K.; Hamidi, N.; Sadler, R.. *Carbon* **2003,** *41*, 893-901.

13.   Yameen, B.; Duran, H.; Best, A.; Jonas, U.; Steinhart, M.; Knoll, W. *Macromol. Chem. Phys.* **2008,** *209*, 1673-1685.

14.   Fyfe, C. A.; Niu, J.; Rettig, S. J.; Burlinson, N. E.; Reidsema, C. M.; Wang, D. W.; Poliks, M. *Macromolecules* **1992,** *25*, 6289-6301.

15.   Gupta, A. M.; Macosko, C. W.. *Macromolecules* **1993,** *26*, 2455-2463.

16.   Wienhold, P. D.; Persons, D. F. *SAMPE J.* **2003,** *39* (6), 6-17.

17.   Kasehagen, L. J.; Macosko, C. W. *Polym. Int.* **1997,** *44*, 237-247.

18.   Georjon, O.; Galy, J. *Polymer* **1998,** *39*, 339-345.

19.   Georjon, O.; Galy, J. *J. Appl. Polym. Sci.* **1997,** *65*, 2471-2479.

20.   Koh, H. C. Y.; Dai, J.; Tan, E. *J. Appl. Polym. Sci.* **2006,** *102*, 4284-4290.

21.   Goertzen, W. K.; Kessler, M. R. *Composites Part A* **2007,** *38*, 779-784.

22.   Hamerton, I.; Howlin, B. J.; Klewpatinond, P.; Takeda, S. *Macromolecules,* **2009,** *42*, 7718-7735.

23.   Hwang, H. J.; Li, C. H.; Wang, C. S. *J. Appl. Polym. Sci.* **2005,** *96*, 2079-2089.

24.   Shimp, D. A.; Ising, S. J.; Christenson, J. R., "Cyanate Esters -- A New Family of High Temperature Thermosetting Resins" in *High Temperature Polymers and Their Uses*, Society of Plastics Engineers: Cleveland, OH, 1989; pp 127-140.

25.   Guenthner, A. J.; Yandek, G. R.; Wright, M. E.; Petteys, B. J.; Quintana, R.; Connor, D.; Gilardi, R. D.; Marchant, D. *Macromolecules* **2006,** *39*, 6046-6053.

26.   Shimp, D. A.; Craig, W. M. "New Liquid Dicyanate Monomer for Rapid Impregnation of Reinforcing Fibers" in *34th International SAMPE Symposium*, SAMPE International: 1989; pp 1336-1346.

27.   Snow, A. W.; Armistead, J. P. *Naval Research Laboratory Memorandum Report 6848*; Naval Research Laboratory: Washington, DC, 1991.

28.   Shimp, D. A.; Ising, S. J. in *35th International SAMPE Symposium*, SAMPE International: 1990; p 1045.

29.   Pascault, J. P.; Williams, R. J. J. *J. Polym. Sci., Part B: Polym. Phys.* **1990,** *28*, 85-95.

30.   Ishida, H.; Allen, D. J. *J. Polym. Sci., Part B: Polym. Phys.* **1996,** *34*, 1019-1030.

31.   Shieh, J.-Y.; Lin, C.-Y.; Huang, C.-L.; Wang, C.-S. *J. Appl. Polym. Sci.* **2006,** *101*, 342-347.

32.   Bicerano, J., *Prediction of Polymer Properties*. 3rd ed.; Marcel Dekker, Inc.: New York, 2002; p 756.

33.   Lide, D. R., *CRC Handbook of Chemistry and Physics*. 82nd ed.; CRC Press: Boca Raton, 2001.

34.   Seitz, J. T. *J. Appl. Polym. Sci.* **1993,** *49*, 1331-1351.

35.   Badrinarayanan, P.; Kessler, M. R. *Compos. Sci. Technol.* **2011,** *71*, 1385-1391.

36.   Wright, M. E., *Polymer Preprints* **2004,** *45 (2)*, 294.

37.   Guenthner, A. J.; Yandek, G. R.; Mabry, J., M; Lamison, K. R.; Vij, V.; Davis, M. C.;
        Cambrea, L. R. "Insights into moisture uptake and processability from new cyanate ester
        monomer and blend studies" in *SAMPE International Technical Conference*, SAMPE
        International Business Office: Salt Lake City, UT, 2010; Vol. 55, pp 42ISTC-119.

38.   Guenthner, A. J.; Lamison, K. R.; Yandek, G. R.; Masurat, K. C.; Reams, J. T.; Cambrea,
        L. R.; Mabry, J. M. *Polymer Preprints* **2011,** *52(2)*, in press.

39.   duMouchel, W. H.; O'Brien, F. L. "Integrating a Robust Option into a Multiple
        Regression Computing Environment" in *Computer Science and Statistics: Proceedings
        of the 21st Symposium on the Interface,* Alexandria, VA, American Statistical
        Association: Alexandria, VA, 1989.

40.   Holland, P. W.; Welsch, R. E. *Communications in Statistics Part A-Theory and Methods*
        1977, *6*, 813-827.

41.   Huber, P. J., *Robust Statistics*. John Wiley & Sons: Hoboken, NJ, 1981.

42.   Street, J. O.; Carroll, R. J.; Ruppert, D. *American Statistician* **1988,** *42*, 152-154.

Table of Contents Graphic – for Table of Contents use only

Title: New Insights into Structure-Property Relationships in Thermosetting Polymers from Studies of Co-Cured Polycyanurate Networks

Authors: Andrew J. Guenthner, Kevin R. Lamison, Vandana Vij, Josiah T. Reams, Gregory R. Yandek, and Joseph M. Mabry
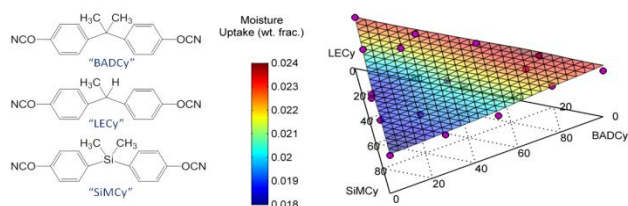
"New Insights into Structure-Property Relationships in Thermosetting Polymers from Studies of Polycyanurate Co-Networks"

Andrew J. Guenthner,[1]* Vandana Vij,[2] Kevin R. Lamison,[2] Josiah T. Reams,[3] Gregory R. Yandek,[1] and Joseph M. Mabry[1]

[1]Air Force Research Laboratory, Propulsion Directorate, Edwards AFB, CA 93524
[2]ERC Corporation, Edwards AFB, CA 93524
[3]National Research Council / Air Force Research Laboratory, Edwards AFB, CA 93524
*author correspondence: andrew.guenthner@edwards.af.mil

S1. Detailed Results of Robust Regression

Table S1 provides descriptive information about the variables analyzed. For convenience, each variable has also been assigned a numeric code and grouped by analysis technique in the order DSC, TGA (N_2), TGA (Air), TMA (Dry), TMA (Wet), density and derived data, and, finally, water uptake. Table S2 lists the regression coefficients (with significance categories indicated), standard error, quality of normal probability and residual plots, and notable outliers (in both smoothed and unsmoothed data) for each regression performed. Figures S1.1 – S1.31 and S2.1 – S2.31 are the associated normal probability plots and residual plots (using unsmoothed Studentized residuals) for all variables analyzed. Figures S3.1 – S3.31 show ternary composition diagrams with the smoothed Studentized residuals mapped by color. Generally, in the smoothed data colormaps, colors ranging from light blue (-0.5) to yellow (+0.5) are expected based on random variation. Negative deviations can be distinguished quickly from positive deviations by noting that the dashed gridlines are filled in only for regions with negative deviation. In addition to the numerous tables and graphs, the following text provides a summary of the key findings for each variable of interest, and, at the end of each section, there is an extended discussion of how the results for the different variables of interest relate to one another.

DSC Data

S1.1 Melting Point (variable 1). Only 7 of the 16 compositions produced DSC scans with a measurable melting point, which was always in excess of 45 °C, thus great caution is required in interpreting the data. The predicted melting point of BADCy (79 ± 3 °C) agrees well with the known value (79 °C)[S1] and the extrapolated melting point of LECy (36 ± 10 °C) also is close to the reported value of 29 °C.[S1] Interestingly, the regression predicts a value of 34 ± 3 °C for the melting point of SiMCy, which is about 20 °C too low, even though all six other observed melting points are predicted to within 1.5 °C by the regression. The two possibilities are: 1) the agreement for all measured samples but pure SiMCy is a fortuitous chance, and 2) differences in crystal ordering between pure SiMCy and its monomer blends affect the melting point. The regression predicts a melting point of about 55 °C for the 50/50 BADCy / SiMCy blend, however, physical observation of the blends at elevated temperatures suggest the melting point is in fact lower (somewhere between room temperature and 40 °C), thus the predictions of the regression deviate significantly from reality for more than one composition, making the former possibility more likely. Other than the major deviation for pure SiMCy, the normal probability (Figure S1.1) and residual (Figure S2.1) plots for melting point appear typical. The smoothed Studentized residuals (Figure S3.1) are dominated by the SiMCy anomaly, and given the small number of data points, are otherwise not informative.

S1.2 Enthalpy of cure (variable 2). No significant trends were found. The average of all measurements was 86 kJ/mol, while the predicted value at the centroid of composition (equal mixture of components) was 87 ± 7 kJ/mol. The range of all values reported was 75 – 99 kJ/mol, with no unusual features in either the normal probability (Figure S1.2), residual (Figure S2.2), or smoothed residual (Figure S3.2) plots. Thus, all data was consistent with a set of 16

measurements having an average of 86 kJ/mol and a standard deviation of 7 kJ/mol. Both the average and standard deviation agreed with expectation based on previously reported DSC measurements of transition-metal catalyzed dicyanate esters (which tend to be a bit lower in cure enthalpy than the uncatalyzed value of ~100 kJ/mol).[S1] The results suggest that changes in the center of the monomer, remote from the terminal cyanate ester reactive groups, make little difference in the thermodynamics of the reaction, as expected.

S1.3 Peak Cure Temperature (variable 3). As with the enthalpy of cure, there were no significant trends, the data set was consistent with an average peak cure temperature of 202 °C and a standard deviation of about 7 °C. The normal probability plot (Figure S1.3) and residual plot (Figure S2.3) showed a single outlier at t (Studentized) = +2.66, but the smoothed residuals (Figure S3.3) showed no significant features. Also no other properties measured on the same batch were highly anomalous, thus the slightly larger than expected deviation was most likely simply due to random error. The results suggests that both the thermodynamics of cure and the main portion of the reaction kinetics of cure were unaffected by monomer composition (among those monomers studied). Comparisons of the DSC curves themselves did show a slightly earlier onset of cure for SiMCy as compared to BADCy and LECy, but this difference may reflect slight differences in sample purity.

S1.4 Post-cure T_g by DSC (variable 4). As mentioned briefly in the main body of the paper, the outstanding feature of the regression is a systematically low set of values for mixtures rich in SiMCy (though not for SiMCy itself). As can be seen from Table 1 in the main body of the paper, the predicted values for the pure components are similar to those found for fully cured samples measured by dynamic TMA. For all blend batches with both measurements available, the DSC value was on average just 4 °C cooler with a standard deviation of 9 °C in the

distribution of differences (the standard errors for the regressions were 6 °C for DSC and 9 °C for dynamic TMA measurements). Hence, no significant difference in results between the two techniques was found.

The normal probability (Figure S1.4) and residual (Figure S2.4) plots for the regression show two outliers, at t = -2.05 and t = -2.65, both for samples rich in SiMCy. These two samples were in fact the only two to show T_g values lower than any of the pure components. In contrast, all T_g values for BADCy / LECy co-networks fell in between the predicted pure component values (despite a difference of only 10 °C). For BADCy / SiMCy co-networks, despite a difference of 33 °C in T_g values, the co-networks had T_g values only 2 °C and 4 °C higher than the observed value for pure SiMCy at 25 wt% and 50 wt% BADCy, respectively. The SiMCy rich networks thus appear to have depressed T_g values, as indicated by the smoothed data (Figure S3.4, also shown in Fig. 12 in the main body of the paper).

Extended Discussion. Since both the DSC and fully cured dynamic TMA data sets gave similar T_g values, it would be expected that deviations associated with specific compositions would show up in both data sets, yet the T_g values determined from dynamic TMA of fully cured samples (variable 16) did not show the large deviations present in the DSC data. The dynamic TMA data did, however, show negative deviations (though smaller) for the two SiMCy / LECy co-networks mentioned above. The greater deviations seen in DSC data may reflect the lower standard error of the measurement, since the deviation itself is around -10 °C in most cases, which is close to t = -2 for DSC data but only t = -1 (i.e. hard to distinguish from random variation) in the dynamic TMA data. In addition, analysis of the dry TMA data yielded a T_g for pure SiMCy of 260 °C, as compared to 267 °C by DSC (the previously reported value was 265 °C). [S2] This difference would tend to accentuate the deviation in the DSC data while masking it

in the TMA data. Thus, when considered in more detail, there is in fact reasonable agreement as to the presence of these deviations between the two data sets.

As noted in the main body of the paper, other deviations, such as high density, lower water uptake, and better than expected thermal stability were also seen in similar compositions, though, interestingly, the largest deviations were found at different compositions in each case. The best instance of coincidence occurred for co-networks consisting of 75 wt% SiMCy and 25 wt % LECy, which showed a lower than normal (t = -2.05) T_g, higher than normal (t = +2.07) density, and insignificantly less than normal (t = -0.33) water uptake with thermo-chemical stability as expected (t = +0.04 for the decomposition rate in air). It should be noted that the other unusual sample according to DSC T_g (67 wt% SiMCy, 16 wt% BADCy, 16 wt% LECy) showed t-values of +0.76 for density, +0.57 for water uptake, and +0.21 for decomposition rate in air, thus exhibiting only a coincidence in statistically insignificant deviations.

TGA Data (Nitrogen)

S1.5 Onset of Decomposition in N_2 (variable 5). No significant trends were found. The 5% mass loss temperature under nitrogen was found to be 418 °C on average, with a standard deviation of just 2 °C. The normal probability (Figure S1.5) and residual (FigureS2.5) plots showed two outliers, at t = -2.95 and t = -2.23, for 25 wt% BADCy / 75 wt% LECy and pure SiMCy, respectively. However, given the very small standard error of the regression, the actual deviations amount to just 6 °C and 4 °C, respectively. The smoothed residuals (Figure S3.5) also show significant negative deviation among the BADCy / LECy co-networks, as well as for pure SiMCy. Again, though, the magnitude of these effects is very modest (the average deviations are only -4 to -5 °C), and the data for onset of decomposition in air (variable 11) shows only slight coincidence of deviations. Thus, the effect, if it exists, is too weak to analyze reliably.

S1.6 Primary Peak Mass Loss Rate under N$_2$ (variable 6). As is evident from Fig. 11 in the main body of the paper, the maximum weight loss rate (which can be inferred from the maximum slope of the mass loss curve) was significantly lower for SiMCy (at 6.1 ± 1.6 %/min.) than for LECy (10.9 ± 1.6%/min.), with BADCy having a predicted rate of 9.4 ± 1.6 %/min (the difference between SiMCy and BADCy was significant only at 94% confidence). With the data collected in air (see variable 12), a systematic negative deviation in peak decomposition rate was seen for the multi-component samples when compared to the prediction based on linear regression (see Figure S3.6). As discussed in the main body of the paper (see the discussion of Figure 10), this deviation is due to the non-coincidence of the component degradation peaks, resulting in a spreading out of the primary weight loss. Even though in terms of the absolute deviations seen in the smoothed data, the effect is marginal for most compositions, the coincidence of the effect in two separate data sets along with a highly plausible explanation leads to the conclusion that the features seen in Figure S3.6 are due to true compositional effects. The normal probability plot (Figure S1.6) shows some slight clustering, while the residual plot (Figure S2.6) looks as expected.

S1.7 Secondary Peak Mass Loss Rate under N$_2$ (variable 7). Only 8 of the 16 compositions studied showed a discernible secondary peak in the mass loss rate, and they tended to be samples with little or no SiMCy present. The secondary mass loss peak was, in all cases, quite small when compared to the primary peak when it was discernable, and thus the peak mass loss rates are likely to be influenced by the nature of the primary weight loss peak as well. In particular, a broader primary weight loss peak might obscure, or even "bury", the secondary peak. Indeed, the broader primary weight loss associated with SiMCy (see Fig. 11 in the main body of the text) may explain the lack of a secondary peak in samples rich in SiMCy.

Overlap of the primary and secondary peaks may also explain the differences observed among the three component monomers. Although BADCy showed a higher secondary peak loss rate than LECy, the difference was of marginal significance. While there was a significant difference between SiMCy and LECy at 95% confidence, the lack of data for SiMCy-rich samples makes the result difficult to interpret. The standard error of the regression was well below the observed loss rates at the secondary peak, and the normal probability (Figure S1.7) and residual (Figure S2.7) plots showed the expected behavior for normally distributed random errors; thus, the secondary peak, when discernible, did seem to be a well-defined feature of the mass loss curves. However, the smoothed residuals show a very large feature in the SiMCy rich region of the ternary composition diagram (Figure S3.7), a feature that may simply reflect a paucity of available data and interference from the primary peak rather than a true departure from linearity.

S1.8 Primary Peak Loss Temperature under N_2 (variable 8). Like the onset of decomposition, no statistically significant differences among the network components were observed. The samples showed an average peak weight loss temperature of $429 \pm 5°C$ with a predicted value from the regression of $428 \pm 5 °C$. Normal probability (Figure S1.8) and residual (Figure S2.8) analysis showed only one possible outlier at $t = +2.45$ (25 wt% BADCy, 75 wt% SiMCy), otherwise the distribution of residuals was as expected. The 25 wt% BADCy / 75 wt% SiMCy sample showed a residual amounting to $t = +1.26$ in the primary mass loss temperature in air (see variable 14), and similar compositions did show some corresponding positive deviations, both in nitrogen and (marginally) in air, in the smoothed residuals (Figure S3.8). Thus, SiMCy-rich samples do appear to show a somewhat higher peak decomposition temperature than expected under nitrogen, although for reasons that remain unclear.

S1.9 Secondary Mass Loss Peak Temperature under N_2 (variable 9). Perhaps as a result of overlap with the much larger primary loss peak, the secondary peak temperature (which was only seen in 8 samples, mainly those poor in SiMCy) was more variable than the primary peak loss and decomposition onset temperatures. No significant trends due to compositional variation were observed. The secondary peak loss temperature averaged 513 ± 24 °C, and no outliers or unusual features in the normal probability (Figure S1.9) or residual (Figure S2.9) plots were seen. The smoothed residuals (Figure S3.9) show a strong negative deviation in SiMCy-rich compositions, but as with the secondary mass loss rate (variable 7), this feature may be caused by a scarcity of available data or interference from the primary loss peak.

S1.10 Char Yield under N_2 (variable 10). Under nitrogen, the estimated char yields of BADCy and SiMCy were nearly identical, at 49 ± 4% and 48 ± 3%, respectively, while the char yield for LECy was significantly higher at 57 ± 3%. Although no outliers were observed and no unusual features were seen in the normal probability (Figure S1.10) and residual (Figure S2.10) plots, the smoothed residuals did show some correlation with composition (Figure S3.10). In particular, samples that contained around 50 wt% SiMCy (especially with LECy) tended to show significant positive deviations, while pure SiMCy and samples rich in SiMCy tended to show negative deviations. This pattern is the result of a steep rise in char yield as SiMCy loading decreases, followed by a leveling off (or even a slight decrease) in char yield with further decreases in loading. It is unclear why, at low loadings SiMCy appears to offer a protective effect under nitrogen while at high loadings it significantly decreases char yield.

TGA Data (Air)

S1.11 Onset of Decomposition in Air (variable 11). As is generally true for cyanate esters in which the cyanurate ring and its connections represent the weak links in terms of thermal

stability, the onset of degradation in air was no different than the onset of degradation in nitrogen. Both the average observed value as well as the predicted value at the centroid of composition were 416 ± 3 °C (compared to 418 ± 2 ° C under nitrogen). No significant trends due to composition were found, and no anomalies were seen in either the normal probability (Figure S1.11) or residual (Figure S2.11) plots, with the largest deviation having an absolute value of t of 2.17. The smoothed residuals showed a single potentially significant positive anomaly at 75 wt% LECY / 25 wt% SiMCy, however, the isolated nature of this anomaly (neighboring points show little deviation) in addition to its absence under nitrogen (variable 5) indicate that it is likely to be due to random error.

In absolute terms, in both nitrogen and air, the maximum observed deviations are about 6°C away from the average. Because the standard deviation for the data under nitrogen is smaller, however, the larger deviations translate into t-scores with a higher absolute value. Thus, it may have been the case that the higher intrinsic variability of the data in air obscured the deviations. As a check, the onset of decomposition temperatures for nitrogen and air were ranked (tied ranks and replicate composition values were averaged). The rankings showed a Pearson correlation coefficient of -0.09, indicating that the deviations did not correlate.

S1.12 Primary Peak Mass Loss Rate in Air (variable 12). The peak mass loss rates for all three monomers showed a similar pattern in air as under nitrogen, being (in air) 8 ± 2 % / min. for SiMCy, 11 ± 2% / min. for LECy, and 14 ± 2 % / min for BADCy. The largest of these differences (SiMCy / BADCy), however, is only significant at 94% confidence. No significant outliers were observed, and the normal probability plot (Figure S1.12) appeared as expected. The residual plot (Figure S2.12), however, appeared to show higher variability for samples that decomposed at higher rates (or, alternatively, for LECy-rich networks). As mentioned in the

main body of the paper, a systematic negative deviation was found for the multi-component systems (Figure S3.12) when compared to the pure components, due to the non-coincidence of the decomposition peaks of the components (see Figure 10 and the related discussion).

S1.13 Secondary Peak Mass Loss Rate in Air (variable 13). It should be noted that in most cases, in air, the secondary mass loss exhibited peak rates at or near the upper limit of the temperature range investigated, that is, 600 °C. As a result, unlike the nitrogen data, only the peak loss rate (and not the peak temperature) was investigated as a variable for samples analyzed in air. Interestingly, among all the TGA-related variables investigated, the secondary mass loss peak rate in air showed some of the most definitive contrast among the three monomers, with the rate for SiMCy (2.6 ± 1.5 % / min.) being significantly lower than that for BADCy (9.1 ± 1.4 %/min.) or LECy (6.4 ± 1.4 %/min.). The only unusual features in the normal probability (Figure S2.14) and residual (Figure S2.13) plots were some clustering, no outliers were observed, and the smoothed residuals showed no anomalies (Figure S3.13). The standard error of the regression was relatively large at about 1.8% / min., which may have obscured some deviations, along with the fact that the secondary maximum was often found at 600 °C, on the edge of the measurement envelope. The lower secondary mass loss rate of SiMCy has been attributed to the formation of a protective oxide layer during the primary mass loss. [S2]

S1.14 Primary Peak Mass Loss Temperature in Air (variable 14). The behavior of this variable very closely resembles that observed under nitrogen (variable 8), with no significant trends due to compositional differences observed, and an average value of 427 ± 4°C (compared to 429 ± 5°C under nitrogen). The largest outlier (pure SiMCy) had a t-score of just -2.18, so no significant outliers were found. As was done with the decomposition onset temperatures, the primary mass loss temperatures under nitrogen and in air were ranked and analyzed for

correlation. The resultant Pearson correlation coefficient on the ranks was +0.42, thus the observed variations in the peak decomposition temperature under nitrogen and in air were somewhat related. And while the normal probability plot (Figure S1.14) for this variable looked as expected, the residual plot (Figure S2.14) had a slightly unusual appearance, with a tendency for positive deviation found in samples with low predicted values. The smoothed residuals (Figure S3.14) showed no significant patterns with respect to composition.

S1.15 Char Yield in Air (variable 15). The estimated values were $51 \pm 6\%$ for SiMCy, $20 \pm 6\%$ for BADCy, and $41 \pm 6\%$ for LECy. The differences between SiMCy and BADCy, and between BADCy and LECy were thus significant, while the difference between SiMCy and LECy was not. The normal probability (Figure S1.15) and residual (Figure S2.15) plots looked as expected, and no significant outliers were found. However, the smoothed residuals (Figure S3.15) revealed a clear pattern of positive deviations for the multi-component samples. In fact, the highest char yield of any single sample was 75 wt% LECy / 25 wt% SiMCy, at 50%, compared to 43% for pure SiMCy (as measured) and 32% for pure LECy (as measured). These deviations may result from two simultaneous effects: first, a strong protective effect of SiMCy and LECy on BADCy in mixtures, with a weaker protective effect of SiMCy in mixtures with LECy (due to the lower difference in char yields between the pure components), and second, a heterogeneity effect, like that seen in the decomposition rates, in which some of the second stage of thermo-oxidation is "smeared out" to temperatures beyond 600 °C, thereby improving the char yield at this temperature. As mentioned in the discussion of the secondary mass loss peak rate data (variable 13), the maximum in the secondary rate was often found at 600 °C (the edge of the measurement envelope) and the standard error of the regression was unusually large, thus the

characteristic pattern for the "smearing out" of the peak rate (seen in variables 6 and 12) may have been obscured by measurement limitations.

   Extended Discussion.   The similarity of both onset and primary decomposition temperatures and primary decomposition rates under nitrogen and in air, along with the lack of compositional dependence of these temperatures suggests, as has been reported previously based on mechanistic studies, that the primary degradation mechanism in the early stages of mass loss is the breaking of the ester bond and subsequent destruction of cyanurate rings,[S1] the kinetics of which should show little or no dependence on composition (for the monomers considered herein). On a mass basis, the fraction of cyanurate rings is about 5% lower in SiMCy than in BADCy, and about 10% lower than in LECy. While these differences can explain the general trend towards lower primary mass loss rates in SiMCy, they are too small to explain the magnitude of the observed difference. The higher char yields in air of SiMCy and LECy can be attributed partly to reduced mass loss in both primary and secondary peaks. Under nitrogen, however, the broadness of the mass loss peak in SiMCy compensates for its lower peak value, leading to similar overall mass loss and char yield, while for LECy, the higher char yield appears to most likely be due to a smaller secondary mass loss peak (LECy also has the highest aromatic content by weight of the monomers studied).

TMA Data (Dry)

S1.16 Fully-Cured Dry Glass Transition Temperature as Measured by Loss Peak (variable 16).   The results, which showed significant differences among all three components, are summarized in Table 1 of the main body of the paper. The normal probability plot (Figure S1.16) showed two outliers (one of the pure LECy replicates and 25 wt% BADCy / 75 wt% LECy) at t = -2.34 and t = -2.63, respectively. Note, however, that the other LECy replicate and

25 wt% SiMCy / 75 wt% LECy showed t = +1.40 and +1.36, respectively. The residual plot (Figure S2.16) also showed some concavity, which may simply reflect the large spread in reported values for LECy-rich samples. The smoothed data (Figure S3.16) does show a pattern of positive deviations for multi-component networks and negative deviations for single-component rich systems, but of a magnitude that implies only marginal significance. Note also that the features seen in the smoothed DSC data are not obvious in the smoothed TMA data. The TMA data do reflect a somewhat different cure cycle (24 hrs at 210 °C, then heating to 350 °C) than the DSC data (heating to 350 °C only). Additional reasons for the apparent discrepancy are provided in the "Extended Discussion" of the DSC data (section S1.4).

S1.17 As-Cured Dry Glass Transition Temperature as Measured by Loss Peak (variable 17). Please note: the extent of cure as determined by the diBenedetto equation was not taken into account for analysis of variable 17. The variable thus represents an alternative case to the one presented in the main body of the paper. In this alternate case it is assumed that variations in cure are simply part of the undefined experimental error and that the primary variation in glass transition temperature results only from a Gordon-Taylor type rule of mixing and systematic composition-driven deviations.

In this alternative analysis, no significant differences among the glass transition temperature values (averaging 266 °C, with a standard deviation of 19 °C) were found. The standard error of the regression, as expected, was close to the standard deviation of the data, at 20 °C. These variations were much larger than normal for TMA measurements (for comparison, the regression for fully cured samples showed a standard error of 9 °C), while repeated TMA measurements of the same sample are often reproducible to within 1 °C. Both the added variability, and the fact that this analysis failed to detect clear differences in glass transition

13

temperature, point to variations in the degree of cure as the primary source of variations in glass transition temperature. In general, a close relationship exists between the as-cured glass transition temperature of a thermosetting polymer and the cure temperature. Although cyanate esters are unusual in that the glass transition temperature can significantly exceed the cure temperature, the difference between the two temperatures has been shown to be fairly similar for different materials. Thus, the as-cured glass transition temperatures of the samples reflect the extent of cure that was possible at 210 °C. Put another way, LECy and SiMCy, having more flexible bonds, cured more readily at 210 °C than did BADCy, however the higher fully-cured glass transition temperature of BADCy compensated for the lower degree of cure, resulting in similar as-cured glass transition temperatures.

The normal probability plot (Figure S1.17) for variable 17 had an unusual feature, namely the lack of a low-end tail. The residual plot (Figure S2.17) also appears a bit asymmetric for the same reason. The smoothed residuals (Figure S3.17) showed, if anything, an unusually low level of deviation. The latter result probably derives from the large standard error of the regression, meaning any deviations from a compositional rule of mixtures (for as-cured glass transition temperatures) were obscured by other factors. The appearance of the normal probability plot may relate to the cause of the variation. In oven-cured samples held at temperature for a long period of time, both temperature overshoots and undershoots may occur. However, in cyanate esters it has been seen that the degree of cure, in systems cured below the glass transition temperature, is much more sensitive to temperature than to time. Thus, even a few minutes at elevated temperature during an overshoot will affect the degree of cure, making the degree of cure sensitive to the maximum temperature seen by the sample, rather than to the set point of the oven. In an undershoot scenario, the oven will eventually reach the set point, and

though cure will be delayed, there will be no impact on the final degree of cure achieved. An overshoot scenario, however, will result in additional cure. Thus, for these samples the degree of cure will not be distributed normally; instead, the distribution should appear to be a normal distribution with a missing low-end tail, just as was observed.

For all of the above reasons, variations in the degree of cure were deemed important in the as-cured samples and included when appropriate as a variable in the residual (using the diBenedetto equation to estimate it as described in the Experimental section of the main body of the paper). It should be noted, though, that although the effect on glass transition temperature was noticeable, the differences amount to a standard deviation of just over 2% in the overall extent of cure achieved. Although attributing all glass transition temperature variations to differences in cure (which is the overall effect of the chosen data analysis procedure) may overstate the actual differences in cure, based on the observed variations in the TMA and DSC data, the estimated degree of conversion was accurate to within about 1%. Moreover, conversion was retained as a regression variable only when its inclusion resulted in a statistically significant effect or a very noticeable decrease in the standard error of the regression (these two conditions generally coincided), thus, in every case in which it was used, there was ample justification.

S1.18 Peak Value of tan delta in As-Cured Samples (variable 18). In addition to the peak temperatures for both loss and tan delta as indicators for the glass transition temperature, widely reported analyses of dynamic mechanical data have sometimes included the peak value of tan delta itself as well as the value of the storage modulus above the glass transition temperature as important indicators of physical properties. Thus, in our analysis of dynamic TMA data, the peak value of tan delta as well as the ratio of the storage component of the stiffness above and below the glass transition temperature were also studied as possible variables of interest. The

ratio, rather than the absolute value, for the storage component of stiffness was used since the lack of a precisely measured contact area precludes a meaningful determination of the absolute storage modulus in dynamic TMA (which relies on compression by a partially contacted probe rather than bulk deformation of the sample). Both the absolute value of the tan delta peak as well as the storage ratio have been related to the cross-link density in the system, with a high cross-link density expected to reduce the peak value of tan delta while increasing the ratio of storage stiffness (which we report as the value 30 °C above the glass transition divided by that 30 °C below the glass transition).

Analysis of the tan delta peak values for as-cured samples showed some difference between the estimated value for SiMCy (0.51 ± 0.06) and BADCy (0.62 ± 0.06) with LECy having an intermediate value (0.58 ± 0.06). Even the largest of these differences, however, is of somewhat marginal significant (93% confidence). When the degree of cure was also included, no decrease in the standard error of the regression was observed, and the effect of cure itself was found to be positive (contrary to expectation) and insignificant ($t = 1.1$), thus the degree of cure was not retained as a regression variable. The normal probability plot (Figure S1.18) for the retained regression (composition only) showed a broader than expected distribution, with up to six seeming outliers, while the residual plot (Figure S2.18) showed no anomalies. Interestingly, the smoothed residuals (Figure S3.18) showed a large positive deviation in LECy/SiMCy co-networks. It should be noted that the peak value of tan delta may reflect some instrumental effects; for instance, sudden changes in probe contact force often lead to irreversible deformation (the crushing of asperities) that show up as increased loss and, consequently, a peak in tan delta, during measurement. Both the tan delta peak value (as well as storage stiffness ratio) might thus be influenced by factors such as the smoothness and hardness of the sample surface that depend

16

on viscosity and cure characteristics of the materials under study in ways not well characterized. Thus, in the absence of very strong statistical trends, further discussion of possible causes of the observed features of the data is not warranted.

S1.19 Storage Stiffness Ratio in As-Cured Samples (variable 19). When conversion was not taken into account, no significant trends were observed; however, when conversion was included, the standard error of the regression decreased from 0.09 to 0.07, and the effect of cure was found to be highly significant while compositional effects were found to be insignificant. At full cure, the predicted ratio was found to be 0.22 ± 0.05 on average, with an increase in conversion of 1% resulting in a decrease of 0.029 ± 0.007 in the ratio (note, a higher ratio indicates a higher storage stiffness above the glass transition temperature). However, the ratio for the fully cured samples was in fact measured on the second heating, and failed to match the prediction (see the discussion of variable 22). In addition, as discussed previously, instrumental effects cannot be ruled out, thus no cause for the observed trend could be identified. As for the data, the normal probability (Figure S1.19) and residual (Figure S2.19) plots looked as expected, with just one outlier (pure SiMCy at $t = +3.17$), and no other significant features seen in the smoothed residuals (Figure S3.19).

S1.20 Fully-Cured Dry Glass Transition Temperature as Measured by tan delta Peak (variable 20). In yet another alternative analysis, the peak temperature of the tan delta function rather than the loss component of stiffness was used as the indicator of the glass transition temperature for fully cured samples. This alternative was analyzed due to the common practice of using the tan delta peak, rather than the loss peak, as an indicator of the glass transition temperature. (The onset of a decline in the storage stiffness is also sometimes used, but this variable was not analyzed).

As expected, the analysis using tan delta peaks gave essentially the same results as that conducted with loss peaks, with the differences in predicted glass transition temperature among the pure components being identical to those found from loss peak (variable 16), but with the actual temperatures shifted higher by 3-6 °C. The standard error of the regression was also just slightly higher, at 9 °C. The residuals were also very similar; the difference between residuals in the loss peak data and the corresponding residuals in the tan delta peak data formed a normal distribution with mean of -0.1 °C and standard deviation 1.5 °C, which is close to the precision of the instrument. Thus, the normal probability (Figure S1.20), residual (Figure S2.20), and smoothed residual (Figure S3.20) plots looked identical for the two data sets. Analysis of the tan delta peak data was therefore judged completely redundant, and the loss peak was judged to be the preferred indicator of the glass transition due to its slightly smaller variability and because it takes place at a lower temperature, thereby reducing the risk of a false reading due to *in-situ* cure. As a result, analysis of tan delta peak temperatures is not reported for any other TMA measurement types.

S1.21 Peak Value of tan delta for Fully-Cured Samples (variable 21). The peak value of tan delta for fully cured samples showed no trends of even marginal significance. The average value, at 0.45, was a bit lower than that seen in as-cured samples, but the standard deviation, at 0.12, was about twice as large. The normal probability plot (Figure S1.21) looked decidedly non-linear, but the residual plot (Figure S2.21) looked as expected while smoothed residuals (Figure S3.21) showed almost no traces of variation. Hence, all that can be said about this variable is that it is likely even less meaningful than its as-cured counterpart (variable 18) due to significantly increased uncontrolled variability.

S1.22 Storage Stiffness Ratio in Fully-Cured Samples (variable 22). Although a significant effect of the degree of conversion was found on the storage modulus ratio in as-cured samples, the data from the fully cured samples did not offer corroborating evidence for an effect of cure. Namely, the average value of the stiffness ratio was 0.314 with a standard deviation of 0.075 for fully cured samples, and 0.297 with a standard deviation of 0.080 for as-cured samples. Note that the regression based on as-cured samples predicted that fully cured samples would show an average value of 0.22, thus, the predicted effect was not observed. Moreover, when only composition was used as a variable for both as-cured and fully-cured data sets, the Studentized residuals showed a Pearson correlation coefficient of 0.54. If in fact conversion were the key determinant of the ratio, the coefficient would be expected to equal zero. Unlike the corresponding as-cured data (variable 19), there were no outliers in this data set, the normal probability (Figure S1.22) and residual (Figure S2.22) plots looked as expected, and there were no significant features in the smoothed residuals (Figure S3.22).

Note that although peak tan delta and storage component of stiffness ratio data were also collected for the wet and wet/re-heated TMA samples, based on the analysis of the dry TMA data, these variables were not expected to yield useful information and thus their analysis is not reported herein.

S1.23 Linear Coefficient of Thermal Expansion (CTE, at 150 °C, on 1st heating, variable 23). Note that due to the thermal lag computation, the "1st heating" actually features three ramps during which the temperature passes 150 °C while heating. The second and third of these are used for determination of the CTE, since probe contact tends to be worse during the first thermal lag loop. Since the final cure temperature was 210 °C, the thermal lag cycling (to 200 °C) will

not affect the data. As a result, each data point was replicated, allowing for higher confidence in the results than would have otherwise been possible.

The degree of conversion was found to be significant at 96% confidence, thus it was included as a regression variable in the "as-cured" data discussed here.   An interesting result is that the "as-cured" data provided an estimate of the CTE at full cure, while the data from the 2nd heating to 350 °C ("fully cured" samples, see variable 24) provided an experimental check of the predictive power of the extrapolation (see the discussion below).   The CTE in "as-cured" samples was found to be significantly affected by composition, with predicted values (extrapolated to 100% conversion) of 59 ± 2 ppm / °C, 64 ± 2 ppm / °C, and 74 ± 2 ppm / °C for BADCy, LECy, and SiMCy, respectively.   These values are close to previously reported values for BADCy and LECy, [S1] but lower than previously reported for SiMCy. [S2]   Also as discussed in the main body of the paper for the experimentally-derived fully cured values, the differences among the three monomers correlate as expected to the glass transition temperatures of the fully cured networks.   According to the regression, for every 1% increase in conversion, the CTE decreases by 0.30 ± 0.014 ppm / °C.   This level of sensitivity is very close to what has been previously reported (when translated into volumetric expansion coefficient) for BADCy. [S3]   The normal probability plot (Figure S1.23) for the robust regression showed some clustering at the low end of the distribution, while the residual plot (Figure S2.23) looked as expected.   The clustering at the low end of the distribution may be associated with the fact that, as revealed by the smoothed residuals (Figure S3.23), there is a systematic trend towards negative deviation for the mixtures with systematic positive deviations for systems rich in, or comprised solely of, a single component.   As explained in the main body of the paper for the experimental data on fully

cured samples, this effect is due to having interlocked segments with differing levels of expansion.

S1.24 Linear Coefficient of Thermal Expansion for Fully Cured Samples (at 150 °C , 2nd heating to 350 °C, variable 24). As mentioned previously, by simply re-heating the samples used for CTE measurements a second time to 350 °C, a "fully cured" rather than as "as-cured" value for CTE was obtained experimentally. In this case, values for heating and cooling at 150 °C were used, rather than values from multiple passes, in order to reduce uncertainties. A separate examination of the values obtained on heating and on cooling showed a systematic difference of 2.4 ± 1.9 °C, with the values obtained on cooling being on average smaller. Since this difference was not statistically significant, the data were pooled for the robust regression. The results were similar to those found by extrapolation of the "as-cured" data, with fully cured network CTE values of 56 ± 3 ppm / °C for BADCy, 62 ± 3 ppm / °C for LECy, and 69 ± 3 ppm / °C for SiMCy. The normal probability plot (Figure S1.24) and residual plot (Figure S2.24) looked as expected, with no significant outliers given the number of data points. The smoothed residuals (Figure S3.24) displayed the same systematic deviations as the "as-cured" samples, as described in more detail in the main body of the paper.

Extended Discussion. Although for BADCy and LECy, the two CTE measurement techniques gave statistically identical values, the experimental fully cured network values were lower in all cases. To check further, a predicted value based on the "as-cured" data was computed for each mixture and compared to the experimental value. The differences formed a surprisingly narrow distribution with a mean 3.4 ppm / °C and a standard deviation of only 0.7 ppm / °C, with the experimental values being lower. Note that systematic effects due to cooling (if they existed) would account for only 1.2 ppm / °C, since they would have been present in

21

only half the data. Possible explanations for the discrepancy include a systematic error in the assessed degree of cure (though this would have to be 5 - 10%, which seems highly unlikely given the sensitivity of the glass transition temperature to such changes), thermal degradation of the samples on heating to 350 °C, or, a change in the level of contact between the sample and the TMA probe (the "as-cured" samples had never been in a softened state and thus were likely to have exhibited looser probe contact).

Although many different variables based on dry TMA measurements were analyzed, there were, in the end, just four important measurements afforded by the technique. The fully cured T_g, which closely matches the same measurement by DSC, the degree of cure based on the diBenedetto equation, the fully cured CTE, and the effect of conversion on CTE. The tan delta peak temperature was shown to be a redundant feature, with the tan delta peak value being essentially constant, as was the storage stiffness ratio, for the range of blends studied.

TMA (Wet)

S1.25 "Wet" Glass Transition Temperature (Based on Loss Peak) for As-Cured Samples (variable 25). It should be noted that "wet" glass transition data were gathered on as-cured samples that were boiled for 96 hours in distilled water, then heated at 20 °C / min. to minimize drying *in-situ*. Weighing of samples pulled from the instrument during intentionally interrupted runs indicated that at least 80% of the absorbed water was retained during the measurement.

Interestingly, the effect of composition on wet glass transition temperature was not significant, with the predicted values for pure components being 207 ± 10 °C for BADCy, 203 ± 10 °C for LECy, and 186 ± 10 °C for SiMCy, and the average for all measurements being 199 °C with a standard deviation of 12 °C. The SiMCy/BADCy trend, however, is marginally significant with a confidence level of 93%. Note also that the order and approximate relative

difference among wet glass transition temperatures matches that of the dry glass transition temperatures; it is the range of the differences that has been compressed by more than 50%. The standard error of the regression (about 12 °C) is also compressed by about 40% relative to that of the as-cured dry glass transition temperature. Due to the small temperature range of the data and the effect of additional sources of variation, the effect of cure was not discernible in the data (inclusion in the regression gave an estimated effect of 2 ± 23 °C for every 1% increase in cure). Both normal probability (Figure S1.25) and residual (Figure S2.25) plots were reasonably consistent with expectations. The smoothed residuals (Figure S3.25) showed only one unusual feature; a large positive deviation in wet glass transition temperature for the 50 wt% /50 wt% SiMCy/LECy co-networks, which by itself showed a deviation of $t = +2.67$. The SiMCy / LECy sample also shows a large negative anomaly in moisture uptake, thus its kinetics of degradation were likely slower than expected, resulting in retention of a higher wet glass transition temperature.

Extended Discussion. In order to further investigate the wet glass transition temperature, a robust regression was performed using only the as-cured dry glass transition temperature (loss peak) and the water uptake as input variables, and ignoring differences in composition. The results (regression 25a) show effects significant at 98% confidence for dry glass transition temperature and 93% confidence for water uptake. As expected, the regression predicts a 45% decrease in the range of glass transition temperatures, with an adjustment of 28 ± 14 °C (decrease) for every 1 wt% increase in water uptake. Such effects would be expected if the hydrolysis of the network were to degrade the glass transition temperature in line with the diBenedetto equation. If one assumes $\lambda = 0.4$ (as measured for the dry samples) in the diBenedetto equation, then the implication of the contraction in the range of the glass transition

23

temperature would be that about 70% of the cross-linking has been reversed by hydrolysis, yet the actual glass transition temperature values are consistent with only around 10% loss of cross-link density. In addition, the former implication also requires that the fully de-polymerized network would have a glass transition temperature of about 155 °C, which is, though unexpected, close to the final glass transition temperature obtained by others for BADCy after allowing it to degrade for several thousand hours until equilibrium was reached. [S1]

As for the regression itself, it resulted in normal probability (Figure S1.25a) and residual (Figure S2.25a) plots that looked as expected, but with smoothed residuals (Figure S3.25a) showing a large positive deviation for BADCy / LECy co-networks. This deviation can be traced to a single outlier, the 75 wt% BADCy / 25 wt% LECy co-network, with t = +5.03. Although the wet glass transition temperature of this network was replicated very well, the dry as-cured glass transition temperature indicated the lowest level of conversion among all the samples prepared. Had the "dry" sample achieved a more typical degree of cure, the wet glass transition temperature would not seem unusual. Moreover, in terms of composition, the sample deviation is quite moderate (only t = +1.12 on average). Thus, one simple explanation for the deviation would be that the sample retained for "dry" glass transition temperature measurement failed to achieve a typical degree of conversion (perhaps due to a random event during mixing and cure), whereas the samples chosen for "wet" measurement cured normally.

S1.26 Glass Transition Temperature (Based on Loss Peak) of "Wet" Samples after Heating to 350 °C ("Re-Heated Wet T_g", variable 26). Note that after heating to 350 °C, no moisture is left within the sample. In most cases, heating past the "wet" T_g the first time caused large bubbles to form in the samples. While this effect does not preclude further data collection, and it did not appear to impede measurement of the glass transition, the samples are clearly no longer

"identical" when compared to the first heating. In fact, residual water in the sample is likely to have reacted with uncured cyanate ester groups, generating carbamates and possibly subsequent reaction products that may have altered the network.

Robust regression analysis showed that all compositional effects were highly significant. Whereas BADCy and LECy exhibited marginally higher T_g values (223 ± 10 °C 2nd heating *vs.* 206 ± 10 °C 1st heating, and 217 ± 11 °C 2nd heating *vs.* 203 ± 10 °C 1st heating) on re-heating (keeping in mind the limitations mentioned previously), SiMCy showed a drastic decrease (147 ± 11 °C 2nd heating *vs.* 186 ± 10 °C 1st heating). Since there were no significant variations from a Gordon-Taylor rule of mixtures in the smoothed residuals (Figure S3.26) despite the very large range of values, whatever network degradation or other chemistry may be responsible for the unusual behavior would appear to be either associated with the silicon atom in SiMCy, or perhaps with an impurity in the SiMCy that is not present in BADCy or LECy. The normal probability (Figure S1.26) and residual (Figure S2.26) plots also looked as expected. Note that the pure LECy sample was not tested for this variable, hence the smoothed data does not cover the entire ternary composition range.

Density and Water Uptake

S1.27 Density at 20 °C (variable 27). Note that the density values have not been corrected for the effect of catalyst, which likely resulted in densities about 0.005 lower than those of uncatalyzed material, but would have been nearly identical for all compositions studied, and therefore, should not have significantly affected the regression results. Note also that the regression included conversion as a variable. Significant differences were observed among all three components with the density being highest for LECy (1.220 ± 0.003), followed by BADCy (1.194 ± 0.003), then SiMCy (1.175 ± 0.003). Note that the values represent extrapolations to

100% conversion. The density was found to decrease by 0.0014 ± 0.0006 g/cc for every 1% increase in conversion.   The normal probability (Figure S1.27) and residual (Figure S2.27) plots appeared as expected, with the exception of the value for pure SiMCy, which represented an outlier at $t = -2.93$. The outlying value was the only prominent feature in the smoothed residual plot (Figure S3.27).   More discussion of the density data and its comparison to previously reported values is provided in the main body of the paper.

S1.28 Packing Fraction at 20 °C (variable 28).   Since the van der Waals volume is, by definition, a linear function of the volume fractions of the components, the deviations from linearity for the density and packing fraction at room temperature were identical, and thus the normal probability, residual, and smoothed residual plots (Figures S1.28, S2.28, and S3.28, respectively) were also identical. As with the density at room temperature, all three components showed significantly different packing fractions and a significant effect due to conversion.   The only notable difference between the density and the packing fraction values lies in their relative ranges. Whereas the density values vary over about 4%, the packing fraction values vary over only 1.5%, with the highest value (LECy at 0.629 ± 0.002), followed by BADCy (0.625 ± 0.002) then SiMCy (0.619 ± 0.001), with the listed values representing extrapolations to full conversion, with the packing fraction decreasing by 0.0007 ± 0.0003 for every 1% increase in conversion. The smaller range of variation in packing fraction thus indicates that much of the variation in density can be explained as the expected result of the differences in bond lengths and molecular weight among the constituent monomers.

S1.29 Packing Fraction at 0 K (variable 29). Note that this variable is based on the combination of as-measured density, calculated van der Waals volume, and the measured coefficient of thermal expansion below the glass transition temperature. Since the variations in

26

many of these factors have systematic components (based, for instance, on the presence of multiple network components as discussed in the main body of the paper), a "propagation of error" type calculation of the uncertainties would be quite involved. Instead, we rely on the standard error of the regression to capture these effects quantitatively. Indeed, the standard error for the packing fraction at 0 K was 10-15% larger than that of the packing fraction at 20 °C. This result is in agreement with qualitative expectations, since the net effect of the extrapolated thermal expansion is to change the packing fractions by about 0.04 (or twenty times their variation), with an uncertainty in the magnitude of only about 2%. Thus, variations related to CTE should be about 40% of variations in the measured packing fraction, with the commonly used propagation of uncertainty formula (which ignores systematic effects) predicting about an 8% increase in standard error.

Interestingly, the packing fractions of BADCy and SiMCy at 0 K are statistically identical (at 0.660 ± 0.002 and 0.661 ± 0.002, extrapolated to full conversion), while that of LECy is significantly higher than both (0.667 ± 0.001 at full conversion), with the effect of conversion being a decrease of $0.000\,9 \pm 0.0004$ for every 1% increase in conversion,, essentially the same as found for the packing fraction values at 20 °C. The total range is thus further reduced to about 1% of the average value. These results suggest that the low packing fraction seen for SiMCy results from greater expansion induced by thermal motion in the longer, more flexible C-Si bonds. The difference between LECy and BADCy increases slightly (though insignificantly) at 0 K when compared to the values at 20 °C.

The normal probability (Figure S1.29) and residual (Figure S2.29) plots appear as expected. The smoothed residuals (Figure S3.29) for the packing fraction at 0 K however looked quite different than the corresponding plot for the packing fraction at 20 °C. The large

negative deviation associated with pure SiMCy was no longer present. In its place was a positive deviation for compositions rich in SiMCy and LECy, which, as noted in the main body of the paper, tended to show a combination of unusual characteristics, most notably low moisture uptake. Whether and how the molecular characteristics of these co-networks are related to the more efficient packing at low temperatures remains to be investigated.

S1.30 Packing Fraction at the Cure Temperature (210 °C, variable 30). We chose to investigate this variable, which is also a combination of density, van der Waals volume, and CTE data, since it represents the packing efficiency of the as-formed network. In this case, LECy was still the most efficiently packed (at a packing fraction of 0.607 ± 0.001 at full cure). As at 20 °C, BADCy was marginally less efficient (0.604 ± 0.00 at full conversion), with the difference being somewhat too small to be statistically significant at 95% confidence. SiMCy, on the other hand, was much less efficiently packed (0.594 ± 0.002 at 100% conversion), with the pure SiMCy representing an anomaly of t = -3.62). The effect of conversion was significant only at 94% confidence, though it was equal to a decrease of 0.0007 ± 0.0003 for every 1% increase in conversion, the same value obtained for packing fractions at 20 °C. The normal probability (Figure S1.30), residual (Figure S2.30), and smoothed residual (Figure S3.30) plots appear quite similar to those for the density and packing fraction at 20 °C, only with a somewhat larger negative anomaly for the pure SiMCy.

Extended Discussion. It is worth noting that, at the cure temperature, SiMCy was only 50 °C below its fully cured glass transition temperature (as a result of its larger thermal expansion when considered from the standpoint of fractional free volume theory), whereas BADCy and LECy were 80 – 100 °C below their glass transition temperatures. Thus, the packing fractions of the as-cured (and not yet cooled) network may be understood as driven by

28

two factors, the relatively lower glass transition temperature of SiMCy being most important, and the superposition of intrinsically more efficient packing in LECy being of secondary importance, but still great enough to more than compensate for the small difference in glass transition temperatures between BADCy and LECy). On cooling, the SiMCy shrinks slightly more due to its somewhat larger CTE, but still retains a considerably lower packing fraction. An interesting corollary to this line of reasoning is that a SiMCy network cured at 80 -100 °C below its glass transition temperature should exhibit a higher packing fraction than one cured (to an equal conversion) at 50 °C below its glass transition temperature. This proposition, however, may be difficult to test since the attainable conversion of a cyanate ester near full conversion has been shown to be a very strong function of temperature and a very weak function of time, making it difficult to prepare samples with identical conversions at significantly different final cure temperatures.

S1.31 Moisture Uptake (variable 31): The results for this variable are discussed at length in the main body of the paper. The regression showed significant differences between SiMCy and LECy and between SiMCy and BADCy, with the estimated uptake values being $1.76 \pm 0.11\%$ for SiMCy, $2.34 \pm 0.12\%$ for BADCy, and $2.36 \pm 0.13\%$ for LECy (on a weight basis) when extrapolated to full cure. The effect of cure was quite large, with an increase of 0.05% in uptake for every 1% increase in conversion, although this value is statistically significant at only 94% confidence. As mentioned in the main body of the paper, the 50/50 SiMCy / LECy co-network showed a very large deviation, at $t = -3.79$. This particular deviation was checked for replication (the replicate was not included in the regression), with the uptake of the replicate being 0.19% lower than the original, which is within expectations given a typical variation in cure of about 1% in addition to a standard error of 0.15% for the regression. An additional set of tests on a

sample with the same composition at around 90% conversion gave an even lower uptake of 1.22%. Thus, there is ample evidence that this particular composition truly exhibits an unusual negative deviation in moisture uptake.

The normal probability plot (Figure S1.31) for the data set looks as expected, with the exception of the single outlier, while the residual plot (Figure S2.31) shows some tendency for larger residuals (both positive and negative) at lower uptake values (corresponding to compositions rich in SiMCy). The smoothed residuals (Figure S3.31) were dominated by the single outlier, although the unsmoothed residuals for the other four SiMCy rich blends (not counting pure SiMCy had Studentized residuals given by t = +0.57, -0.33, -0.70, and -0.84), contributing modestly to the systematic effect shown in the smoothed data. The mechanism of interaction by which this particular combination of monomers produces the unusual but highly desirable behavior remains an important subject for future investigations.

Table S-1

Description of variables used

#	Type	Data Points	Name	Function of	Description
01	DSC	7	Melting Point	Composition (mol%)	Peak endotherm temperature (uncorrected) in °C
02	DSC	16	Enthalpy of Cure	Composition (mol%)	Peak area in kJ/mol , assumes equal purity of components
03	DSC	16	Peak Cure Temperature	Composition (mol%)	Peak exotherm temperature in °C
04	DSC	16	Post-cure T_g	Composition (Gordon-Taylor)	Mid-point of observed step transition, in °C. Uses the Gordon-Taylor equation linearized in composition (volume fractions multiplied by K-factors, K-factors based on fully cured T_g ratios)
05	TGA-N2	17	Loss Onset	Composition (wt%)	5% mass loss temperature, in °C
06	TGA-N2	17	Peak Loss Rate	Composition (wt%)	Maximum mass loss rate in % / min.
07	TGA-N2	8	Secondary Peak Loss Rate	Composition (wt%)	Maximum loss rate observed during secondary mass loss (in samples where two separate peaks are discernible in the mass loss rate), in % / min.
08	TGA-N2	17	Primary Peak Loss Temperature	Composition (wt%)	Temperature at which loss rate was maximum, in °C
09	TGA-N2	8	Secondary Peak Loss Temperature	Composition (wt%)	Temperature corresponding to secondary weight loss peak (when discernible), in °C
10	TGA-N2	17	Chari Yield	Composition (wt%)	Mass fraction remaining at 600 °C after heating, in per cent
11	TGA-Air	16	Loss Onset	Composition (wt%)	5% mass loss temperature, in °C
12	TGA-Air	16	Peak Loss Rate	Composition (wt%)	Maximum mass loss rate in % / min.
13	TGA-Air	16	Secondary Peak Loss Rate	Composition (wt%)	Maximum loss rate observed during secondary mass loss (in samples where two peaks are discernible), in % / min.

14	TGA-Air	16	Primary Peak Loss Temperature	Composition (wt%)	Temperature at which loss rate was maximum, in °C
15	TGA-Air	16	Chari Yield	Composition (wt%)	Mass fraction remaining at 600 °C after heating, in per cent
16	TMA-Dry	18	T_g at full cure	Composition (Gordon-Taylor)	Temperature at which loss component of stiffness was maximum, on 2nd heating after ramp to/from 350 °C at 10 °C/min.
17	TMA-Dry	19	T_g as-cured	Composition (Gordon-Taylor)	Temperature at which loss component of stiffness was maximum, on 1st heating to 350 °C at 10 °C/min.
18	TMA-Dry	19	Tan delta at T_g (as-cured)	Composition (vol%)	Maximum value of tan delta on 1st heating
19	TMA-Dry	18	Stiffness ratio (as-cured)	Composition (vol%) and conversion	Ratio of storage component of stiffness at $T_{g,td}$ + 30 °C to that at $T_{g,td}$ – 30 °C where $T_{g,td}$ is the temperature at which tan delta was maximum, all measured on 1st heating
20	TMA-Dry	18	T_g (fully-cured) based on tan delta	Composition (Gordon-Taylor)	Temperature corresponding to peak in tan delta, measured on 2nd heating
21	TMA-Dry	18	Tan delta at T_g (fully cured)	Composition (vol%)	Maximum value of tan delta on 2nd heating
22	TMA-Dry	18	Stiffness ratio (fully cured)	Composition (vol%)	Ratio of storage component of stiffness at $T_{g,td}$ + 30 °C to that at $T_{g,td}$ – 30 °C where $T_{g,td}$ is the temperature at which tan delta was maximum, all measured on 2nd heating
23	TMA-Dry	38	"as cured" CTE	Composition (vol%) and cure	Linear coefficient of thermal expansion based on displacement vs. temperature over the range 145 – 155 °C, includes two data points per sample, one from 2nd thermal lag determination heating and one from 1st heating to 350 °C

24	TMA-Dry	33	"fully cured" CTE	Composition (vol%)	Linear coefficient of thermal expansion based on displacement vs. temperature over the range 145 – 155 °C, includes two data points per sample after 1st heating to 350 °C, one from cooling and one from 2nd heating to 350 °C
25	TMA-Wet	18	"wet" T_g	Composition (Gordon-Taylor)	Temperature corresponding to peak in loss modulus after sample exposed to 85 °C water for 96 hrs, then heated (1st heating)
26	TMA-Wet	15	Reheated "wet" T_g	Composition (Gordon-Taylor)	Temperature corresponding to peak in loss modulus after sample exposed to 85 °C water for 96 hrs, then heated to 350 °C, cooled, and measured (2nd heating)
27	Density	16	Density at 20 °C	Composition (vol%) and cure	Density of $CaCl_2$ solution at 20 °C that gave neutral buoyancy to "as cured" discs at 20 °C
28	Density	16	Packing fraction at RT	Composition (vol%) and cure	Uses van der Waals volume as calculated by the Bicerano method
29	Density	14	Packing fraction at 0 K	Composition (vol%) and cure	Uses CTE at 150 °C for basis of extrapolation and correlation of Bicerano for van der Waals volume. Note: only computed when density and CTE were measured on the same physical sample
30	Density	14	Packing fraction at cure temperature (483 K)	Composition (vol%) and cure	Uses CTE at 150 °C for basis of extrapolation and correlation of Bicerano for van der Waals volume. Note: only computed when density and CTE were measured on the same physical sample
31	Mois-ture uptake	14	Water uptake	Composition (mol%) and cure	Weight gain after 96 hrs at 85 °C; uses only samples with conversion determined simultaneously

Table S2. Key Characteristics of Robust Regressions

Y[a]	C[b]	Const.[c]	BADCy[d]	LECy[e]	Conv.[f]	Std Err[g]	Plot Qual.[h]	Outliers[i]
1	X	**34(4)**	**45(6)**	2(10)	n/a	5	Good –o	+L /+*LM*
2	X	**84(4)**	9(6)	-2(6)	n/a	7	Good	-K / -D
3	X	**198(4)**	3(6)	7(6)	n/a	7	Good-o	+D / none
4	K	**267(3)**	**33(5)**	**23(5)**	n/a	6	Good-o	-HI / *-EHIM*
5	W	**418(1)**	1(2)	-0.3(2)	n/a	2	Good-o	-DL / *-DG* -L
6	W	**6(1)**	*4(2)*	**5(2)**	n/a	2	Fair--1	+P / +P *(Δ)*
7	W	**4.0(0.8)**	*-1.8(0.9)*	**-2.9(0.8)**	n/a	0.4	Good	none / +N
8	W	**430(3)**	-1(4)	-5(5)	n/a	5	Good –o	+M / +M
9	W	**475(34)**	20(41)	65(39)	n/a	18	Good	none / none
10	W	**48(2)**	1(4)	**9(4)**	n/a	4	Good	none / +*BE* -L *(Δ)*
11	W	**415(2)**	1(3)	2(3)	n/a	3	Good	-H / +B -H
12	W	**8(2)**	*6(3)*	4(3)	n/a	3	Fair—2	none / +P *(Δ)*
13	W	**3(1)**	**6(2)**	**4(2)**	n/a	2	Fair—1	none / +A -G
14	W	**430(2)**	-5(4)	-6(4)	n/a	4	Fair--3	-L / -L
15	W	**51(4)**	**-31(7)**	-10(7)	n/a	8	Good	none/ *-ALP+FG(Δ)*
16	K	**266(5)**	**43(8)**	**28(7)**	n/a	9	Fair--4	-AD / -D
17	K	**254(10)**	24(17)	13(16)	n/a	20	Fair--5	+O / none
18	V	**.51(.03)**	*.11(.06)*	.07(.05)	n/a	0.07	Good-o	+G / -L
19	V	**3.2(0.7)**	-.06(.06)	-.05(.06)	**-2.9(0.7)**	0.06	Good-o	+P / +P
20	K	**272(5)**	**40(8)**	**24(8)**	n/a	9	Fair--4	-AD / -D
21	V	**.41(.07)**	.11(.11)	.03(.10)	n/a	0.08	Fair--6	none / none
22	V	**.29(.05)**	.01(.07)	.06(.07)	n/a	0.08	Good	none / none
23	V	**104(14)**	**-15(1)**	**-9(1)**	**-30(14)**	2	Fair—1	+L / +L *(Δ)*
24	V	**69(2)**	**-13(2)**	**-7(2)**	n/a	4	Fair--4	+A / +A *(Δ)*
25	K	**186(7)**	*20(11)*	17(11)	n/a	12	Good-o	none / -A +E +K
26	K	**147(7)**	**76(12)**	**70(14)**	n/a	13	Good	none / -L
27	V	**1.31(0.05)**	**.019(.003)**	**.045(.003)**	**-.14(.06)**	.004	Good-o	+H –L / -L
28	V	**.69(.03)**	**.006(.002)**	**.010(.002)**	**-.07(.03)**	.002	Good-o	+H –L / -L
29	V	**.75(.03)**	-.001(.002)	**.006(.002)**	**-.09(.04)**	.002	Good	none / +H
30	V	**.67(.03)**	**.009(.002)**	**.012(.002)**	**-.07(.03)**	.002	Good	-L / -L
31	X	-0.03(0.02)	**.006(.001)**	**.006(.002)**	*.05(.02)*	.002	Fair--7	-E / *-EFI* +L

Notes for this table are provided on the following page.

The following diagram is helpful in interpreting composition codes:
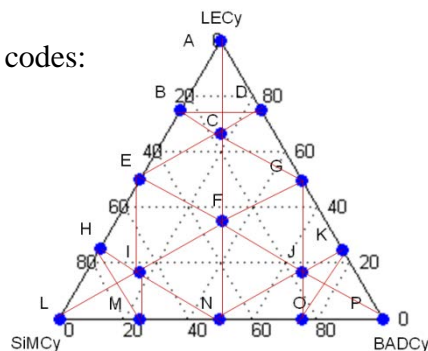
Notes:
a. "Y" indicates the dependent variable, use Table S1 to see the descriptions (by number) for each variable as well as the units of the dependent variable
b. "C" indicates the compositional variable used via the following codes: "K" = Gordon-Taylor adjusted volume fraction, that is $\phi T_{gref}/T_g$, where T_g is the fully cured T_g by DSC and T_{gref} is the fully cured T_g by DSC of SiMCy, and ϕ denotes volume fraction.; "V" = volume fraction, "W" = mass (weight) fraction, "X" = mole fraction
c. The constant in the regression equation, where the variables are the fractions (see note b) of BADCy and LECy in the system, plus (in some cases) conversion. The estimate for SiMCy equals this value when conversion is not taken into account. When taken into account, the constant represents the value for SiMCy at zero conversion (though the valid range of the data is for conversions of 0.95 – 1). For regression terms, bold indicates significance ($p < 0.05$); italic indicates marginal significance ($p \leq 0.05 < 0.1$); and gray text indicates low significance ($p \geq 0.1$).
d. The effect of substituting BADCy for SiMCy.
e. The effect of substituting LECy for SiMCy
f. The effect of conversion, where conversion is a variable from 0.95 to 1, measured for each data point based on the diBenedetto equation and the as-cured T_g (loss peak) from dynamic TMA
g. Standard error of the robust regression, see Table S1 for units
h. Codes for quality of the normal distribution and residual plots: "Good" = as expected, "Good-o" = as expected but with conspicuous outliers by visual examination, "Fair" indicates a minor issue as noted, otherwise the plots look as expected: "Fair-1" = clustering in the normal probability plot; "Fair-2" = tendency for large deviation at high values in the residual plot; "Fair-3" = negative correlation in the residual plot, "Fair-4" = residual plot has negative concavity, "Fair-5" = normal probability plot lacks low tail, residual plot has negative concavity, "Fair-6" = normal probability plot has some curvature; "Fair-7" = residual plot shows more variation at low end
i. Indication of which data points had an absolute value of the Studentized residual (t) greater than two for individual, unsmoothed data points, and greater than 0.5 for smoothed data points (note, this criteria differs slightly from "conspicuous outlier", which is based only on visual inspection). A "+" indicates positive deviation, a "-" indicates negative deviation. Letters prior to the slash represent compositions in the unsmoothed data set, letters after the slash represent compositions in the smoothed data set. Italics indicate a cluster of neighboring points (an indication of significance) in the smoothed data, a "Δ" indicates a smoothed pattern in which multi-component networks tend to deviate oppositely from single-component systems.

The composition codes (from top to bottom on the diagrams in Figures S3.1-S3.31) are, for BADCy, LECy, and SiMCy, respectively, fractions of: "A": 0,1,0; "B": 0,.75,.25; "C" .17,.67,.17; "D" .25,.75,0; "E": 0,.5,.5; "F" .33,.33,.33; "G": .5,.5,0; "H" 0,.25,.75; "I" .17,.17,.67; "J": .67,.17.,17; "K": .75,.25,0; "L": 0,0,1; "M" .25,0,.75; "N" .5,0,.5; "O" .75,0,.25; "P" 1,0,0
Stated another way, they are: Single-component: "A" – LECy, "L" – SiMCy, "P" – BADCy
LECy rich: "B" 75 LECy / 25 SiMCy; "C" 67 LECy / 17 BADCy / 17 SiMCy; "D" 75 LECy / 25 BADCy
BADCy rich: "J" 67 BADCy / 17 LECy / 17 SiMCy; "K" 75 BADCy / 25 LECy; "O" 75 BADCy / 25 SiMCy
SiMCy rich: "H" 75 SiMCy / 25 LECy; "I" 67 SiMCy / 17 BADCy / 17 LECy; "M" 75 SiMCy / 25 BADCy
Others: "E" 50 LECy / 50 SiMCy; "G" 50 BADCy / 50 LECy; "N" 50 BADCy / 50 SiMCy

Table S3. Meta-analysis of significant deviations from linearity listed in Table S2.

Number of variables for which a significant deviation from linearity was reported:

Comp. Code (category)[a]	In unsmoothed data			In smoothed data			In clusters (smoothed data)[b]		
	+	-	Total	+	-	Total	+	-	Total
A (LECy)	1	2	3	3	1	4			0
B (LECy rich)			0	2		2	1		1
C (LECy rich)			0			0			0
D (LECy rich)	1	3	4		4	4		1	1
E (LECy/SiMCy)		1	1	2	2	4	1	2	3
F (all equal))			0	1	1	2	1	1	2
G (LECy/BADCy)	1		1	1	2	3	1	1	2
H (SiMCy rich)	2	2	4	1	2	3		1	1
I (SiMCy rich)		1	1		2	2		2	2
M (SiMCy rich)	1		1	2	1	3	1	1	2
L (SiMCY)	2	5	7	4	7	11	1		1
N (SiMCy/BADCy)			0	1		1			0
J (BADCy rich)			0		1	1			0
K (BADCy rich)		1	1	1		1			0
O (BADCy rich)	1		1			0			0
P (BADCy)	2		2	3	1	4			0
Sub-totals by category[c]									
50% or more LECy	3	6	9	8	9	17	3	4	7
50% or more SiMCy	5	9	14	10	14	24	3	6	9
50% or more BADCy	4	1	5	6	4	10	1	1	2
0 to 50% LECy	9	10	19	16	19	35	5	8	13
0 to 50% SiMCy	6	7	13	14	12	26	4	5	9
0 to 50% BADCy	8	14	22	17	22	39	6	9	15
Grand totals									
All composition	11	15	26	21	24	45	6	9	15

Notes:
a. A "rich" composition is one in which 60% or greater is of a single component, "(A/B)" compositions denote roughly 50/50 mixtures, and "all equal" denotes mixtures in which all three components are approximately equally represented
b. "Clusters" refers to a set of points on the ternary diagram joined by nearest neighbor connections (see the diagram in the notes below Table S2).
c. Expectation values based on a random distribution are 37.5% of total for the "50% or more" categories, and 75% of total for the "0 to 50%" categories. Specifically, the expectation values are: "50% or more" categories: unsmoothed data: 4.125(+), 5.625(-), 9.75 (total); smoothed data: 7.875(+), 9(-), 16.875(total); in clusters: 2.25(+), 3.375(-), 5.625 (total); "0 to 50%" categories: unsmoothed data 8.25(+), 11.25(-), 19.5(total); smoothed data 15.75(+), 18(-), 33.75(total); in clusters: 4.5(+), 6.75(-), 11.25(total)
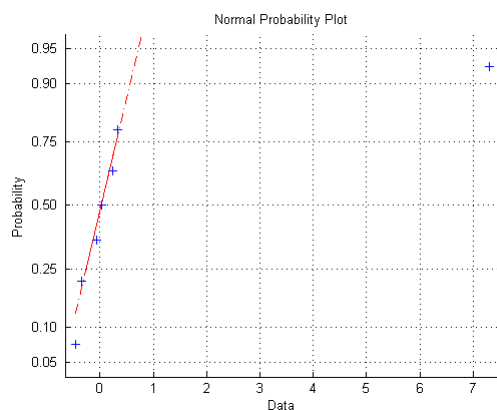
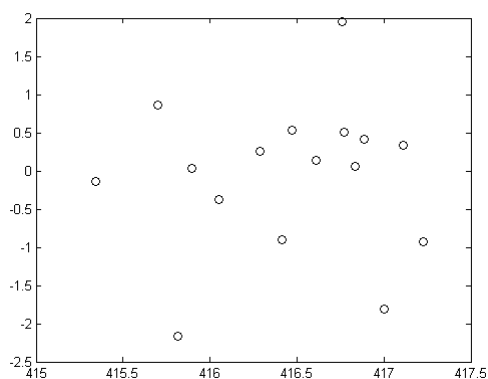**Figure S1.1.** Normal probability plot for variable 1 (DSC melting point). Studentized residuals are plotted on the x-axis.
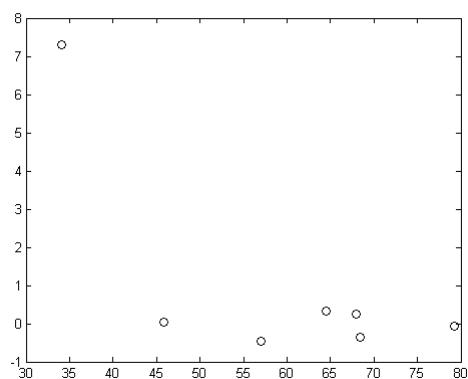
Figure S2.1. Residual plot for variable 1 (DSC melting point). Predicted values (in °C) are plotted on the x-axis and Studentized residuals on the y-axis.
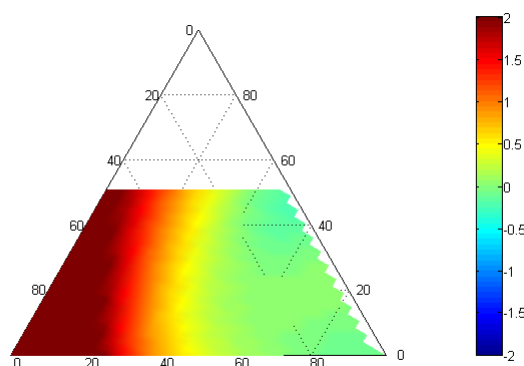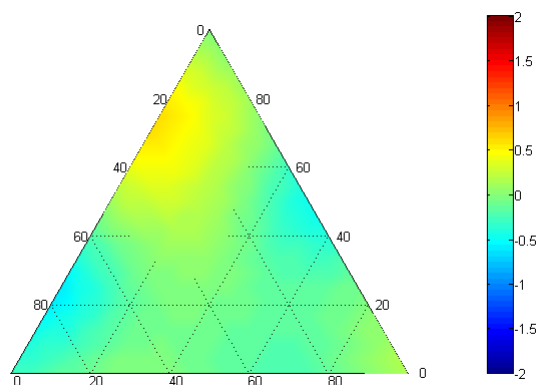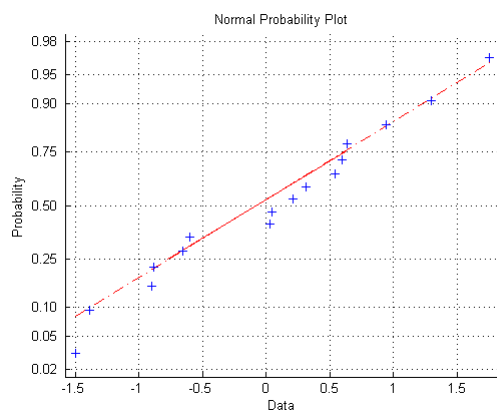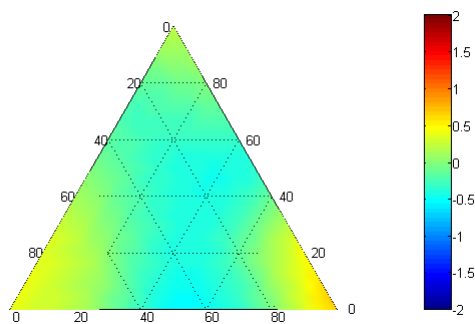

Figure S3.1. Smoothed Studentized residuals (colormap) as a function of composition for variable 1 (DSC melting point). The ternary diagram vertices are lower right: BADCy, lower left: SiMCy, top: LECy
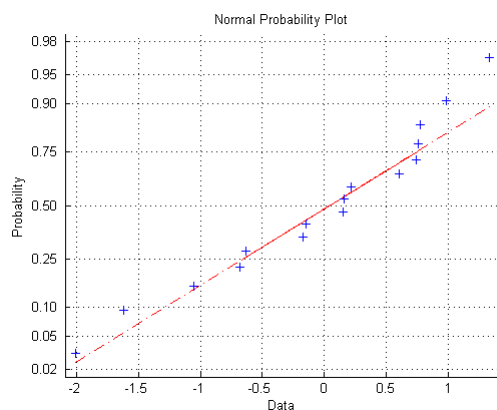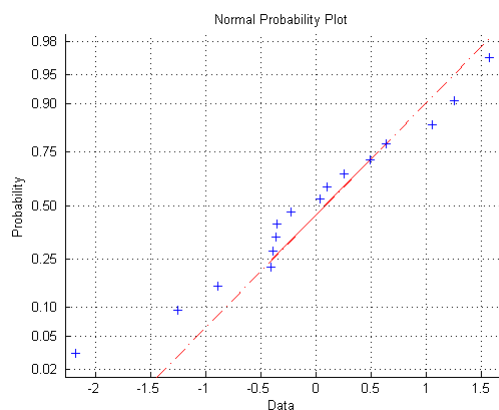
Figure S1.2. Normal probability plot for variable 2 (DSC enthalpy of cure). Studentized residuals are plotted on the x-axis.
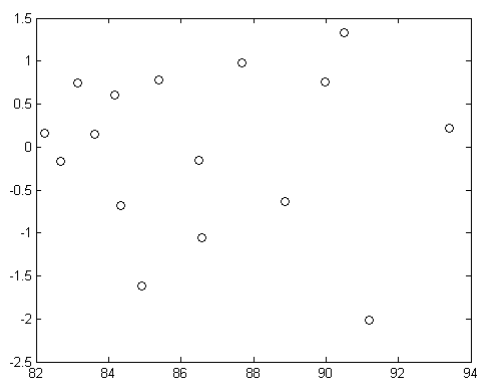
Figure S2.2. Residual plot for variable 2 (DSC enthalpy of cure). Predicted values (in kJ/mol) are plotted on the x-axis and Studentized residuals on the y-axis.
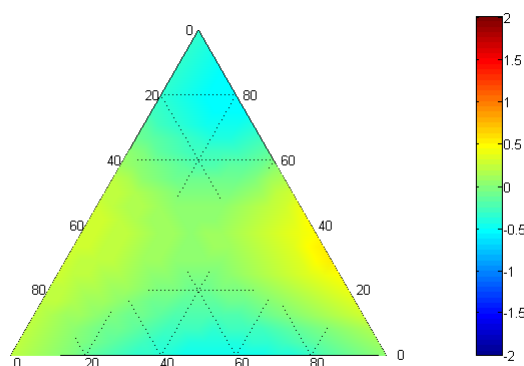
Figure S3.2. Smoothed Studentized residuals (colormap) as a function of composition for variable 2 (DSC enthalpy of cure). The ternary diagram vertices are lower right: BADCy, lower left: SiMCy, top: LECy
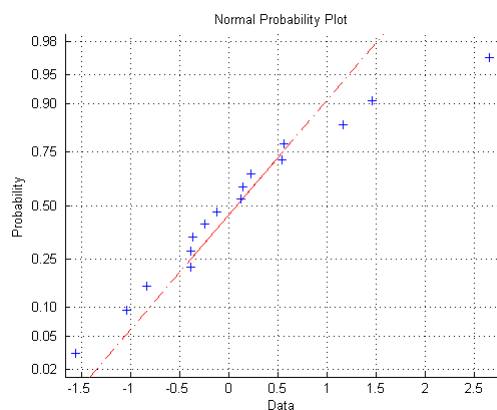
Figure S1.3. Normal probability plot for variable 3 (DSC peak exotherm temperature). Studentized residuals are plotted on the x-axis.
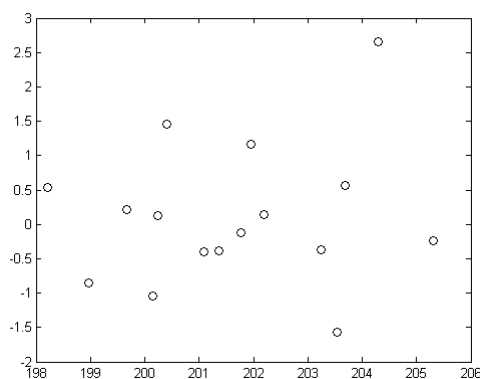
Figure S2.3. Residual plot for variable 3 (DSC peak exotherm temperature). Predicted values (in °C) are plotted on the x-axis and Studentized residuals on the y-axis.
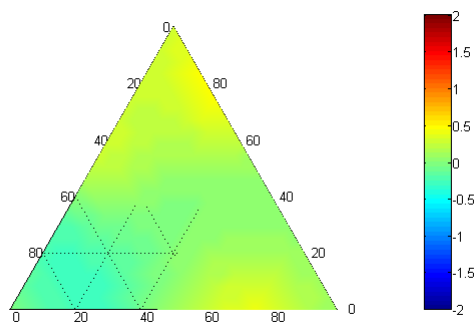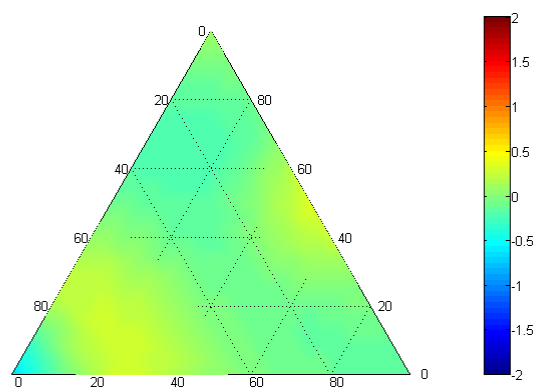

Figure S3.3. Smoothed Studentized residuals (colormap) as a function of composition for variable 3 (DSC peak exotherm temperature). The ternary diagram vertices are lower right: BADCy, lower left: SiMCy, top: LECy
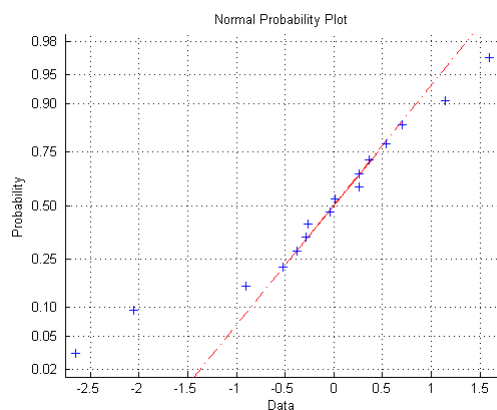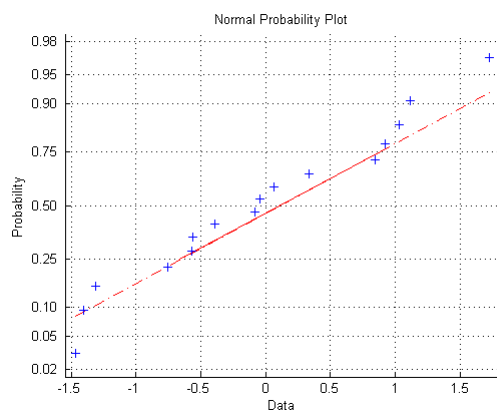
Figure S1.4. Normal probability plot for variable 4 (DSC post-cure T_g). Studentized residuals are plotted on the x-axis.
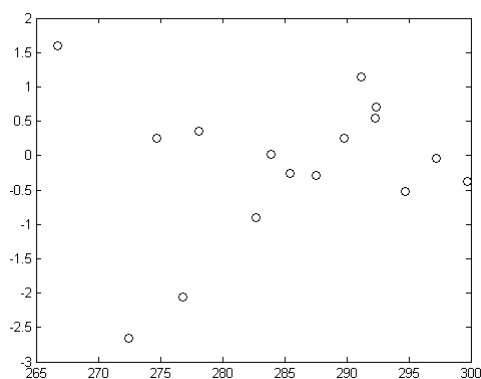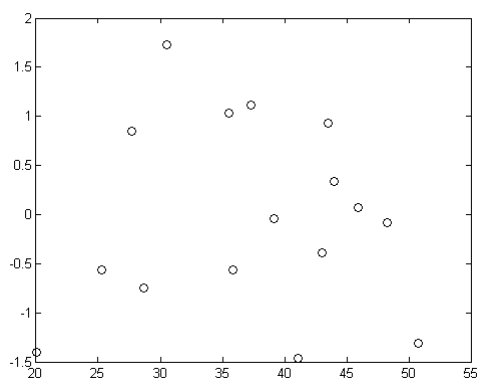

Figure S2.4. Residual plot for variable 4 (DSC post-cure T_g). Predicted values (in °C) are plotted on the x-axis and Studentized residuals on the y-axis.
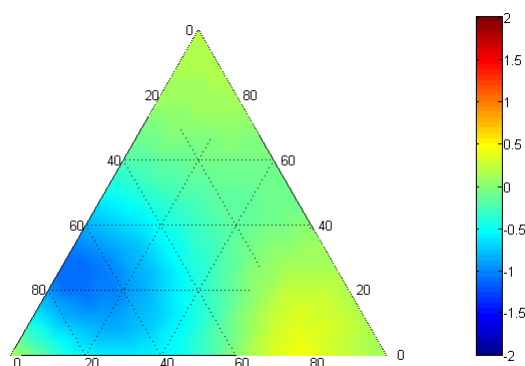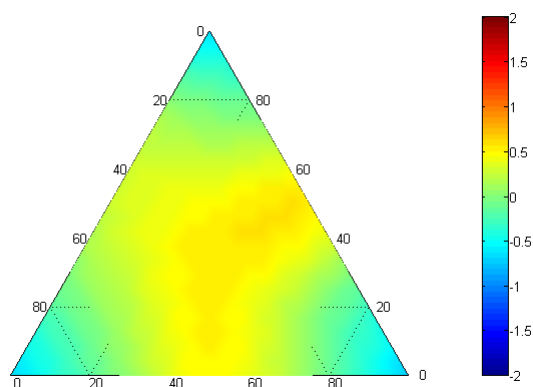

Figure S3.4. Smoothed Studentized residuals (colormap) as a function of composition for variable 4 (DSC post-cure T_g). The ternary diagram vertices are lower right: BADCy, lower left: SiMCy, top: LECy
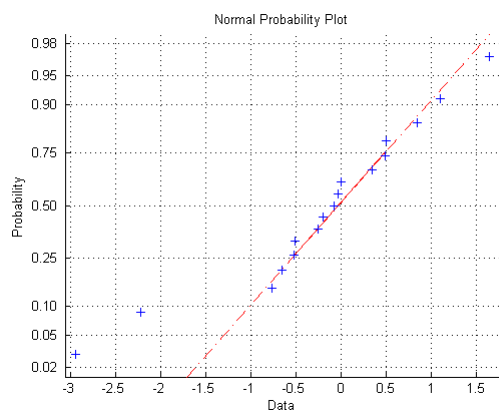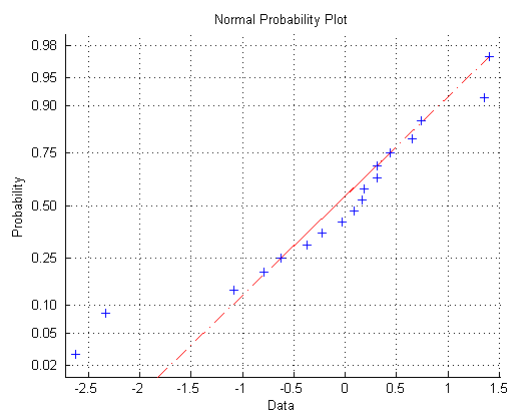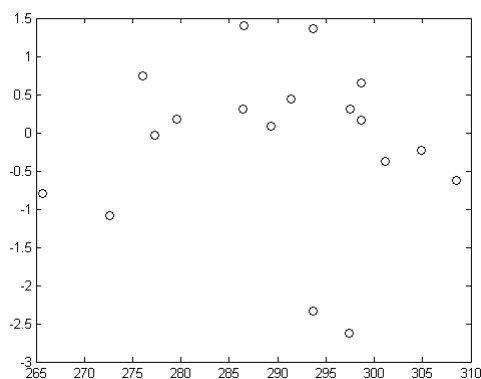
Figure S1.5. Normal probability plot for variable 5 (TGA-N$_2$ onset of decomposition). Studentized residuals are plotted on the x-axis.
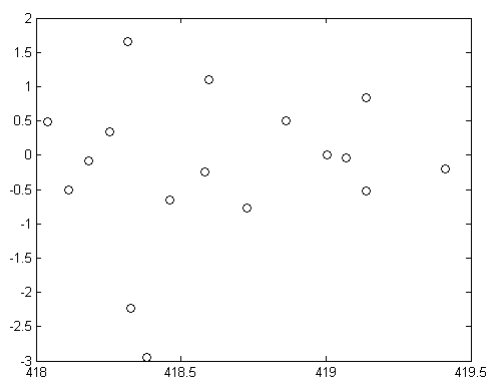
Figure S2.5. Residual plot for variable 5 (TGA-N$_2$ onset of decomposition). Predicted values (in °C) are plotted on the x-axis and Studentized residuals on the y-axis.
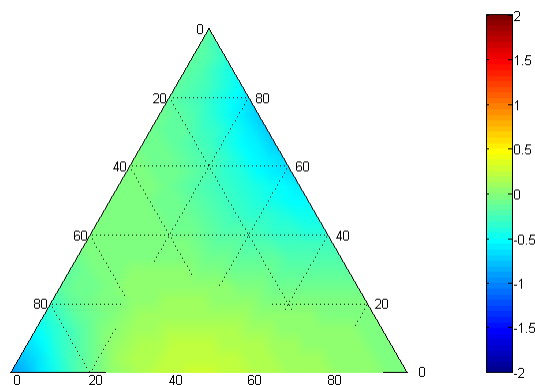
Figure S3.5. Smoothed Studentized residuals (colormap) as a function of composition for variable 5 (TGA-N$_2$ onset of decomposition). The ternary diagram vertices are lower right: BADCy, lower left: SiMCy, top: LECy
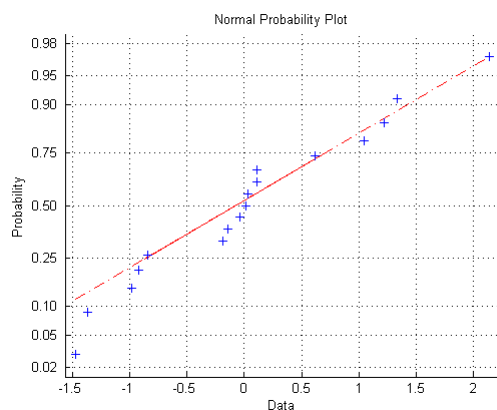
Figure S1.6. Normal probability plot for variable 6 (TGA-N$_2$ peak decomposition rate). Studentized residuals are plotted on the x-axis.
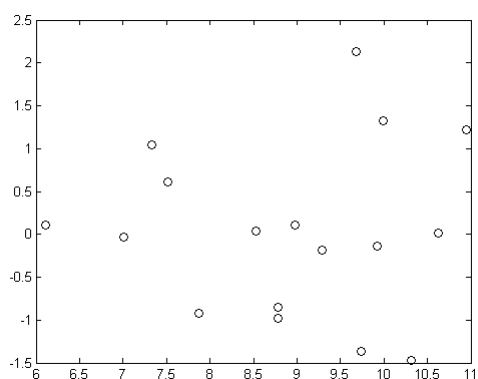
Figure S2.6. Residual plot for variable 6 (TGA-N$_2$ peak decomposition rate). Predicted values (in %/min.) are plotted on the x-axis and Studentized residuals on the y-axis.
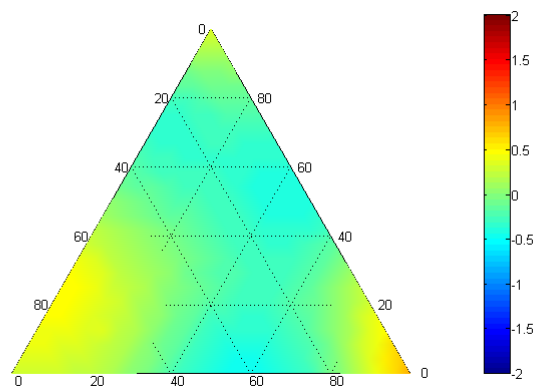
Figure S3.6. Smoothed Studentized residuals (colormap) as a function of composition for variable 6 (TGA-N$_2$ peak decomposition rate). The ternary diagram vertices are lower right: BADCy, lower left: SiMCy, top: LECy
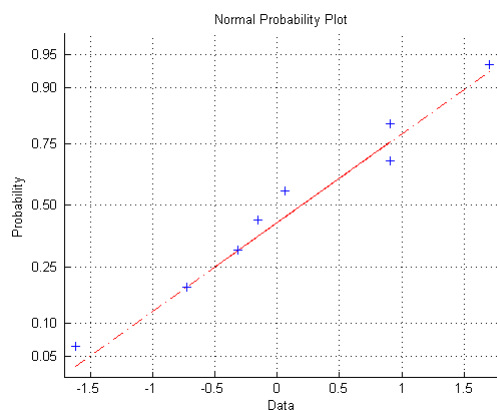
Figure S1.7. Normal probability plot for variable 7 (TGA-N$_2$ secondary peak decomposition rate). Studentized residuals are plotted on the x-axis.
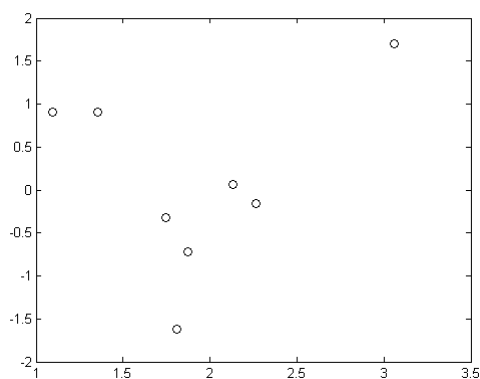
Figure S2.7. Residual plot for variable 7 (TGA-N$_2$ secondary peak decomposition rate). Predicted values (in %/min.) are plotted on the x-axis and Studentized residuals on the y-axis.
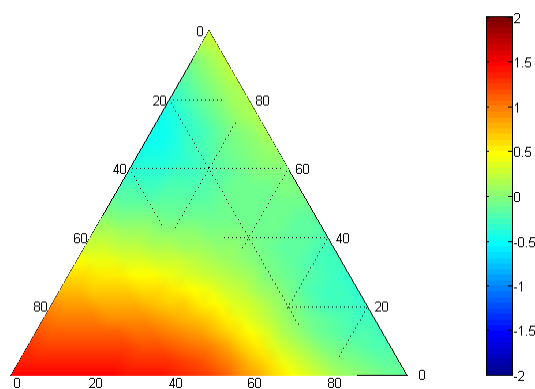
Figure S3.7. Smoothed Studentized residuals (colormap) as a function of composition for variable 7 (TGA-N$_2$ secondary peak decomposition rate). The ternary diagram vertices are lower right: BADCy, lower left: SiMCy, top: LECy
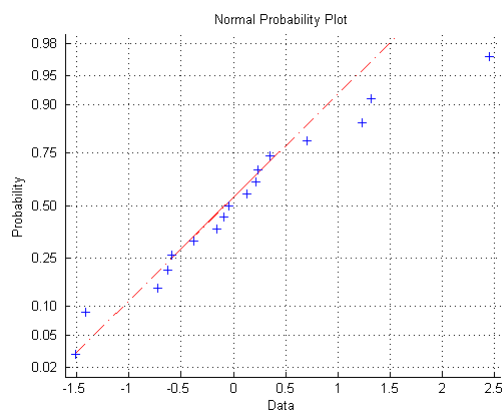
Figure S1.8. Normal probability plot for variable 8 (TGA-N$_2$ peak decomposition temperature). Studentized residuals are plotted on the x-axis.
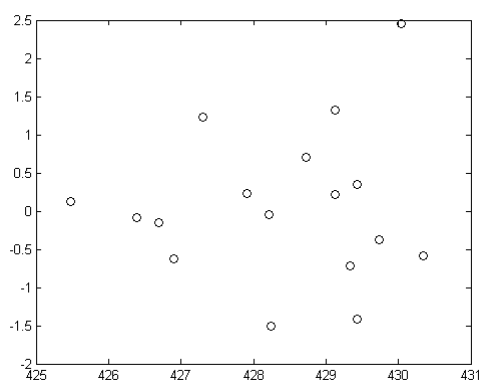
Figure S2.8. Residual plot for variable 8 (TGA-N$_2$ peak decomposition temperature). Predicted values (in °C) are plotted on the x-axis and Studentized residuals on the y-axis.
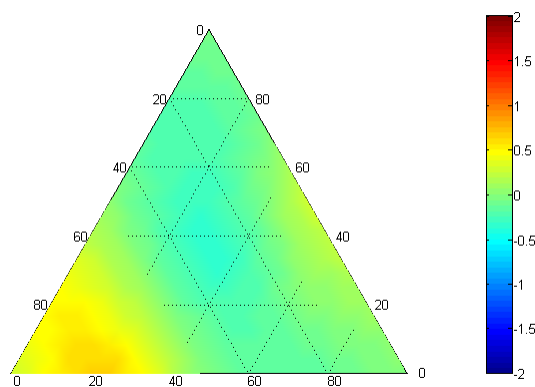
Figure S3.8. Smoothed Studentized residuals (colormap) as a function of composition for variable 8 (TGA-N$_2$ peak decomposition temperature). The ternary diagram vertices are lower right: BADCy, lower left: SiMCy, top: LECy
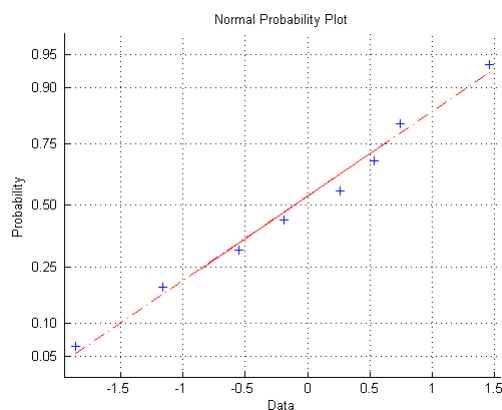
Figure S1.9. Normal probability plot for variable 9 (TGA-N$_2$ secondary peak decomposition temperature). Studentized residuals are plotted on the x-axis.
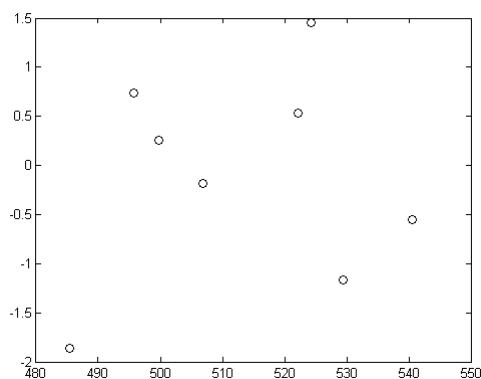
Figure S2.9. Residual plot for variable 9 (TGA-N$_2$ secondary peak decomposition temperature). Predicted values (in °C) are plotted on the x-axis and Studentized residuals on the y-axis.
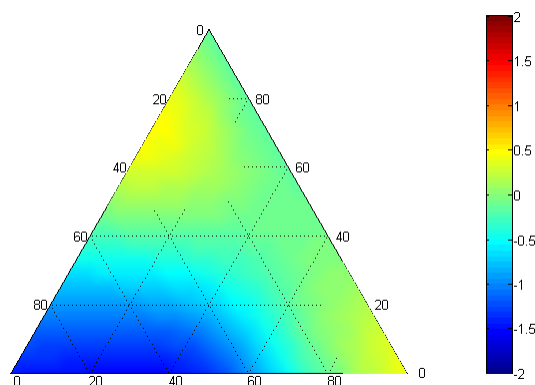
Figure S3.9. Smoothed Studentized residuals (colormap) as a function of composition for variable 9 (TGA-N$_2$ secondary peak decomposition temperature). The ternary diagram vertices are lower right: BADCy, lower left: SiMCy, top: LECy
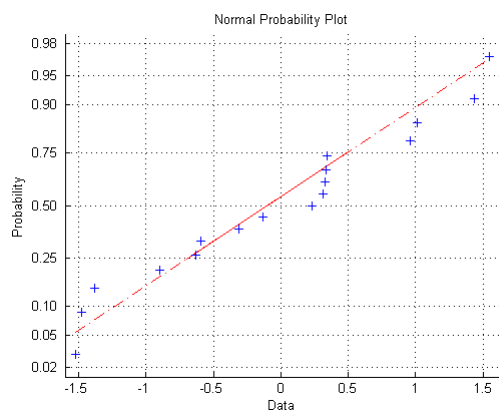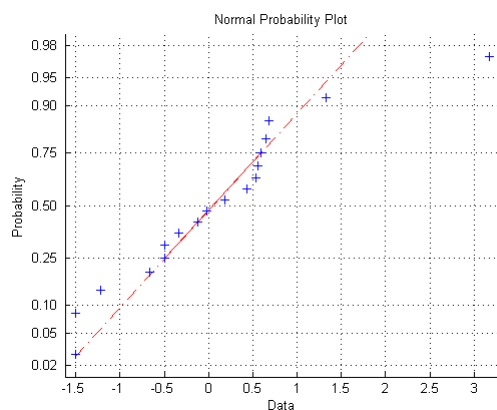
Figure S1.10. Normal probability plot for variable 10 (TGA-N$_2$ char yield). Studentized residuals are plotted on the x-axis.
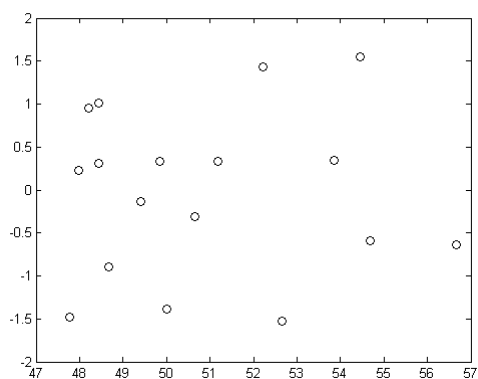
Figure S2.10. Residual plot for variable 10 (TGA-N$_2$ char yield). Predicted values (in wt%) are plotted on the x-axis and Studentized residuals on the y-axis.
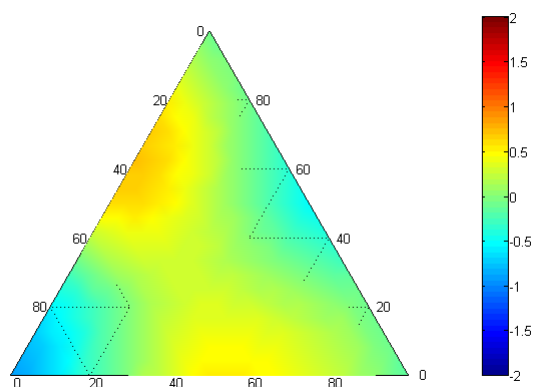
Figure S3.10. Smoothed Studentized residuals (colormap) as a function of composition for variable 10 (TGA-N$_2$ char yield). The ternary diagram vertices are lower right: BADCy, lower left: SiMCy, top: LECy

46
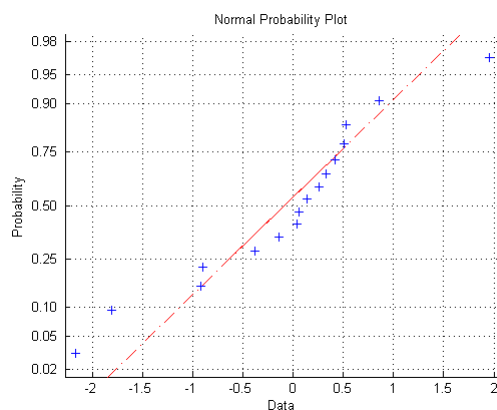
Figure S1.11. Normal probability plot for variable 11 (TGA-Air onset of decomposition). Studentized residuals are plotted on the x-axis.

Figure S2.11. Residual plot for variable 11 (TGA-Air onset of decomposition). Predicted values (in °C) are plotted on the x-axis and Studentized residuals on the y-axis.
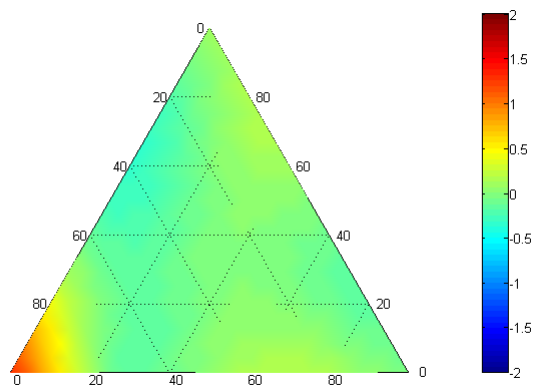

Figure S3.11. Smoothed Studentized residuals (colormap) as a function of composition for variable 11 (TGA-Air onset of decomposition). The ternary diagram vertices are lower right: BADCy, lower left: SiMCy, top: LECy
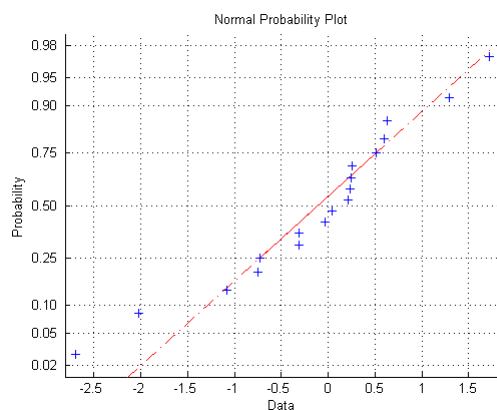
47

Figure S1.12. Normal probability plot for variable 12 (TGA-Air peak decomposition rate). Studentized residuals are plotted on the x-axis.
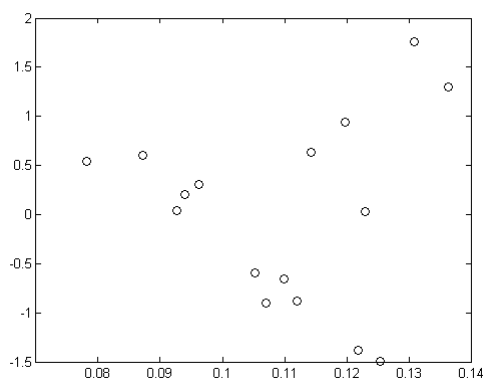
Figure S2.12. Residual plot for variable 12 (TGA-Air peak decomposition rate). Predicted values (in %/min.) are plotted on the x-axis and Studentized residuals on the y-axis.

Figure S3.12. Smoothed Studentized residuals (colormap) as a function of composition for variable 12 (TGA-Air peak decomposition rate). The ternary diagram vertices are lower right: BADCy, lower left: SiMCy, top: LECy
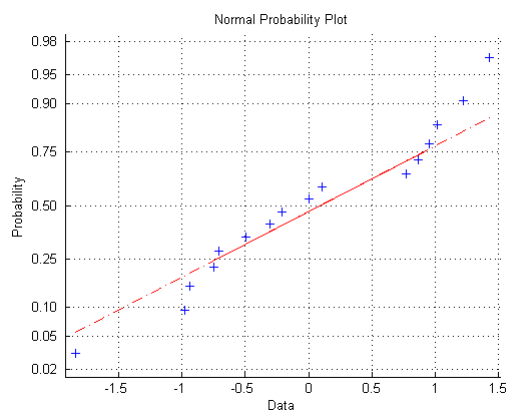
Figure S1.13. Normal probability plot for variable 13 (TGA-Air secondary peak decomposition rate). Studentized residuals are plotted on the x-axis.
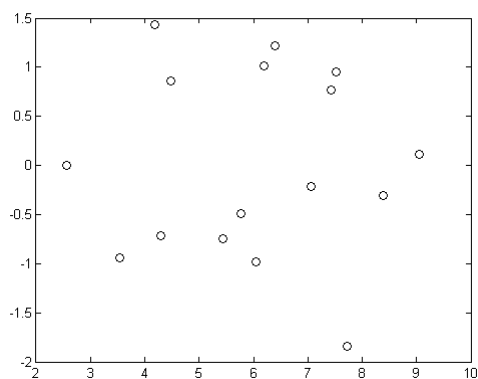
Figure S2.13. Residual plot for variable 13 (TGA-Air secondary peak decomposition rate). Predicted values (in %/min.) are plotted on the x-axis and Studentized residuals on the y-axis.
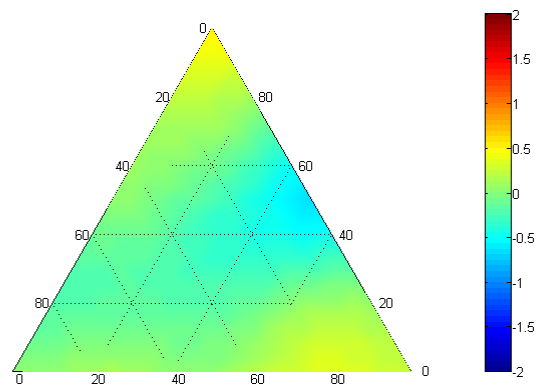
Figure S3.13. Smoothed Studentized residuals (colormap) as a function of composition for variable 13 (TGA-Air secondary peak decomposition rate). The ternary diagram vertices are lower right: BADCy, lower left: SiMCy, top: LECy

Figure S1.14. Normal probability plot for variable 14 (TGA-Air primary peak decomposition temperature). Studentized residuals are plotted on the x-axis.
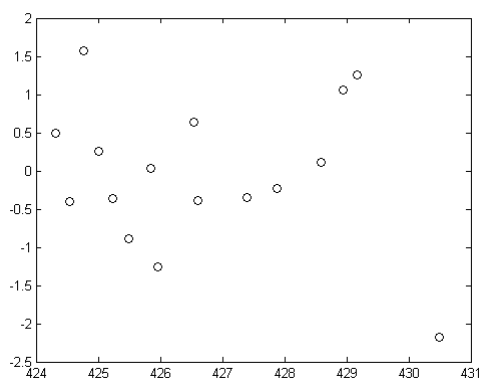
Figure S2.14. Residual plot for variable 14 (TGA-Air primary peak decomposition temperature). Predicted values (in °C) are plotted on the x-axis and Studentized residuals on the y-axis.

Figure S3.14. Smoothed Studentized residuals (colormap) as a function of composition for variable 14 (TGA-Air primary peak decomposition temperature). The ternary diagram vertices are lower right: BADCy, lower left: SiMCy, top: LECy

Figure S1.15. Normal probability plot for variable 15 (TGA-Air char yield). Studentized residuals are plotted on the x-axis.

Figure S2.15. Residual plot for variable 15 (TGA-Air char yield). Predicted values (in wt%) are plotted on the x-axis and Studentized residuals on the y-axis.

Figure S3.15. Smoothed Studentized residuals (colormap) as a function of composition for variable 15 (TGA-Air char yield). The ternary diagram vertices are lower right: BADCy, lower left: SiMCy, top: LECy

Figure S1.16. Normal probability plot for variable 16 (TMA-Dry fully-cured T_g, loss peak). Studentized residuals are plotted on the x-axis.
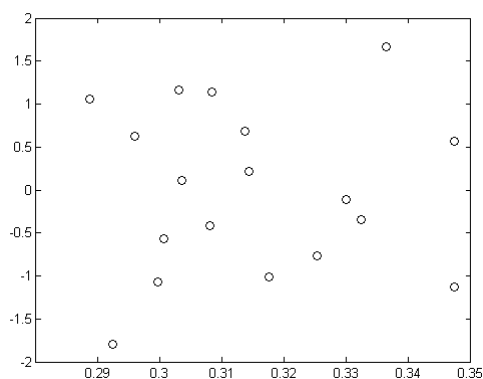

Figure S2.16. Residual plot for variable 16 (TMA-Dry fully-cured T_g, loss peak). Predicted values (in °C) are plotted on the x-axis and Studentized residuals on the y-axis.
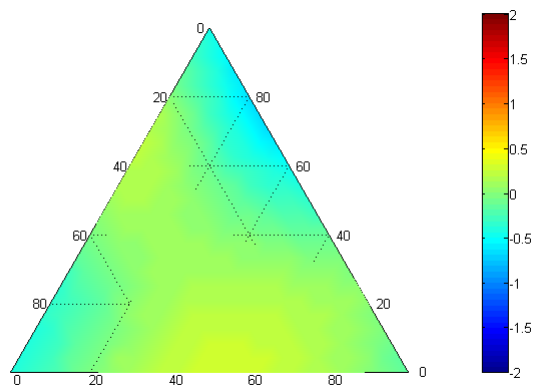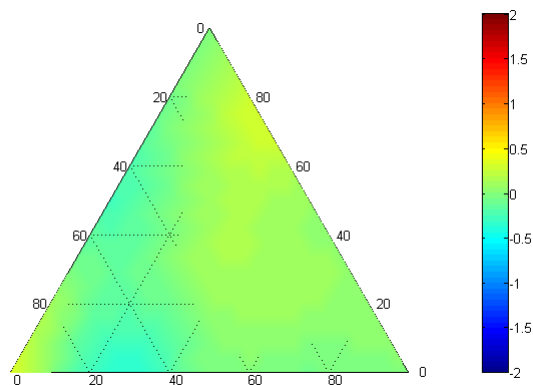

Figure S3.16. Smoothed Studentized residuals (colormap) as a function of composition for variable 16 (TMA-Dry fully-cured T_g, loss peak). The ternary diagram vertices are lower right: BADCy, lower left: SiMCy, top: LECy
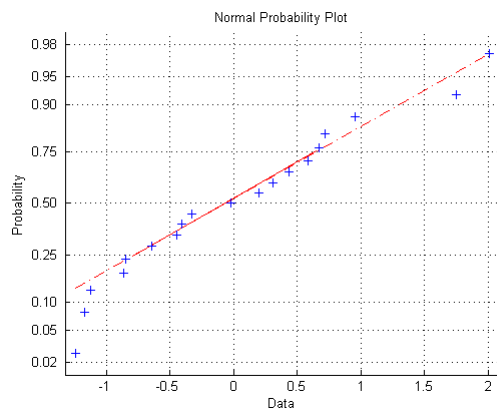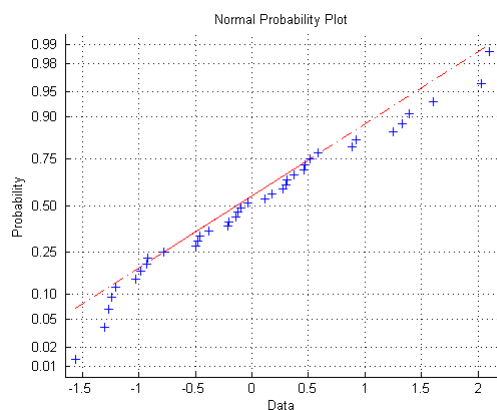
Figure S1.17. Normal probability plot for variable 17 (TMA-Dry as-cured T_g, loss peak). Studentized residuals are plotted on the x-axis.
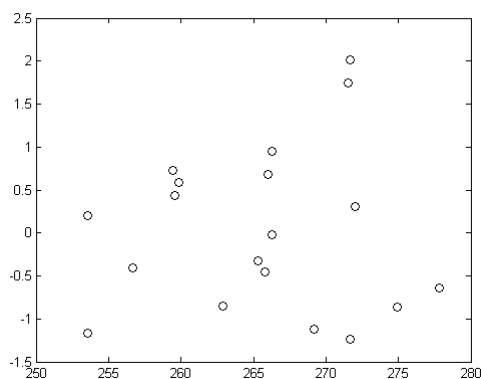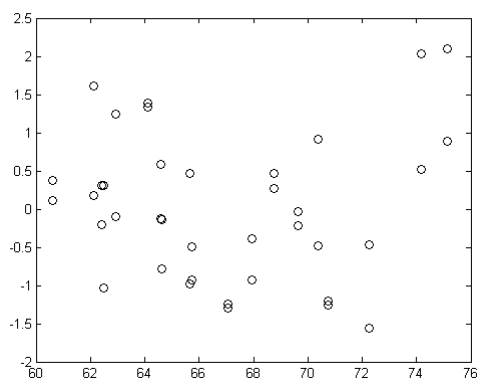

Figure S2.17. Residual plot for variable 17 (TMA-Dry as-cured T_g, loss peak). Predicted values (in °C) are plotted on the x-axis and Studentized residuals on the y-axis.
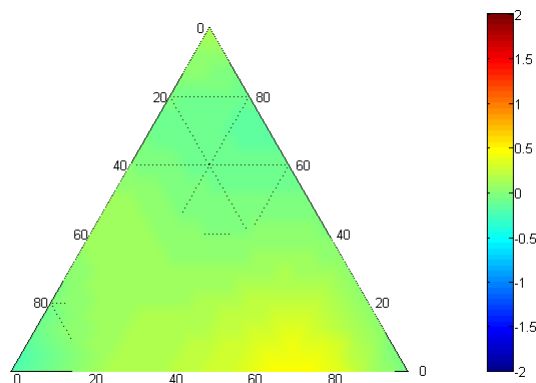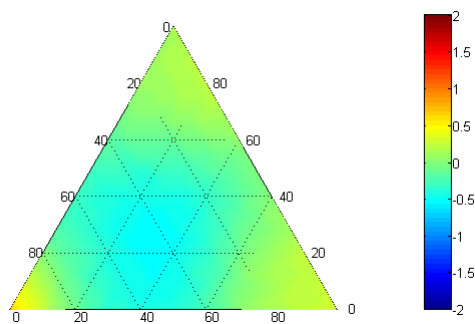

Figure S3.17. Smoothed Studentized residuals (colormap) as a function of composition for variable 17 (TMA-Dry as-cured T_g, loss peak). The ternary diagram vertices are lower right: BADCy, lower left: SiMCy, top: LECy

53
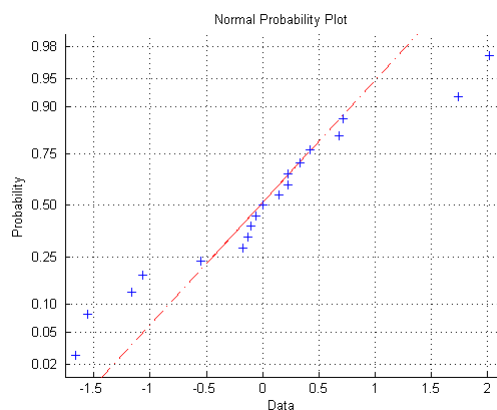
Figure S1.18. Normal probability plot for variable 18 (TMA-Dry as-cured tan delta peak value). Studentized residuals are plotted on the x-axis.
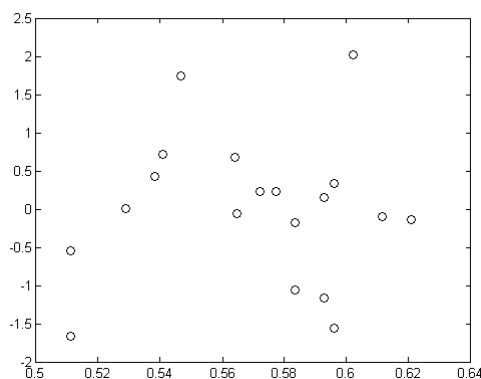
Figure S2.18. Residual plot for variable 18 (TMA-Dry as-cured tan delta peak value). Predicted values (dimensionless) are plotted on the x-axis and Studentized residuals on the y-axis.
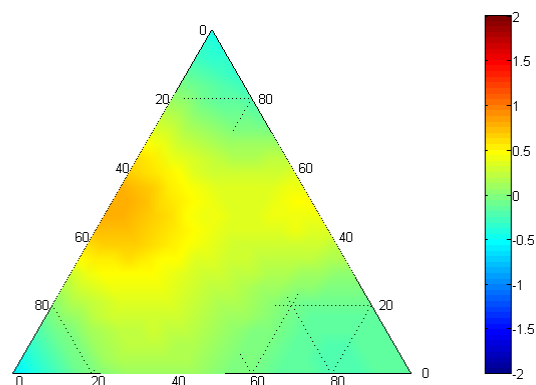
Figure S3.18. Smoothed Studentized residuals (colormap) as a function of composition for variable 18 (TMA-Dry as-cured tan delta peak value). The ternary diagram vertices are lower right: BADCy, lower left: SiMCy, top: LECy
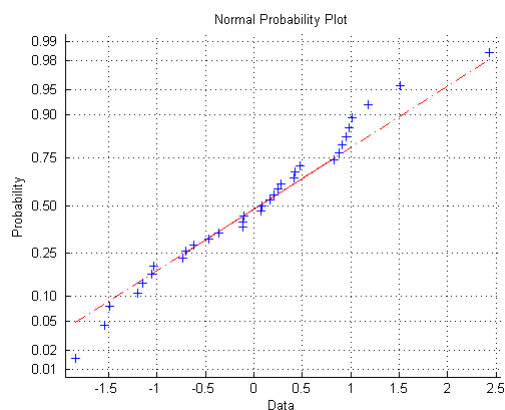
Figure S1.19. Normal probability plot for variable 19 (TMA-Dry as-cured stiffness ratio). Studentized residuals are plotted on the x-axis.
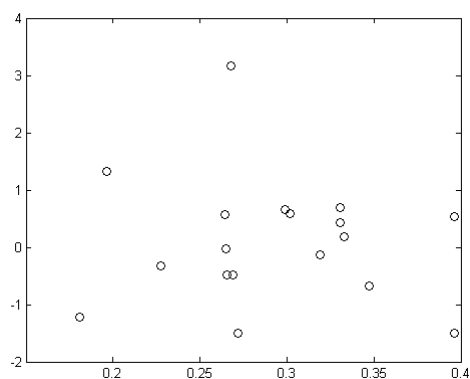
Figure S2.19. Residual plot for variable 19 (TMA-Dry as-cured stiffness ratio). Predicted values (dimensionless) are plotted on the x-axis and Studentized residuals on the y-axis.

Figure S3.19. Smoothed Studentized residuals (colormap) as a function of composition for variable 19 (TMA-Dry as-cured stiffness ratio). The ternary diagram vertices are lower right: BADCy, lower left: SiMCy, top: LECy

Figure S1.20. Normal probability plot for variable 20 (TMA-Dry fully-cured T_g, tan delta). Studentized residuals are plotted on the x-axis.
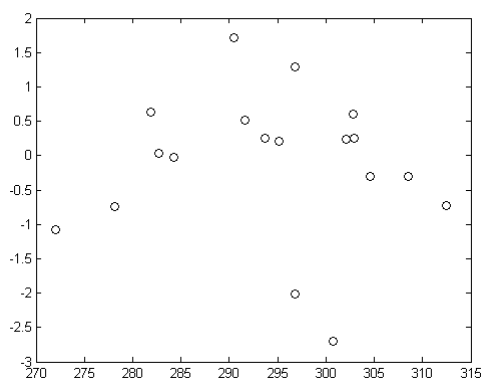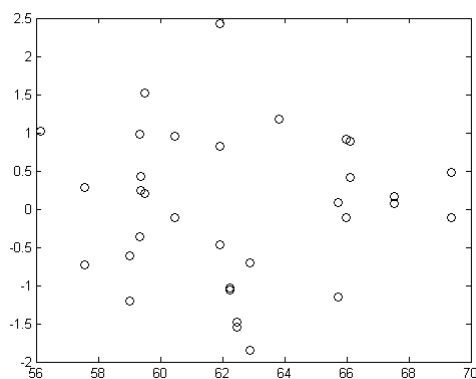

Figure S2.20. Residual plot for variable 20 (TMA-Dry fully-cured T_g, tan delta). Predicted values (in °C) are plotted on the x-axis and Studentized residuals on the y-axis.
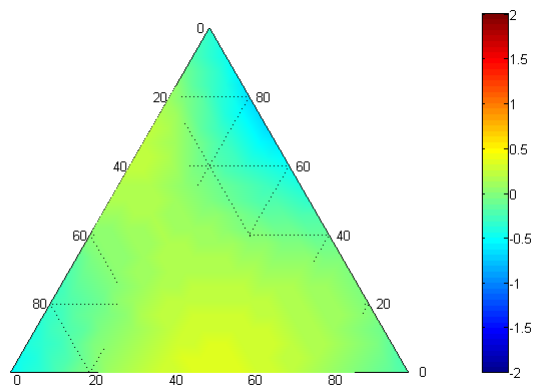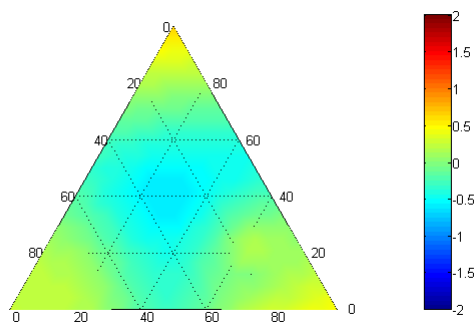

Figure S3.20. Smoothed Studentized residuals (colormap) as a function of composition for variable 20 (TMA-Dry fully-cured T_g, tan delta). The ternary diagram vertices are lower right: BADCy, lower left: SiMCy, top: LECy
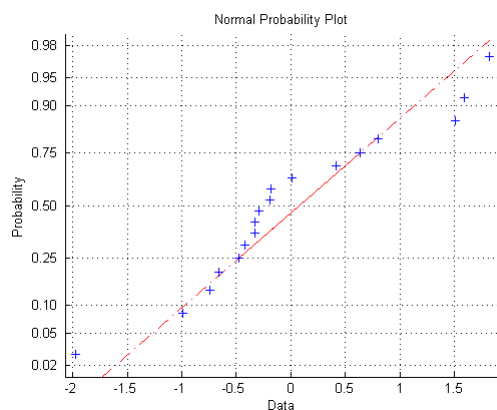
56
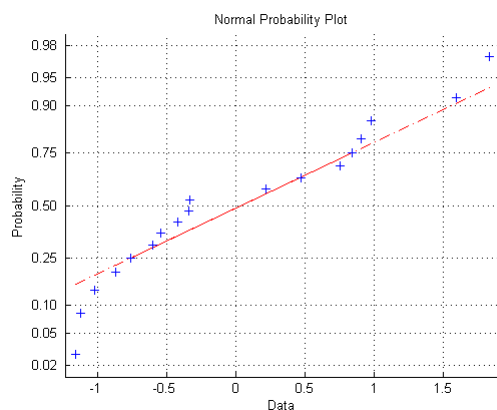
Figure S1.21. Normal probability plot for variable 21 (TMA-Dry fully-cured peak value of tan delta). Studentized residuals are plotted on the x-axis.
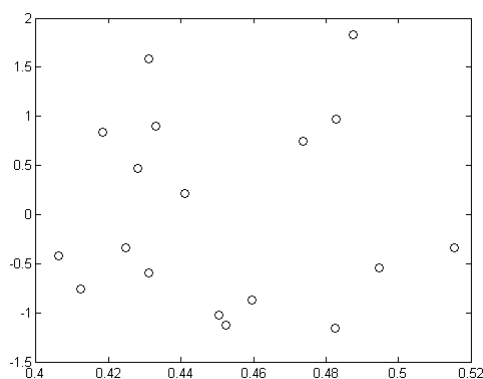
Figure S2.21. Residual plot for variable 21 (TMA-Dry fully-cured peak value of tan delta). Predicted values (dimensionless) are plotted on the x-axis and Studentized residuals on the y-axis.
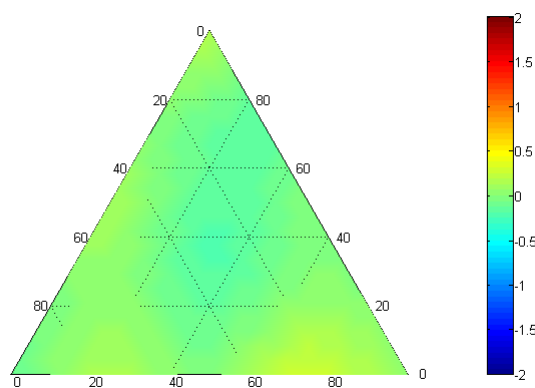
Figure S3.21. Smoothed Studentized residuals (colormap) as a function of composition for variable 21 (TMA-Dry fully-cured peak value of tan delta). The ternary diagram vertices are lower right: BADCy, lower left: SiMCy, top: LECy

57
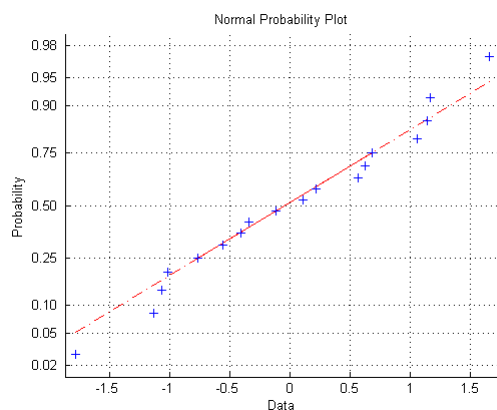
Figure S1.22. Normal probability plot for variable 22 (TMA-Dry fully-cured stiffness ratio). Studentized residuals are plotted on the x-axis.

Figure S2.22. Residual plot for variable 22 (TMA-Dry fully-cured stiffness ratio). Predicted values (dimensionless) are plotted on the x-axis and Studentized residuals on the y-axis.

Figure S3.22. Smoothed Studentized residuals (colormap) as a function of composition for variable 22 (TMA-Dry fully-cured stiffness ratio). The ternary diagram vertices are lower right: BADCy, lower left: SiMCy, top: LECy

Figure S1.23. Normal probability plot for variable 23 (TMA-Dry as-cured CTE). Studentized residuals are plotted on the x-axis.

Figure S2.23. Residual plot for variable 23 (TMA-Dry as-cured CTE). Predicted values (in ppm/ °C) are plotted on the x-axis and Studentized residuals on the y-axis.

Figure S3.23. Smoothed Studentized residuals (colormap) as a function of composition for variable 23 (TMA-Dry as-cured CTE). The ternary diagram vertices are lower right: BADCy, lower left: SiMCy, top: LECy
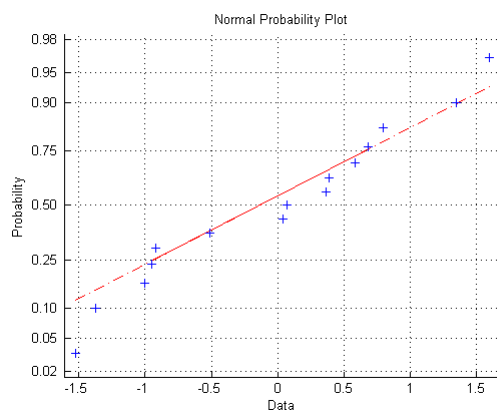
59

Figure S1.24. Normal probability plot for variable 24 (TMA-Dry fully-cured CTE). Studentized residuals are plotted on the x-axis.

Figure S2.24. Residual plot for variable 24 (TMA-Dry fully-cured CTE). Predicted values (in ppm/ °C) are plotted on the x-axis and Studentized residuals on the y-axis.

Figure S3.24. Smoothed Studentized residuals (colormap) as a function of composition for variable 24 (TMA-Dry fully-cured CTE). The ternary diagram vertices are lower right: BADCy, lower left: SiMCy, top: LECy

Figure S1.25. Normal probability plot for variable 25 (TMA-Wet T_g, loss peak). Studentized residuals are plotted on the x-axis.
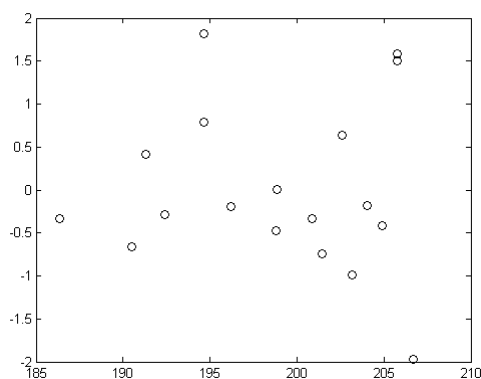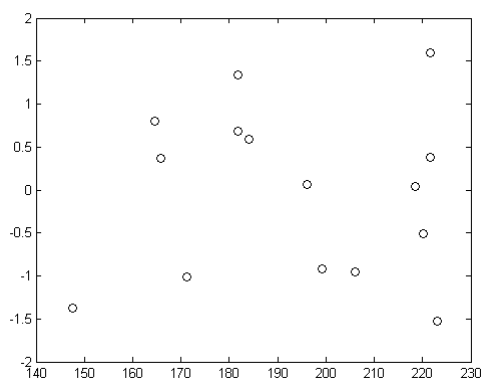

Figure S2.25. Residual plot for variable 25 (TMA-Wet T_g, loss peak). Predicted values (in °C) are plotted on the x-axis and Studentized residuals on the y-axis.
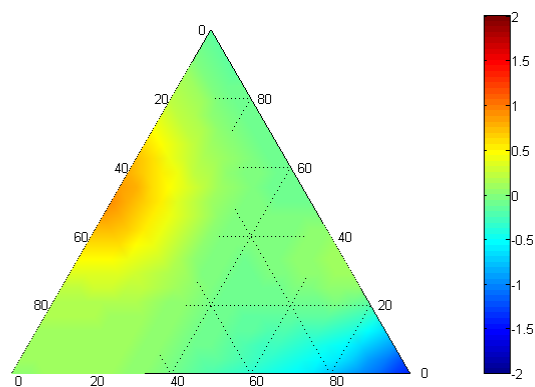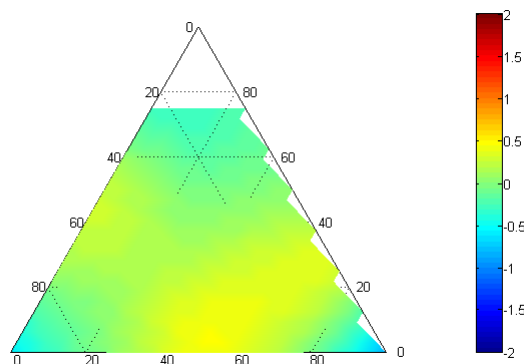

Figure S3.25. Smoothed Studentized residuals (colormap) as a function of composition for variable 25 (TMA-Wet T_g, loss peak). The ternary diagram vertices are lower right: BADCy, lower left: SiMCy, top: LECy
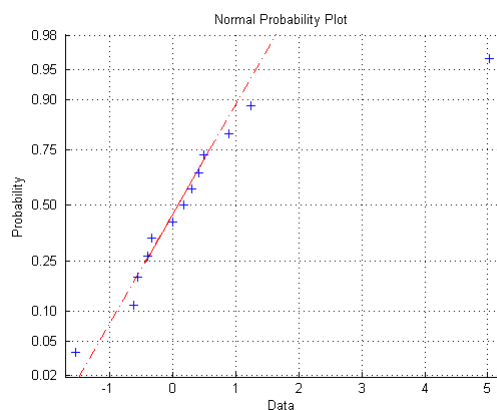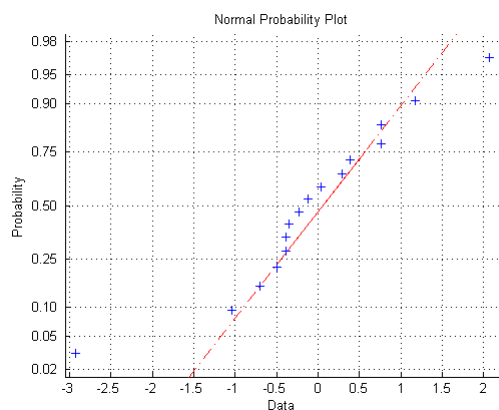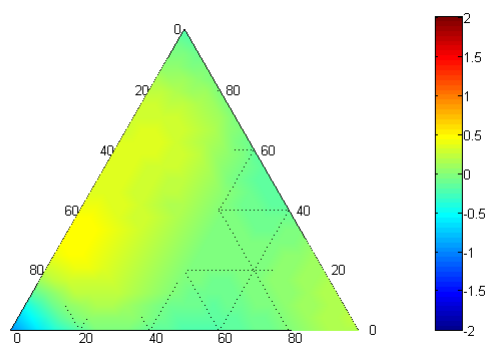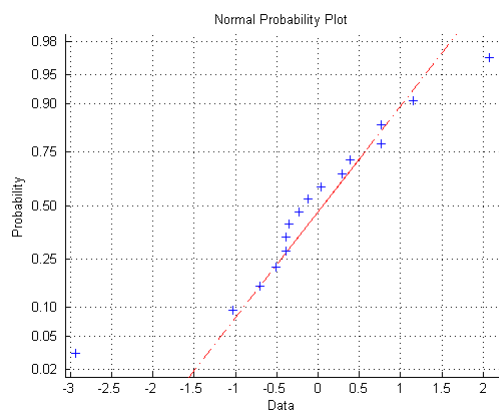
Figure S1.25a. Normal probability plot for regression 25a (TMA-Wet T_g from Dry T_g, Moisture Uptake). Studentized residuals are plotted on the x-axis.
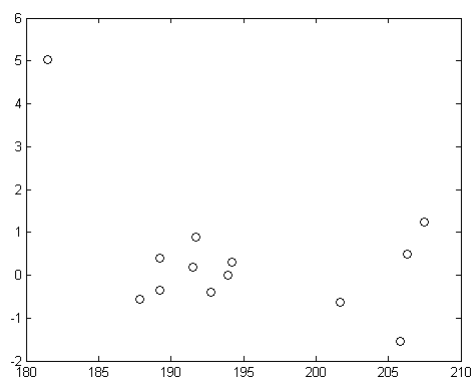
Figure S2.25a. Residual plot for regression 25a (TMA-Wet T_g from Dry T_g, Moisture Uptake). Predicted values (in °C) are plotted on the x-axis and Studentized residuals on the y-axis.
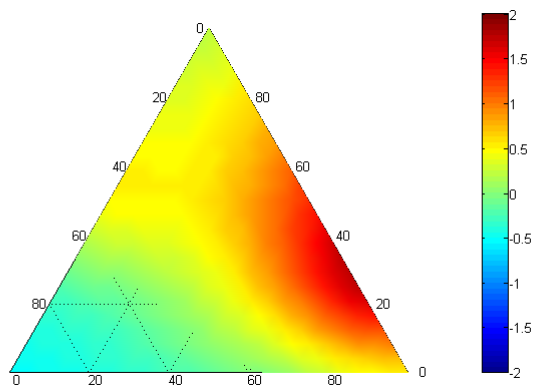
Figure S3.25a. Smoothed Studentized residuals (colormap) as a function of composition for regression 25a (TMA-Wet T_g from Dry T_g, Moisture Uptake). The ternary diagram vertices are lower right: BADCy, lower left: SiMCy, top: LECy

Figure S1.26. Normal probability plot for variable 26 (TMA-Wet Re-heated T_g, loss peak). Studentized residuals are plotted on the x-axis.

Figure S2.26. Residual plot for variable 26 (TMA-Wet Re-heated T_g, loss peak). Predicted values (in °C) are plotted on the x-axis and Studentized residuals on the y-axis.

Figure S3.26. Smoothed Studentized residuals (colormap) as a function of composition for variable 26 (TMA-Wet Re-heated T_g, loss peak). The ternary diagram vertices are lower right: BADCy, lower left: SiMCy, top: LECy

Figure S1.27. Normal probability plot for variable 27 (Density at 20 °C). Studentized residuals are plotted on the x-axis.
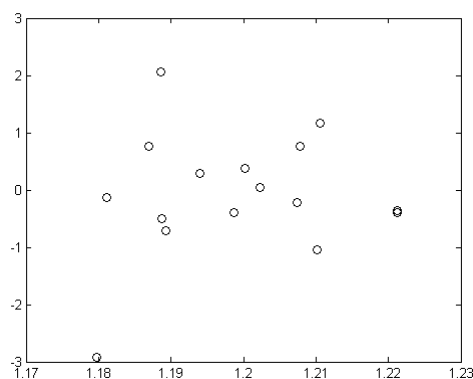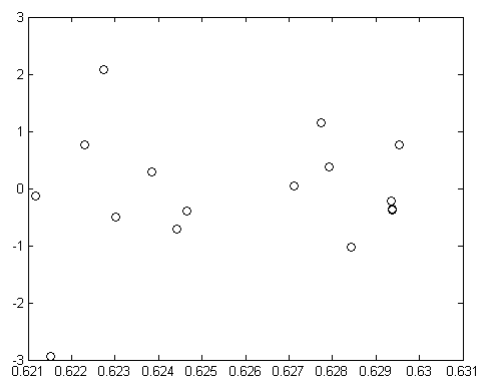

Figure S2.27. Residual plot for variable 27 (Density at 20 °C). Predicted values (in g/cc) are plotted on the x-axis and Studentized residuals on the y-axis.
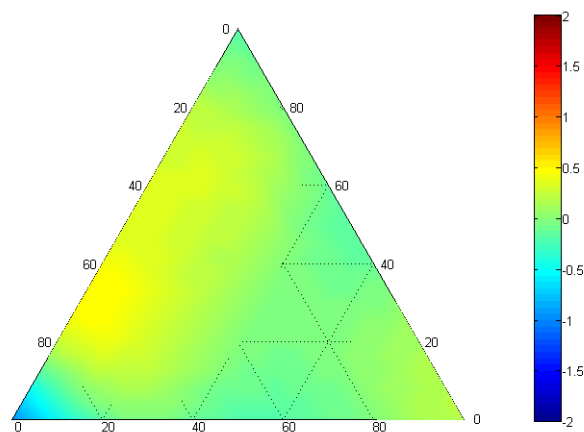

Figure S3.27. Smoothed Studentized residuals (colormap) as a function of composition for variable 27 (Density at 20 °C). The ternary diagram vertices are lower right: BADCy, lower left: SiMCy, top: LECy
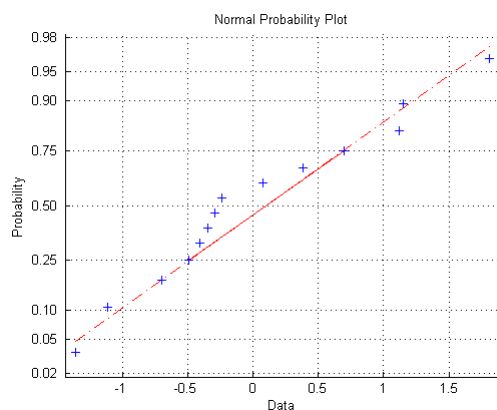
64

Figure S1.28. Normal probability plot for variable 28 (Packing fraction at 20 °C). Studentized residuals are plotted on the x-axis.

Figure S2.28. Residual plot for variable 28 (Packing fraction at 20 °C). Predicted values (dimensionless) are plotted on the x-axis and Studentized residuals on the y-axis.

Figure S3.28. Smoothed Studentized residuals (colormap) as a function of composition for variable 28 (Packing fraction at 20 °C). The ternary diagram vertices are lower right: BADCy, lower left: SiMCy, top: LECy

Figure S1.29. Normal probability plot for variable 29 (Packing fraction at 0 K). Studentized residuals are plotted on the x-axis.
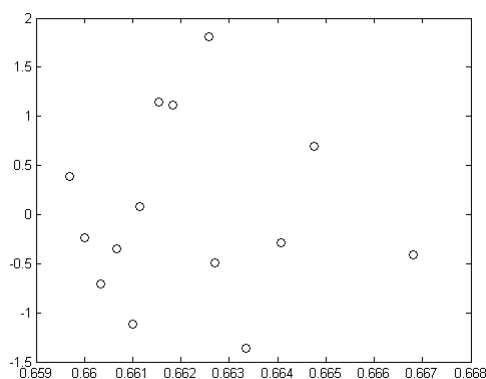

Figure S2.29. Residual plot for variable 29 (Packing fraction at 0 K). Predicted values (dimensionless) are plotted on the x-axis and Studentized residuals on the y-axis.
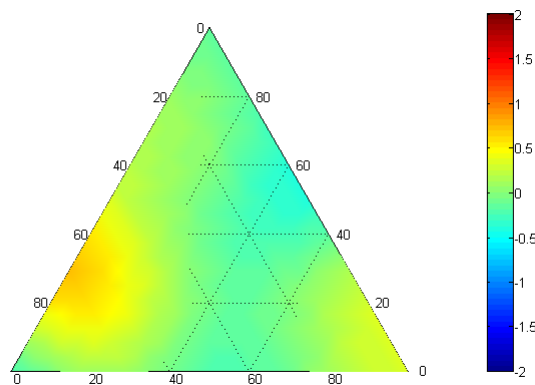

Figure S3.29. Smoothed Studentized residuals (colormap) as a function of composition for variable 29 (Packing fraction at 0 K). The ternary diagram vertices are lower right: BADCy, lower left: SiMCy, top: LECy
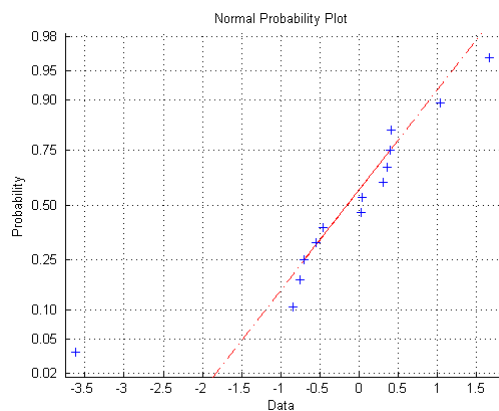
Figure S1.30. Normal probability plot for variable 30 (Packing fraction at 210 °C). Studentized residuals are plotted on the x-axis.
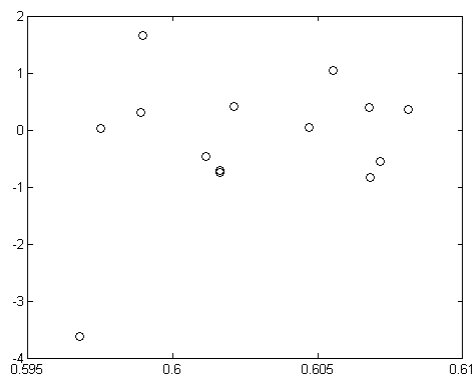

Figure S2.30. Residual plot for variable 30 (Packing fraction at 210 °C). Predicted values (dimensionless) are plotted on the x-axis and Studentized residuals on the y-axis.
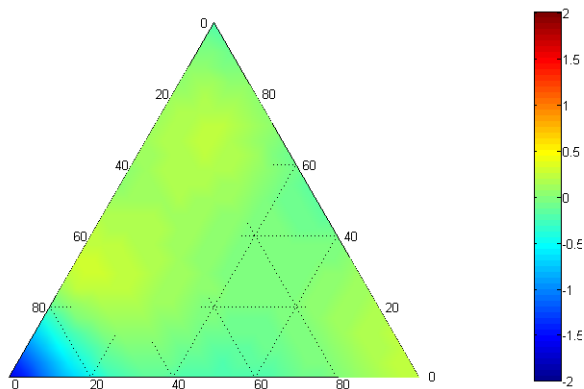

Figure S3.30. Smoothed Studentized residuals (colormap) as a function of composition for variable 30 (Packing fraction at 210 °C). The ternary diagram vertices are lower right: BADCy, lower left: SiMCy, top: LECy
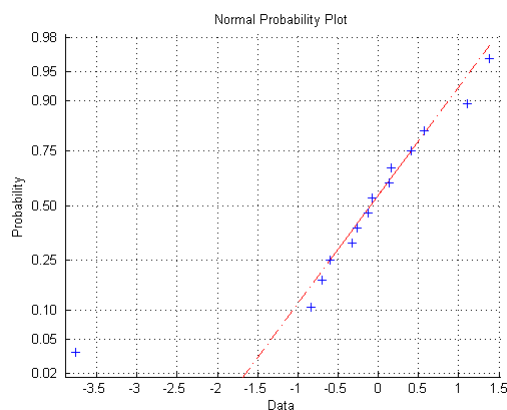
67

Figure S1.31. Normal probability plot for variable 31 (moisture uptake). Studentized residuals are plotted on the x-axis.
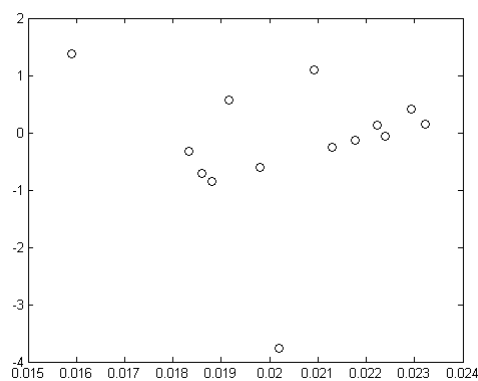

Figure S2.31. Residual plot for variable 31 (moisture uptake). Predicted values (fractional weight gain) are plotted on the x-axis and Studentized residuals on the y-axis.
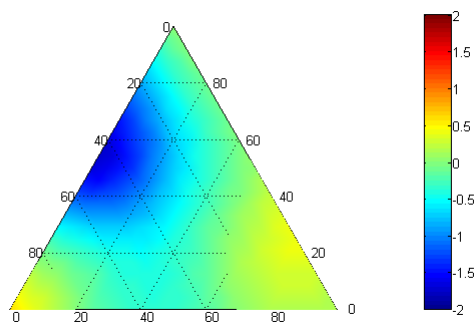

Figure S3.31. Smoothed Studentized residuals (colormap) as a function of composition for variable 31 (moisture uptake). The ternary diagram vertices are lower right: BADCy, lower left: SiMCy, top: LECy

S2. Simple Model for the Coefficient of Thermal Expansion of a Random Co-Polymerized Network

The key assumptions of the very simple model presented here are as follows:

1) Network segments are interpenetrating and randomly arranged in an isotropic orientation

2) Expansion of the network is uniform and isotropic at all length scales

3) The response of any network segment to a thermally-induced stress caused by the constraints imposed by interpenetrating neighbor segments is small enough to be adequately represented as a linearly proportional change in volume, and therefore characterized by a single linear bulk modulus parameter (K).

4) The average change in relative volume in response to a temperature change for all component segments in a given co-network is the same as the average change in volume for all the segments in the corresponding single-component network, and is small enough to be adequately represented by a single linear thermal expansion parameter (α).

For a given change in temperature ΔT, the relative volume of the ith component will change by an amount very well approximated by $\Delta V_i / V_i = 3\alpha_i\Delta T$, which will also be the average response of the network segment comprising the ith component in the absence of constraints. Due to the interpenetrating nature of the network segments, however, constraints are introduced, and for the purposes of the model, it is assumed that these constraints produce a homogeneous change in relative volume ($3\alpha_{eff}\Delta T$). As a result, each network segment is either compressed or dilated by an amount (herein denoted x_i) such that

$$x_i = 3\ \Delta T\ (\alpha_{eff} - \alpha_i) \qquad\qquad\qquad (\text{S-1})$$

Note that compression corresponds to a negative value of x_i, while dilation corresponds to a positive value.   As a result of the displacement from the unconstrained volume, the segments exert a force of their neighbors, given by

$$F_i = - K_i x_i A_i \qquad \text{(S-2)}$$

Where K_i represents the bulk modulus of the ith segment and A_i represents the contact area. Note that in this case, compression creates a positive (dilatory) force on the neighboring segments. Since the medium has a homogeneous effective thermal expansion coefficient, then if we consider a region that is small in comparison to the network as a whole but still encompasses a large number of segments, and further consider the surrounding region, both regions must have a volume expansion given by $3\alpha_{eff}\Delta T$, hence the displacement from equilibrium for the region as a whole must equal zero, and hence the total force from all the segments in contact with the region must sum to zero. For a given component, the total area of contact in an isotropic, homogeneous network with an arbitrary region is given by $\phi_i A$, where ϕ_i represents the volume fraction of the ith component in the network and A is the (arbitrary) surface area of the region in question. For a three component network, then, the need for a macroscopically homogeneous network gives rise to the equation:

$$-(\phi_1 K_1 x_1 + \phi_2 K_2 x_2 + \phi_3 K_3 x_3) A = 0 \qquad \text{(S-3)}$$

Since the area A is arbitrary and the negative sign is a common factor,

$$\phi_1 K_1 x_1 + \phi_2 K_2 x_2 + \phi_3 K_3 x_3 = 0 \qquad \text{(S-4)}$$

Additionally, by instantiating eq. (S-1) for any components (herein, component 1 and 2), and subtracting, the following relation is obtained

$$x_1 - x_2 = 3 \Delta T (\alpha_2 - \alpha_1) \qquad \text{(S-5)}$$

70

Rearranging and expanding to include the third component gives

$$x_2 = x_1 - 3\,\Delta T\,(\alpha_2 - \alpha_1) \; ; \; x_3 = x_1 - 3\,\Delta T\,(\alpha_3 - \alpha_1) \tag{S-6}$$

Substituting (S-6) into (S-4) yields

$$\phi_1 K_1 x_1 + \phi_2 K_2 [x_1 - 3\,\Delta T\,(\alpha_2 - \alpha_1)] + \phi_3 K_3 [\, x_1 - 3\,\Delta T\,(\alpha_3 - \alpha_1)\,] = 0 \tag{S-7}$$

Solving for x_1

$$x_1 = \frac{\phi_2 K_2 [3\Delta T(\alpha_2 - \alpha_1)] + \phi_3 K_3 [3\Delta T(\alpha_3 - \alpha_1)]}{\phi_1 K_1 + \phi_2 K_2 + \phi_3 K_3} \tag{S-8}$$

Then, using the version of eq. (S-1) for component 1, substituting (S-8), and solving for α_{eff} gives:

$$\alpha_{eff} = \frac{\alpha_1 \phi_1 K_1 + \alpha_2 \phi_2 K_2 + \alpha_3 \phi_3 K_3}{\phi_1 K_1 + \phi_2 K_2 + \phi_3 K_3} \tag{S-9}$$

Note that eq. (S-9) has the form of a weighted volumetric rule of mixtures; in this case the weighting factor is simply the bulk modulus.

References

S1.   Hamerton, I., *Chemistry and Technology of Cyanate Ester Resins*. Chapman & Hall: London, 1994.
S2.   Guenthner, A. J.; Yandek, G. R.; Wright, M. E.; Petteys, B. J.; Quintana, R.; Connor, D.; Gilardi, R. D.; Marchant, D. *Macromolecules* **2006,** *39*, 6046-6053.
S3.   Georjon, O.; Galy, J. *Polymer* **1998,** *39*, 339-345.